

Operator learning meets inverse problems: A probabilistic perspective

Nicholas H. Nelsen^{1,2,3*} and Yunan Yang^{2*}

¹Department of Mathematics, Massachusetts Institute of Technology,
Cambridge, MA 02139, USA.

²Department of Mathematics, Cornell University, Ithaca, NY 14853, USA.

³Oden Institute for Computational Engineering and Sciences & Department of
Aerospace Engineering and Engineering Mechanics, The University of Texas at
Austin, Austin, TX 78712, USA.

*Corresponding author(s). E-mail(s): nnelsen@utexas.edu;
yunan.yang@cornell.edu;

Abstract

Operator learning offers a robust framework for approximating mappings between infinite-dimensional function spaces. It has also become a powerful tool for solving inverse problems in the computational sciences. This chapter surveys methodological and theoretical developments at the intersection of operator learning and inverse problems. It begins by summarizing the probabilistic and deterministic approaches to inverse problems, and pays special attention to emerging measure-centric formulations that treat observed data or unknown parameters as probability distributions. The discussion then turns to operator learning by covering essential components such as data generation, loss functions, and widely used architectures for representing function-to-function maps. The core of the chapter centers on the end-to-end inverse operator learning paradigm, which aims to directly map observed data to the solution of the inverse problem without requiring explicit knowledge of the forward map. It highlights the unique challenge that noise plays in this data-driven inversion setting, presents structure-aware architectures for both point predictions and posterior estimates, and surveys relevant theory for linear and nonlinear inverse problems. The chapter also discusses the estimation of priors and regularizers, where operator learning is used more selectively within classical inversion algorithms.

Keywords: inverse map, regularization, neural operator, prior distribution, Bayesian inference, stability estimates, measure transport, pushforward, empirical measure

MSC Classification: 35R30 (Primary) 68T07, 65N21 (Secondary)

Contents

1	Introduction	3
2	Background on inverse problems	5
2.1	Probabilistic methods	8
2.1.1	Bayesian inverse problems	8
2.1.2	Transport maps	9
2.1.3	Nonparametric statistical inverse problems	10
2.1.4	Measure-centric formulations	11
2.2	Regularization methods	15
3	Background on operator learning	17
3.1	Supervised learning of operators	17
3.2	Common architectures	19
3.2.1	Encoder-decoder operator networks	20
3.2.2	Neural operators	21
4	Learning inverse problem solvers	23
4.1	Mathematical formulation	24
4.1.1	Training and evaluating learned inverse maps	25
4.1.2	Noisy data and the range of the forward map	26
4.2	Architectures for data-to-parameter maps	28
4.2.1	Fourier Neural Mappings	28
4.2.2	Operator Recurrent Neural Networks	29
4.2.3	Neural Inverse Operator	31
4.3	Theoretical results	33
4.3.1	Neural operator approximation theory: A case study on EIT	34
4.3.2	Finite-dimensionalizing nonlinear inverse problems	38
4.3.3	Finite-dimensionalizing linear inverse problems	39
4.4	Beyond point estimation: Data-to-posterior maps	42
5	Learning prior distributions and regularizers	44
5.1	Prior learning and Bayesian variational inference	44
5.1.1	Mathematical formulation and architecture choices	46
5.1.2	Theoretical results	49
5.2	Denoising networks and plug-and-play methods	58
5.2.1	Motivation for PnP	58
5.2.2	Theoretical analysis of PnP	59
6	Conclusion and outlook	60

1. Introduction

This chapter centers on operator learning for inverse problems with infinite-dimensional unknown parameters. This setting pervades numerous fields of science and engineering. The observed data can be finite-dimensional, which is realistic, or infinite-dimensional, which is a mathematical idealization useful for theoretical applications or when data is abundant. Mathematically, the relationship between the parameters and data is usually determined by (possibly nonlinear) partial- or integro-differential equations. For example, the parameter could be a spatially varying permeability coefficient function appearing in a physics model for groundwater flow. The measurements could be noisy observations of the associated pressure field at a sparse set of sensors in the domain. While all inverse problems are characterized by some notion of ill-posedness in the sense of Hadamard [1], i.e., lacking existence, uniqueness, or continuity concerning the data, the primary classes of inverse problems that the present chapter surveys are those with inherent instability. This makes the numerical resolution of such problems challenging.

Classical methods for solving inverse problems often rely on hand-crafted regularization techniques, explicit models of the forward process, and iterative optimization routines. While mathematically rigorous, these approaches can be limited in their practical application. They tend to be computationally intensive, sensitive to noise, and may struggle to deliver acceptable accuracy when the forward model is not invertible, ill-conditioned, or only partially known. Moreover, designing effective regularization terms requires deep domain expertise and often involves simplifying assumptions that may not hold in realistic scenarios.

In recent times, deep learning has demonstrated an exceptional ability to accurately solve inverse problems and even outperform classical reconstruction methods in linear and nonlinear imaging inverse problems [2–4]. The subsequent development and success of operator learning methods for the emulation of forward maps of partial differential equations (PDEs) has spurred significant interest in the application of such tools to inverse problems formulated in function spaces [5–18]. Indeed, operator learning serves as an attractive alternative and a complement to classical inversion. Architectures such as neural operators are designed to map between infinite-dimensional spaces of functions. As a byproduct, the tunable parameters of these models are decoupled from the resolution of the discretized data used to train them. This property affords exceptional flexibility at inference time and opens up new directions for multiresolution regularization. Operator learning methods can directly approximate the underlying inverse map purely from data. Furthermore, these methods can also be integrated into hybrid approaches that learn regularizers while respecting known physical structure in the forward map.

The chapter distinguishes between solving a single inverse problem with machine learning [19, 20], e.g., requiring the evolution of a Markov chain or running an optimization solver, and solving or probing families of inverse problems simultaneously, which is enabled by operator learning methods. There is an important and popular line of work that employs operator learning to build fast forward map surrogates to be then used downstream in various inverse problems [21–28]. Under certain conditions,

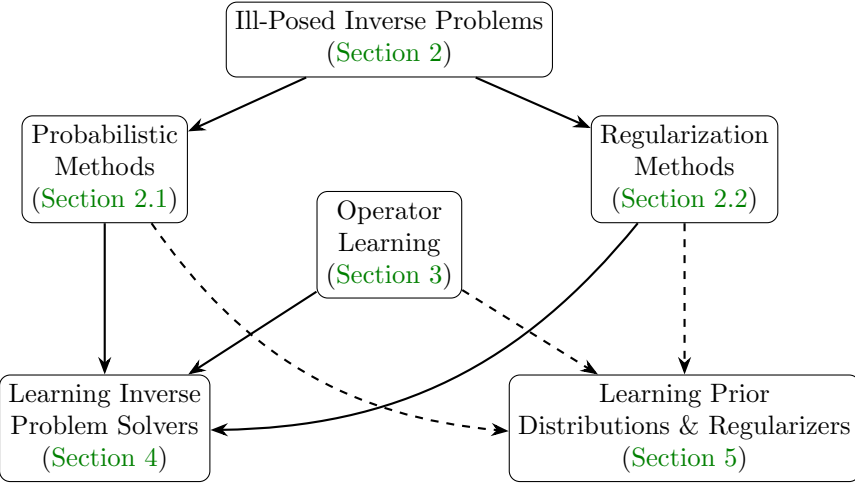


Fig. 1: Overall structure of the chapter.

the error incurred by replacing the true forward operator with the surrogate operator controls the propagated error in the inverse problem solution [29–33]; also see [34, Chp. 3]. However, due to its emphasis on the forward map, such work is outside of the scope of the present chapter. Instead, the chapter focuses on the machine learning of quantities specific to inverse problems and their underlying mathematical structure.

Another area of research that is contemporary in data-driven inverse problems but beyond the scope of the chapter is generative modeling based on the dynamical transport of measure. This research direction is timely and ever-expanding, encompassing the rapid advances in score-based diffusion models [35–38], flow matching [39], and stochastic interpolants [40–42]. These frameworks enable sampling from posterior distributions, interpolating between distributions, or learning regularizers implicitly from data. They can offer scalable alternatives to classical sampling algorithms or variational inference. Instead, the present chapter restricts its attention to more established Bayesian and numerical analysis methodologies for these tasks. The main topics of the chapter are (*i*) the learning of end-to-end inverse problem solvers directly from data and (*ii*) the learning of priors and regularizers for use in traditional inverse problem solvers.

Outline

This chapter reviews the current landscape of data-driven inverse problem solvers and regularizers based on operator learning. It places a particular focus on probabilistic formulations and theoretical insights. Unless otherwise specified, the chapter works in the continuum. This means that all functions, operators, and measures are viewed as elements of infinite-dimensional metric spaces, and no appeal is made to a particular type of discretization. As illustrated in [Fig. 1](#), the chapter is organized as follows.

[Sections 2](#) and [3](#) provide the necessary preliminaries on inverse problems and operator learning, respectively. On the inverse problems side, [Section 2](#) discusses

probabilistic and deterministic solution methods. It places particular emphasis on the expanding *measure-centric* viewpoint, which casts certain inverse problems into ones where either the data or parameter are themselves probability distributions. Subsequently, [Section 3](#) reviews the fundamental components of the operator learning framework, including training data assumptions, loss functions, and popular architectures.

The bulk of the chapter is concentrated in [Section 4](#), which concerns the end-to-end operator learning approach that seeks to directly map observed data to the unknown parameters that solve the inverse problem. It reveals features unique to inverse map learning, describes several structure-exploiting operator learning architectures for both point prediction and posterior estimation, and surveys some theoretical guarantees.

[Section 5](#) studies prior and regularizer learning from the perspectives of variational inference and denoising. This subject adopts a more specialized viewpoint than the previous section, focusing solely on machine learning to estimate sub-components within a larger analytical inversion procedure. The theoretical analysis discusses the stability properties of the prior-to-posterior map under prior perturbations and the convergence properties of learned Tikhonov regularizers.

[Section 6](#) concludes the chapter with an outlook toward challenges and future opportunities at the interface of operator learning and inverse problems.

2. Background on inverse problems

Inverse problems concern the recovery of unknown parameters from indirect, and often noisy, observations. Consider a data model of the form

$$y = \mathcal{G}(u) + \eta, \quad (2.1)$$

where $\mathcal{G}: \mathcal{U} \rightarrow \mathcal{Y}$ is a forward operator (also known as the parameter-to-data map), $u \in \mathcal{U}$ is the unknown parameter to be inferred, $y \in \mathcal{Y}$ is the observed data, and η models measurement noise or model error. The inverse problem is to recover u from y . In many applications arising from science and engineering, \mathcal{G} is nonlinear, the parameter space \mathcal{U} is an infinite-dimensional Banach space, and the data space \mathcal{Y} is high- or infinite-dimensional as well. The inherent nonlinearity and the high- or infinite-dimensional nature of many practical inverse problems can introduce significant mathematical and computational challenges.

More fundamentally, the inverse problem of recovering u from y is often *ill-posed* in the sense of Hadamard: solutions may not exist, may not be unique, or may not depend continuously on the data [1]. Regarding the last difficulty, the inverse problem solution's sensitivity to noise in y makes naïve inversion schemes unstable and unreliable. To address this challenge, one may introduce additional information, such as smoothness, sparsity, or statistical structure, through *regularization* techniques or by adopting a *probabilistic* framework to capture uncertainty and stabilize the solution. This section reviews approaches in both directions.

A canonical example of a severely ill-posed nonlinear inverse problem is *electrical impedance tomography* (EIT) [43]. EIT is a noninvasive imaging technique used to

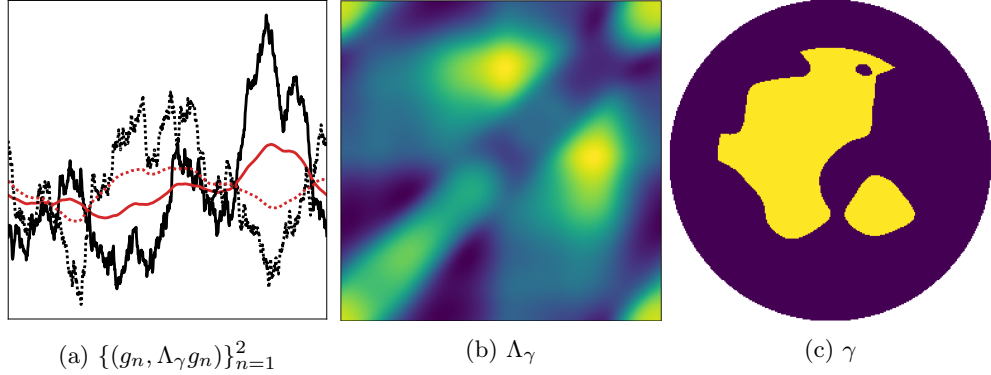


Fig. 2: Electrical impedance tomography from [Example 1](#). The domain Ω is the unit disk in \mathbb{R}^2 . The boundary manifold $\partial\Omega$ is identified as the one-dimensional unit torus \mathbb{T} by transforming into polar coordinates. [Figure 2a](#) displays two pairs of randomly sampled Neumann data (g_n , black) and corresponding Dirichlet data ($\Lambda_\gamma g_n$, red) on the torus. In [Fig. 2b](#), the full NtD map Λ_γ is represented numerically using its $L^2(\partial\Omega \times \partial\Omega)$ integral kernel function; this kernel function is further shifted, re-scaled, and transformed to the torus to aid visualization. The true realization of the conductivity γ generating these measurements under the forward map $\gamma \mapsto \Lambda_\gamma$ is shown in [Fig. 2c](#). Solving the inverse conductivity problem amounts to evaluating the inverse map $\Lambda_\gamma \mapsto \gamma$.

reconstruct the internal conductivity field of an object by making electrical measurements on the object's boundary. Spatial variations in the conductivity correspond to different regions of interest in the object, such as malignant biological tissue in hospital patients or distinct Earth subsurface structures in a geophysical context. Due to its well-understood mathematical properties, EIT has emerged as a prototypical non-linear benchmark inverse problem for both traditional inverse solvers and deep learning methods [\[12, 13, 44, 45, 45–52\]](#). This chapter works with the idealized continuum measurement version of the problem, which is known as *Calderón's problem* [\[53\]](#). For convenience, we will use the Calderón problem and EIT terminology interchangeably. The following EIT example will appear frequently throughout the chapter.

Example 1 (electrical impedance tomography). EIT aims to recover an unknown conductivity field $u = \gamma \in L^\infty(\Omega; \mathbb{R}_{>0})$ from measurements corresponding to the Neumann-to-Dirichlet (NtD) map $\mathcal{G}(\gamma) := \Lambda_\gamma$ of the elliptic PDE

$$\begin{cases} \nabla \cdot (\gamma \nabla \phi) = 0 & \text{in } \Omega, \\ \gamma \frac{\partial \phi}{\partial \mathbf{n}} = g & \text{on } \partial\Omega. \end{cases} \quad (2.2)$$

The NtD map $\Lambda_\gamma \in \mathcal{L}(H^{-1/2}(\partial\Omega); H^{1/2}(\partial\Omega))$ is a continuous linear operator from the dual Sobolev space $H^{-1/2}(\partial\Omega) = (H^{1/2}(\partial\Omega))^*$ into the trace Sobolev space $H^{1/2}(\partial\Omega)$ of $H^1(\Omega)$ boundary values [\[54\]](#). It maps the current density g to the voltage $\phi|_{\partial\Omega}$, i.e.,

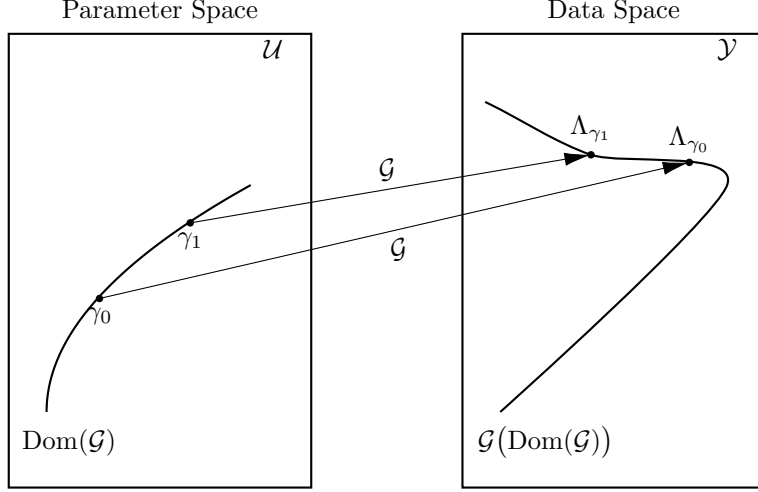


Fig. 3: Stability within the range of $\mathcal{G}: \gamma \mapsto \Lambda_\gamma$ from Example 1, Eq. (2.3).

$\Lambda_\gamma g = \phi|_{\partial\Omega}$ according to (2.2), both of which are functions on the smooth boundary $\partial\Omega$ of a bounded domain $\Omega \subset \mathbb{R}^d$. Figure 2 illustrates the main components of the EIT problem.

The problem of finding γ from Λ_γ is hard. Indeed, we wish to recover a function, often in an infinite-dimensional space, on the interior of Ω only by probing the boundary $\partial\Omega$. More quantitatively, EIT is severely ill-posed from a stability perspective. That is, for sufficiently smooth conductivities γ_0 and γ_1 bounded away from zero and infinity, it holds that

$$\|\gamma_0 - \gamma_1\|_{L^\infty(\Omega)} \lesssim \log^{-\beta} \left(\|\Lambda_{\gamma_0} - \Lambda_{\gamma_1}\|_{\mathcal{L}(H^{-1/2}(\partial\Omega); H^{1/2}(\partial\Omega))}^{-1} \right) \quad (2.3)$$

whenever $\delta = \|\Lambda_{\gamma_0} - \Lambda_{\gamma_1}\|_{\mathcal{L}(H^{-1/2}(\partial\Omega); H^{1/2}(\partial\Omega))}$ is small enough [55]. This means that for the parameter error $\|\gamma_0 - \gamma_1\|_{L^\infty(\Omega)}$ to be less than ε , it suffices for the measurement error δ to be exponentially small: $\delta \lesssim \exp(-\varepsilon^{-1/\beta})$. This estimate only holds in the range of the forward map $\mathcal{G}: \gamma \mapsto \Lambda_\gamma$. See Fig. 3 for a visualization. Similar results remain valid outside of the range of \mathcal{G} , as will be discussed in Sections 4.1.2 and 4.3.1. These extensions are useful to handle realistic noisy measurements.

The remainder of this section provides an overview of inverse problem solution methods. Section 2.1 considers techniques to solve inverse problems that heavily rely on ideas from probability and statistics. In contrast, Section 2.2 discusses a complementary viewpoint based on the functional-analytic regularization of inverse problems. We refer the reader to [56] for a more targeted review of the probabilistic and regularization approaches to inverse problems.

2.1. Probabilistic methods

In inverse problems, the observed data are typically indirect, incomplete, heterogeneous, and corrupted by noise. Such data challenges lead to inherent ambiguity in the recovered parameters. To address such ambiguity, probabilistic approaches formulate inverse problems in terms of probability measures, which promotes a systematic treatment of uncertainty in addition to resolving ill-posedness. The central goal is not only to recover an estimate of the unknown parameter u from the model (2.1), but also to quantify the uncertainty associated with that estimate. Such probabilistic approaches offer richer solution concepts than pointwise methods do. Indeed, uncertainty quantification (UQ) offers a principled approach to assessing the reliability and confidence of inferred inverse problem solutions, which is crucial for downstream decision-making, model validation, and risk assessment.

The *Bayesian approach* treats the unknown parameter as a random variable (Section 2.1.1). It computes the posterior distribution given the data, combining a prior distribution with a likelihood informed by the forward model and measurement process. This allows for both point estimates, such as the maximum a posteriori (MAP) point or posterior mean, and principled UQ through posterior variances, credible sets, and predictive distributions.

Sampling methods rooted in the *transportation of measure* offer flexible ways to represent and visualize uncertainty, particularly in high-dimensional, multi-modal, and non-Gaussian settings (Section 2.1.2). They can be viewed as a scalable alternative to traditional Bayesian posterior sampling algorithms such as Markov chain Monte Carlo (MCMC).

In contrast, *frequentist approaches* to statistical inverse problems draw on non-parametric statistics, minimax theory, and empirical risk minimization (Section 2.1.3). These methods yield confidence intervals, model selection procedures, and adaptive estimators with frequentist guarantees.

The *measure-centric perspective* formulates new inverse problems, or reinterprets existing ones, by modeling parameters or data as elements of the space of probability measures (Section 2.1.4). As a special case, the so-called stochastic inverse problem framework focuses on pushing forward or pulling back probability measures through the forward map \mathcal{G} . It emphasizes consistency between distributions over the parameter and data spaces and enables uncertainty propagation even in poorly identified regimes.

Each of these methodologies contributes a complementary lens on the incorporation of uncertainty into the solution procedure for inverse problems.

2.1.1. Bayesian inverse problems

The Bayesian approach to inverse problems is perhaps the most well-developed of all the probabilistic methods mentioned earlier. In recent decades, there has been significant progress and success in integrating Bayesian inference with statistical inverse problems formulated in function spaces [57, 58]. This has led to comprehensive well-posedness theory, approximation theory, and posterior consistency theory [59, 60] on the one hand, and scalable computational algorithms on the other hand [61, 62]. By

leveraging an inherently infinite-dimensional framing, the Bayesian approach is naturally applicable to inverse problems from continuum applied mathematics and scientific computing.

The Bayesian statistician models all quantities in the inverse problem (2.1) probabilistically. The noise η is assumed to be a random variable with distribution $\nu_0 := \text{Law}(\eta)$. This and the forward map \mathcal{G} defines the *likelihood* of observing y given the parameter u ; we denote by $\nu_{\mathcal{G}(u)} := \text{Law}(y | u)$ the pushforward of ν_0 under the translation-by- $\mathcal{G}(u)$ map. The core of any Bayesian procedure is the *prior distribution* specification. The parameter u is modeled as a random variable with distribution $\mu \in \mathcal{P}(\mathcal{U})$, the prior. The prior probability measure μ represents the modeler's beliefs and existing knowledge before observing any data. The prior μ is known to regularize the ill-posedness of the inverse problem. Popular choices in infinite dimensions include Gaussian priors, Besov priors, or data-driven pushforwards thereof [60].

The Bayesian solution to the inverse problem is not just a single point estimate of the parameter $u \in \mathcal{U}$, but instead the entire posterior probability distribution $\mu^y := \text{Law}(u | y) \in \mathcal{P}(\mathcal{U})$ obtained by conditioning the prior on the random variable y according to (2.1). Assume that $\nu_{\mathcal{G}(u)}$ has density $\exp(-\Phi(u; \cdot))$ with respect to ν_0 for all u , μ almost everywhere (a.e.). Then, under some mild conditions that can be verified on a case-by-case basis, the infinite-dimensional Bayes' rule [60, Thm. 14, pp. 9–10] shows that the posterior is given by

$$\begin{aligned} \mu^y(du) &= \frac{1}{Z_\mu^y} \exp(-\Phi(u; y)) \mu(du), \quad \text{where} \\ Z_\mu^y &:= \int_{\mathcal{U}} \exp(-\Phi(u'; y)) \mu(du'). \end{aligned} \tag{2.4}$$

The formula (2.4) is valid for every y a.e. under the joint distribution of (u, y) . The normalizing constant Z_μ^y , also known as the *evidence*, depends on both the data y and the prior μ . The potential function $\Phi: \mathcal{U} \times \mathcal{Y} \rightarrow \mathbb{R}$, also called the negative log-likelihood, depends on the forward map \mathcal{G} . A typical example is the Gaussian likelihood. Taking $\mathcal{Y} = \mathbb{R}^J$ and $\nu_0 = \mathcal{N}(0, \Gamma)$ for some positive definite $\Gamma \in \mathbb{R}^{J \times J}$, we have $\Phi(u; y) = \frac{1}{2} \|\Gamma^{-1/2}(y - \mathcal{G}(u))\|_{\mathbb{R}^J}^2$ [57].

There is by now a mature understanding of the statistical and computational [63] performance of Bayesian posterior solutions to linear [59, 64–71] and nonlinear inverse problems [58, 72, 73], especially those arising from PDEs [74–77]. In PDE problems, the map \mathcal{G} is typically factorized as $\mathcal{G} = \mathcal{O} \circ \mathcal{F}$, where $\mathcal{F}: \mathcal{U} \rightarrow \mathcal{V}$ is a parameter-to-solution operator and $\mathcal{O}: \mathcal{V} \rightarrow \mathcal{Y}$ is the solution-to-data operator, i.e., the observation operator. Here, the solution refers to the entire PDE solution, which is usually not fully observable in practice. While the interaction between \mathcal{O} and \mathcal{F} can substantially influence statistical accuracy [78], for the purposes of this chapter we are content with working with \mathcal{G} alone.

2.1.2. Transport maps

Computational measure transport is a general paradigm that seeks to represent a target probability measure $\nu = \mathsf{T}_\#^* \rho$ as the pushforward of some easy-to-sample reference

probability measure ρ under a measurable function T^* [79]. Thus, if $u \sim \rho$ is a sample from ρ , then $y = \mathsf{T}^*(u) \sim \nu$ is a sample from ν . Such a task can be accomplished by solving the minimum divergence estimation problem

$$\min_{\mathsf{T} \in \mathcal{T}} \mathsf{d}(\nu, \mathsf{T}_\# \rho) \quad (2.5)$$

for some statistical distance or divergence d and hypothesis class of transport maps \mathcal{T} . One can also add a regularizer to penalize the transport maps. Problem (2.5) falls under the umbrella of variational inference. By adjusting the choice of d , \mathcal{T} , and ρ , one derives different measure transport algorithms, including those that enable conditional sampling of joint distributions. While the solution to (2.5) is generally not “optimal” in the sense of optimal transport [80], connections to optimal transport can still be made, especially if d is taken to be a Wasserstein distance [81].

Specializing to the Bayesian setting discussed in Section 2.1.1, to solve inverse problems with measure transport, one typically seeks a prior-to-posterior map $\mathsf{T} = \mathsf{T}^{(\mu, y)}$ such that $\mu^y = \mathsf{T}_\# \mu$ [34, Chp. 5], where μ^y is the posterior (2.4) corresponding to prior μ and observed data y . The dependence of T on μ and y is implicit from the previous equality. While not usually done, in some applications it makes sense to explicitly parametrize the dependence of T on μ or y . This way, problem (2.5) does not have to be re-solved every time μ or y is changed, which can be prohibitively expensive. There is work along these lines that develops *amortized solvers* for Bayesian inverse problems [81, 82]. This amounts to methods that, given a new piece of data y , can rapidly produce a representation of the posterior distribution corresponding to that y without re-training or additional optimization. Using measure transport, this is equivalent to approximating the map $y \mapsto \mathsf{T}^{(y)}$, where $\mathsf{T}^{(y)}$ is the divergence minimization solution for a particular y . The amortized estimation of the data-to-posterior map is arguably a more challenging task than merely emulating the data-to-parameter inverse map, because now the output space is the metric space $\mathcal{P}(\mathcal{U})$ of probability measures supported on \mathcal{U} , rather than just the linear parameter space \mathcal{U} itself. We return to data-to-posterior estimation in Section 4.4.

2.1.3. Nonparametric statistical inverse problems

Nonparametric statistical inverse problems depart from the Bayesian and transport map settings by only modeling the noise η as a random variable [83–86]. The unknown parameter u is thought of as some fixed, true function that generates data y according to (2.1). Several examples can be formulated this way, such as derivative estimation, denoising, deconvolution, or the inverse heat equation [64, 83].

The canonical model for a nonparametric statistical inverse problem is

$$y = \mathcal{G}(u) + \frac{\sigma}{\sqrt{N}} \xi, \quad (2.6)$$

where ξ is a (typically Gaussian) white noise process indexed by the Hilbert space $\mathcal{Y} = L^2(\Omega)$. The forward operator $\mathcal{G}: \mathcal{U} \rightarrow \mathcal{Y}$ is usually linear in theoretical studies,

although there are some exceptions [76, 87]. The parameter σ scales the noise, and the number N represents the “amount of information” available for recovery.

The use of the notation N and the choice of white noise are for the following reason. The idealized problem (2.6) is known to be equivalent—in a precise statistical sense [74, 83]—to the nonparametric inverse regression problem

$$y_n = (\mathcal{G}(u))(x_n) + \sigma \xi_n \quad \text{for } n \in \{1, \dots, N\}, \quad (2.7)$$

where $\xi_n \stackrel{\text{i.i.d.}}{\sim} \mathcal{N}(0, 1)$ are independent and identically distributed (i.i.d.) standard Gaussians and the $\{x_n\}$ are some observed design points in the domain Ω . Thus, N represents the sample size of available data. The finite-sample problem (2.7) is also known as statistical inverse learning [88, 89].

Theoretical analysis is easier for the continuum model (2.6). However, it must be carefully interpreted (i.e., in a weak sense) because $\|\xi\|_{\mathcal{Y}} = \infty$ almost surely if \mathcal{Y} is infinite-dimensional. Thus, infinite-dimensional statistical inverse problems are characterized by “large” noise realizations. The error in reconstructions of the parameter u is measured on average with respect to the noise. The parameter u is assumed to belong to a bounded set of functions, typically the unit ball in some smoothness class such as a Sobolev or Besov space. To solve the inverse problem, one develops estimators that aim to minimize the worst-case average error over this set of functions. This is the minimax framework, which enables the classification of estimators as minimax optimal or not [83, Sec. 2].

2.1.4. Measure-centric formulations

Distribution-valued data is becoming increasingly common in modern data science [90–94]. Usually numerically realized as unstructured point clouds of arbitrary size, measure-valued data appear in a wide range of scientific applications including probabilistic weather forecasting [95], biomedical modeling [96], and computational geometry [97], to name a few. It is natural to wonder if inverse problems can also be formulated in the space of probability measures in order to take advantage of these substantial developments.

There is indeed an emerging *measure-centric* line of research on distributional inversion [98–103]. For example, measure-valued parameters arise in continuum formulations of optimal experimental design [104–106]. The calibration of physical models using diverse data sources leads to inverse problems where both the parameters and the measurements are measure-valued [107, 108]. Unlike Bayesian inversion from Section 2.1.1, it is worth emphasizing that in these frameworks, the underlying state space for the parameters is a space of distributions. Applying Bayesian ideas in the setting of measure-valued parameters would require a notion of posterior distribution over the probability measure space, which would be an interesting yet challenging future direction. The focus in this subsection—and other parts of the chapter more broadly—is on non-Bayesian inverse problems with observed data belonging to the space of probability measures. We now elaborate on this setting.

Collections of measurements

The starting point is the assumption that instead of observing a single measurement $y \in \mathcal{Y}$, we observe an unordered collection of data $Y^M := \{y_m\}_{m=1}^M$, i.e., a point cloud. A key point is that $M = M(u)$ is allowed to depend on the unknown parameter u of the inverse problem. This has implications for inversion routines that are repeatedly called to solve the inverse problem for different data realizations. Different measure-valued inverse problem frameworks arise from the particular data-generating model that is assumed for Y^M . This subsection now presents three such models.

Suppose that the forward map \mathcal{G} and the noise distribution $\pi := \text{Law}(\eta)$ are known quantities. For $m \in \{1, \dots, M(u)\}$, the first data-generating model is

$$y_m = \mathcal{G}(u) + \eta_m, \quad \text{where } \eta_m \sim \pi. \quad (2.8)$$

The goal is to find u from $Y^{M(u)}$. The variation in each y_m is due to a new realization of noise η_m ; the parameter u is the same across realizations.

The second model now varies the parameter realizations via

$$y_m = \mathcal{G}(u_m) + \eta_m, \quad \text{where } u_m \sim \mu \quad \text{and } \eta_m \sim \pi. \quad (2.9)$$

This setup corresponds to measurements of the fixed system \mathcal{G} at varied parameter configurations $u_m \sim \mu$ [107]. The goal here is to perform *distributional inversion* by finding $\mu \in \mathcal{P}(\mathcal{U})$ from Y^M , where $M = M(\mu)$. The unknown measure μ could represent a Bayesian prior or some inherent physical uncertainty, for example. Suppose either \mathcal{G} or π is unknown. In that case, the joint recovery of either of these objects in addition to μ becomes an instance of blind deconvolution [108], which is a notoriously difficult nonlinear inverse problem.

The last model, which will be particularly relevant for the EIT problem from [Example 1](#), is the generalized regression model

$$y_m = \mathcal{G}_m(u) + \eta_m, \quad \text{where } \eta_m \sim \pi \quad (2.10)$$

and $\{\mathcal{G}_m\}_{m=1}^{M(u)}$ is a (potentially random) family of “forward maps.” The goal of this inverse problem is to find u from the known pairs $\{(\mathcal{G}_m, y_m)\}_{m=1}^{M(u)}$.

A traditional inversion approach for (2.8) or (2.10) would involve stacking all M equations on \mathcal{Y} into a single equation on the product space \mathcal{Y}^M [62]. Then, the enlarged inverse problem can be solved with Bayesian or optimization methods. However, this strategy may impose an ordering on the indices $\{1, \dots, M\}$ that is not fundamental to the inverse problem. It also raises difficulties when applying operator learning to approximate the inverse map $Y^{M(u)} \mapsto u$ because such a map would have to be re-trained from scratch if $M = M(u)$ changes when u changes. Relatedly, a naïve attempt to solve (2.9) by solving $M(\mu)$ individual inverse problems does not take into account correlations between points from the statistical model. One path forward is to work with distribution-valued data instead.

Lifting to the space of probability measures

We unify the preceding perspectives by lifting equations on the data space \mathcal{Y} to equations on the infinite-dimensional space $\mathcal{P}(\mathcal{Y})$ of probability measures over \mathcal{Y} . To this end, let δ_z denote the Dirac measure, or atom, defined by $\delta_z(A) = 1$ if $z \in A$ and $\delta_z(A) = 0$ otherwise. We identify the point cloud $\{y_m\}_{m=1}^M$ with the empirical probability measure $\nu^M \in \mathcal{P}(\mathcal{Y})$ defined by

$$\nu^M := \frac{1}{M} \sum_{m=1}^M \delta_{y_m}. \quad (2.11)$$

By letting ν^M be our representation of the point cloud data, we can design inversion procedures that are robust to the number M of measurements and are also invariant—or at least equivariant—to permutations of the indices of the atoms in ν^M . At the population level for (2.8), we seek $u \in \mathcal{U}$ such that

$$\nu^{M(u)} \approx \pi * (\mathcal{G}_\# \delta_u), \quad (2.12)$$

where $\mathcal{G}_\# : \mathcal{P}(\mathcal{U}) \rightarrow \mathcal{P}(\mathcal{Y})$ is the pushforward operator under \mathcal{G} and $*$ denotes convolution of measures [107]. The right-hand side of (2.12) is the distribution of y_m from (2.8). Closeness of this distribution to $\nu^{M(u)}$ should be quantified by a statistical distance that is still meaningful when applied to two empirical measures, such as maximum mean discrepancy (MMD) or the family of Wasserstein metrics. This then suggests an optimization principle for finding u .

Similarly, the lifted version of the second data model from (2.9) is

$$\nu^{M(\mu)} \approx \pi * (\mathcal{G}_\# \mu), \quad (2.13)$$

where now $M = M(\mu)$ is allowed to depend on μ . Transport map generative models have been used to find μ from $\nu^{M(\mu)}$ according to (2.13) [107, 108].

For clarity, we defer the discussion of lifting the third model, (2.10), until we describe it in the concrete setting of EIT. Regardless, all three of the preceding multi-measurement inverse problems can be written as finding a distribution $\mu \in \mathcal{P}(\mathcal{U})$ from $\mathcal{P}(\mathcal{Y})$ -valued data

$$\nu^{M(\mu)} \approx \nu := \mathcal{G}(\mu). \quad (2.14)$$

The lifted forward operator $\mathcal{G} : \mathcal{P}(\mathcal{U}) \rightarrow \mathcal{P}(\mathcal{Y})$ acts on probability measures, but in the case that u is deterministic, we identify u with the Dirac measure $\mu \equiv \delta_u$ in (2.14). In the case of (2.12) and (2.13), the right-hand side of these displays shows that $\mathcal{G} = \pi * \mathcal{G}_\#$ is the composition of a convolution with a pushforward. Both convolution and pushforward, and hence \mathcal{G} , can be interpreted as “linear” operations on measures under certain conditions. However, the measure-centric framework is still amenable to more complicated and highly nonlinear operators \mathcal{G} if they arise.

Application to EIT

Calderón's problem from [Example 1](#) is formulated at the continuum level as finding $\gamma \in \mathcal{U}$ from noisy data $Y := \Lambda_\gamma + \Xi$ belonging to a space of linear operators. Here, Ξ is an abstract operator-valued noise process. The NtD map Λ_γ represents all possible current-voltage pairs on the boundary. However, practical EIT hardware only permits a finite number $M = M(\gamma)$ of boundary measurements [\[54, 109\]](#). For $m \in \{1, \dots, M(\gamma)\}$, we observe functions g_m and

$$y_m = \Lambda_\gamma g_m + \eta_m, \quad \text{where} \quad g_m \sim \rho \quad \text{and} \quad \eta_m \sim \pi. \quad (2.15)$$

The known distribution $\rho \in \mathcal{P}(\mathcal{X})$ over a space \mathcal{X} of current patterns represents the experimental design of the EIT imaging system. See [Fig. 2a](#) for a visualization. The goal is to recover the conductivity γ from the point cloud $\{(g_m, y_m)\}_{m=1}^{M(\gamma)}$. One approach is to perform a two-stage recovery: first, estimate the nuisance parameter Λ_γ via regression, then use Λ_γ to perform inversion using the continuum Calderón framework. However, it is desirable to avoid the nuisance parameter Λ_γ and instead directly reconstruct γ from the raw data boundary measurement pairs $\{(g_m, y_m)\}_{m=1}^{M(\gamma)}$.

We do so as follows. First, we relate the EIT data model [\(2.15\)](#) to the general regression model [\(2.10\)](#) by defining $\mathcal{G}_m(u) := \Lambda_u g_m$. Then by lifting the observed data to the joint space $\mathcal{P}(\mathcal{X} \times \mathcal{Y})$, we obtain the measure-valued inverse problem

$$\frac{1}{M(\gamma)} \sum_{m=1}^{M(\gamma)} \delta_{(g_m, y_m)} \approx (\delta_0 \otimes \pi) * (\text{Id}, \Lambda_\gamma)_\# \rho =: \mathcal{G}(\delta_\gamma). \quad (2.16)$$

In the display, $\delta_0 \otimes \pi \in \mathcal{P}(\mathcal{X} \times \mathcal{Y})$ is a product measure. Under the measure-centric perspective, the inverse problem solution operator corresponding to [\(2.16\)](#) maps $\mathcal{P}(\mathcal{X} \times \mathcal{Y})$ to \mathcal{U} , that is, a joint probability measure over functions on the boundary to functions on the interior. We will return to this measure-to-function viewpoint on EIT in [Section 4.2.3](#).

Stochastic inverse problems

A special case of [\(2.9\)](#) and its lifting [\(2.13\)](#) is when $\pi = \text{Law}(\eta) = \delta_0$. This noiseless setting leads to the so-called *stochastic inverse problem* (SIP)

$$\nu = \mathcal{G}_\# \mu. \quad (2.17)$$

The data is $\nu \in \mathcal{P}(\mathcal{Y})$ and the unknown is $\mu \in \mathcal{P}(\mathcal{U})$. There is a growing body of work on SIPs [\[103, 110, 111\]](#) and related methodologies, such as *data-consistent inversion* [\[112–115\]](#). These approaches extend classical inverse problem frameworks by treating both the data and the unknown parameters as probability measures and modeling their relationships through forward operators defined between metric spaces of probability spaces. Recent advances in SIPs have leveraged variational optimization in probability measure spaces, explored the effects of different statistical divergences (e.g., f -divergences and Wasserstein distances) used for parameter reconstruction,

addressed challenges in conditional and marginal recovery, and introduced dynamical solution techniques. These methods provide robust stability estimates, convergence guarantees, regularization effects, and uncertainty quantification [100, 102, 116]. A comparison between SIPs and Bayesian inverse problems can be found in [117].

Distributional inversion greatly benefits from modern techniques for analysis in probability measure spaces, including structured transport maps [79, 118, 119] and Wasserstein gradient flows [102, 116, 120, 121]. These techniques are also relevant for learning distribution-informed priors in standard Bayesian inversion workflows, especially in scenarios where data from multiple sources must be incorporated [107, 108, 122]. Although the forward operator in most SIP formulations is based on a pushforward map that links the parameter distribution to the observed data distribution as in (2.17), alternative operators between probability measure spaces have also gained attention. For example, the cryo-EM imaging problem is a notable instance of an SIP where the forward operator itself involves randomness [123].

2.2. Regularization methods

In contrast to the chapter so far, this subsection adopts a more deterministic viewpoint on inverse problems. Here, the goal is to solve the equation

$$y = \mathcal{G}(u) \quad (2.18)$$

for the unknown parameter $u \in \mathcal{U}$. However, instead of the exact observation $y \in \mathcal{Y}$, we are provided with a perturbed measurement

$$y^\delta \in \mathcal{Y}, \quad \text{where} \quad d_{\mathcal{Y}}(y, y^\delta) \leq \delta. \quad (2.19)$$

In (2.19), $d_{\mathcal{Y}}$ is a distance function on the data space and δ quantifies the magnitude of the measurement error. In this setting, reconstruction accuracy is studied for the worst-case data perturbation satisfying (2.19). This departs from the nonparametric statistical inverse problems setting of Section 2.1.3, which considers average-case error with respect to random noise in the measurements.

Such inverse problems are ill-posed: the forward operator \mathcal{G} may be non-invertible or ill-conditioned, making the solution highly sensitive to small perturbations in the data. To mitigate this instability, *regularization* incorporates prior information or constraints on the parameter space \mathcal{U} to stabilize the inversion process [124, 125]. Regularization strategies for inverse problems of the form (2.18)–(2.19) are commonly grouped into three broad paradigms: direct methods (e.g., spectral filtering via the SVD), implicit techniques (e.g., early stopping and the dynamics of gradient descent), and variational formulations (e.g., Tikhonov and total variation regularization).

Of the three classifications, this chapter centers mostly on variational regularization. Variational regularization is an optimization approach [126]. The solution is obtained by minimizing a composite objective:

$$\min_{u \in \mathcal{U}} \left\{ d_{\mathcal{Y}}(\mathcal{G}(u), y^\delta) + \lambda R(u) \right\}, \quad (2.20)$$

where $R: \mathcal{U} \rightarrow \mathbb{R}$ is a chosen regularizer and $\lambda \geq 0$ is a regularization parameter. The first term in (2.20) quantifies data misfit, while the second term involving R encodes prior knowledge about the parameter u . Classical choices for the regularization functional R include Tikhonov's quadratic penalty $R(u) = \|u\|_{\mathcal{U}}^2$ [127–129] and total variation (TV) regularization $R(u) = \|\nabla u\|_{L^1}$ [130–132], which promote smoothness and edge sparsity, respectively. While handcrafted regularizers have proven to be effective in specific applications [133–136], they often fall short in capturing the complex, high-dimensional structures present in real-world data. Moreover, the choice and tuning of the hyperparameter λ remain significant practical challenges [137].

In recent years, data-driven approaches have significantly improved the quality of reconstructions by learning regularizers or priors directly from data [138–140]. Modern machine learning techniques for regularization can be categorized based on their training paradigm and model type [141]. In supervised approaches, networks are trained on paired examples (y, u) to learn either the full inverse map or a regularization functional. In contrast, unsupervised methods aim to model the distribution of u (i.e., a prior μ) using only samples of u from historical datasets. There are also untrained approaches, such as Deep Image Prior (DIP) [142], which impose priors implicitly during instance-specific inversion without requiring any offline training. Most of these methods require or assume some knowledge about the forward operator \mathcal{G} .

Among these advances, score-based diffusion models have emerged as powerful priors for use in solving inverse problems. These models leverage learned gradients of log densities to guide stochastic sampling conditioned on observed data. This enables unsupervised, high-fidelity reconstructions that replace traditional hand-crafted regularizers with learned generative dynamics. Current research efforts are focused on improving the efficiency of these models while incorporating physics-based constraints [143–146].

More recently, operator learning, which focuses on estimating mappings between function spaces, is gaining significant attention in the context of inverse problems. Beyond the more common tasks of learning forward or inverse operators from paired data, the operator learning framework offers new opportunities to derive or incorporate regularization techniques to tackle challenging inverse problems. Section 5 will explore two key categories of methods for learning priors and regularization mechanisms: Bayesian variational inference and denoising-driven regularization, notably the plug-and-play technique.

Variational inference methods aim to approximate prior distributions by learning them from within a parametric family of probability measures. This is achieved by optimizing statistical divergence-based objective functions. In contrast, plug-and-play methods leverage the insight that denoisers inherently encode prior information. By embedding a learned denoiser into iterative optimization algorithms, typically replacing a proximal operator, plug-and-play methods regularize inverse problems without requiring an explicit prior. As we will examine, these prior-learning and regularization approaches can be interpreted within the broader framework of operator learning, where the mathematical properties of the learned operators (e.g., Lipschitz continuity, monotonicity) play a crucial role in ensuring algorithmic stability and convergence when solving inverse problems.

3. Background on operator learning

Supervised operator learning lifts finite-dimensional vector-to-vector regression to infinite-dimensional function-to-function regression. The framework designs approximation architectures at the continuum level. Consequently, these architectures exhibit robustness to the level of discretization used during numerical implementation [147, Sec. 2.3, pp. 8–9]. This is a core distinction between operator learning and traditional machine learning. Once trained, operator learning models can be deployed at different discretizations of the input and output spaces without additional effort, while at the same time producing consistent predictions. The primary motivators for operator learning are the acceleration of scientific computation and the discovery of physical laws from real data. Operator learning has been particularly successful in surrogate modeling of parametrized PDEs and their corresponding downstream tasks, such as uncertainty propagation or engineering design optimization, based on these PDE parameter-to-solution map surrogates.

Operator learning developed independently from the field of inverse problems and does not explicitly rely on ideas from that field. However, it is known that forward operator learning [148–151]—and nonparametric regression more generally [152]—can be interpreted as a linear inverse problem with a non-compact forward map. The non-compact linear forward map arises from the point evaluations of the unknown and possibly nonlinear target operator at the randomly sampled input data points. This perspective has proven to be highly effective in the study of linear regression and kernel methods, where sharp error estimates are developed by combining concentration of measure techniques in Hilbert spaces with concrete manipulations of integral operators [153–155].

Another related line of work exploits the Green’s function structure of differential operators to derive data-efficient operator learning algorithms that are inspired by numerical linear algebra [156–159]. This framework is generalized to a statistical setting that allows for recovery of kernels in possibly nonlinear operators that do not necessarily admit Green’s functions [150, 160–162]. In contrast, the present chapter focuses on solving a variety of inverse problems that arise from the physical, imaging, and data sciences, rather than the specific non-physical inverse problem associated with the act of supervised learning.

For a more comprehensive overview of operator learning from a mathematical and theoretical perspective, we refer the reader to these recent survey articles [159, 163, 164]. The present section only covers material that is necessary for inverse problem purposes. Section 3.1 presents the basic components of an operator learning workflow, while Section 3.2 defines common neural operator architectures that appear frequently in the rest of this chapter.

3.1. Supervised learning of operators

Suppose that $\mathcal{X}_1 = \mathcal{X}_1(\Omega_1; \mathbb{R}^{p_1})$ and $\mathcal{X}_2 = \mathcal{X}_2(\Omega_2; \mathbb{R}^{p_2})$ are input and output Banach spaces of vector-valued functions defined on bounded Euclidean subsets Ω_1 and Ω_2 , respectively. Let $F: \mathcal{X}_1 \rightarrow \mathcal{X}_2$ denote the target operator that we wish to learn. As a concrete example, consider $F: L^\infty(\Omega; \mathbb{R}_{>0}) \rightarrow H^1(\Omega; \mathbb{R})$ defined by $\gamma \mapsto \phi$ in (2.2).

This is a nonlinear operator defining the coefficient-to-solution map of the elliptic boundary value problem (2.2). More generally, we could also consider learning the well-posed forward operator \mathcal{G} appearing in inverse problems such as (2.1). These examples are representative of much of the field of operator learning: approximation of well-defined, potentially very smooth, forward processes that map physical parameters to PDE solutions or quantities of interest.

In supervised operator learning, we first assume that a dataset of labeled pairs $\{(u_n, y_n)\}_{n=1}^N \subset \mathcal{X}_1 \times \mathcal{X}_2$ is available for training. The $u_n: x \mapsto u_n(x)$ are the input functions and the $y_n: x' \mapsto y_n(x')$ are the possibly noisy output functions

$$y_n = \mathsf{F}(u_n) + \xi_n. \quad (3.1)$$

In statistical learning, the data are assumed to be i.i.d. samples from some joint distribution over $\mathcal{X}_1 \times \mathcal{X}_2$. Such an assumption may not hold for highly correlated processes, such as time series or optimal experimental designs. Nonetheless, in this section we further assume that $u_n \stackrel{\text{i.i.d.}}{\sim} \mu$ for some $\mu \in \mathcal{P}(\mathcal{X}_1)$ and that $\xi_n \equiv 0$ for all n . Often in operator learning, the labeled data are not passively given, but instead are actively queried using the map F as a black box. Thus, the training data distribution μ is frequently specified by the user. While it is of considerable interest to determine optimal choices for μ [11, 165–168], in practice μ is usually taken to be a Gaussian measure over \mathcal{X}_1 with a specified covariance structure such as Matérn or exponential [159, Sec. 4.1]. Then μ is sampled i.i.d. to generate the random functions $\{u_n\}$, and consequently $\{y_n\}$ after querying $u_n \mapsto \mathsf{F}(u_n)$. The noise-free condition $\xi_n \equiv 0$ is justified when the data arises from high-fidelity numerical solvers with controlled discretization errors; this is a typical use case in operator learning.

The overall goal in operator learning is to estimate the operator F from the given data. The most popular way to do so is by performing the *empirical risk minimization* (ERM)

$$\min_{\Psi \in \mathcal{H}} \frac{1}{N} \sum_{n=1}^N \ell(y_n, \Psi(u_n)). \quad (3.2)$$

Solving this optimization problem is referred to as *training*. In (3.2), $\ell: \mathcal{X}_2 \times \mathcal{X}_2 \rightarrow \mathbb{R}$ is a loss functional and \mathcal{H} is the hypothesis space of possible operator approximations. The loss is often taken to be the squared loss $\ell(y, y') = \|y - y'\|_X^2$ or non-squared norm loss $\ell(y, y') = \|y - y'\|_X$ in any Banach space $X \supseteq \mathcal{X}_2$. Usually X equals the Lebesgue space $L^q(\Omega_2; \mathbb{R}^{p_2})$ for $q = 1, 2$ or the Sobolev space $H^k(\Omega_2; \mathbb{R}^{p_2})$ for $k = 1, 2$. The relative loss

$$\ell(y, y') = \frac{\|y - y'\|_X}{\|y\|_X + \epsilon} \quad (3.3)$$

is also popular; here $\epsilon \geq 0$ is a small numerical stability parameter. Practically, the function space norms appearing in the loss ℓ are discretized with quadrature rules and finite difference schemes.

For parametric hypothesis classes based on deep learning, (3.2) is typically solved with variants of mini-batch stochastic gradient descent (SGD) and accelerated with graphics processing unit (GPU) computing. However, there are more structured operator learning models, such as those based on kernels or random features [169–171], that do not require the explicit minimization (3.2) with SGD, e.g., because of closed-form expressions for minimizers. These methods still benefit from GPU acceleration, however.

Once a minimizer or approximate minimizer $\widehat{\Psi}$ of (3.2) is obtained, it remains to assess its accuracy as an approximation to F . It is theoretically convenient, especially in universal approximation results, and also practically desirable in safety-critical applications, to consider the uniform error over a fixed compact subset K of \mathcal{X}_1 :

$$\sup_{u \in \mathsf{K}} \ell(\mathsf{F}(u), \widehat{\Psi}(u)) \quad \text{or} \quad \sup_{u \in \mathsf{K}} \|\mathsf{F}(u) - \widehat{\Psi}(u)\|_X. \quad (3.4)$$

However, we cannot expect the worst-case error (3.4) to be small by only training in the empirical norm (3.2), which is an averaged quantity. The most used accuracy metric in practice is the expected risk

$$\mathbb{E}_{u \sim \mu} [\ell(\mathsf{F}(u), \widehat{\Psi}(u))]. \quad (3.5)$$

When $\mathcal{X}_2 \subseteq L^2$ and ℓ is chosen as (3.3), we then obtain the popular *expected relative L^2 error*

$$\mathbb{E}_{u \sim \mu} \left[\frac{\|\mathsf{F}(u) - \widehat{\Psi}(u)\|_{L^2(\Omega_2; \mathbb{R}^{p_2})}}{\|\mathsf{F}(u)\|_{L^2(\Omega_2; \mathbb{R}^{p_2})} + \epsilon} \right] \quad (3.6)$$

with respect to the training distribution μ . Other test accuracies are defined by choosing different function spaces X and loss functions ℓ . The out-of-distribution error with respect to some $\mu' \neq \mu$ is also relevant in applications [148, 166]; in this case, one would replace every instance of μ by μ' in the preceding displays. See [159, Sec. 4.2.1] for other choices of loss functions or loss augmentations. The expectations in expressions such as (3.5) and (3.6) are evaluated numerically by averaging over a finite set of held-out test samples.

More broadly, operator learning as a field extends beyond the supervised setting considered here. The present chapter will touch on some unsupervised operator learning problems in Section 5. We also refer the reader to [151, Chapter 6.2] for other examples.

3.2. Common architectures

By now, there are dozens of variants of operator learning architectures. For an overview of some of these and their shared structure, see [159, 163, 164, Sec. 3] and [169, 172]. What these models share is a conceptually continuous design that decouples model parameters from any fixed discretization. Some operator learning methods of note that we do not study in detail in this chapter include continuum transformers for

functions and probability measures [5, 13, 95, 173–175], function space random features [169, 176], kernel methods and Gaussian processes [171], and nonparametric linear operator parametrizations [148, 149, 156–158, 165, 170, 177]. The remainder of this subsection describes two important parametric classes: encoder-decoder networks in Section 3.2.1 and neural operators in Section 3.2.2. They correspond to a hypothesis space \mathcal{H} in (3.2) given by

$$\mathcal{H} := \{\Psi(\cdot; \theta) : \mathcal{X}_1 \rightarrow \mathcal{X}_2 \mid \theta \in \Theta\} \quad (3.7)$$

for some parameter set Θ of high but finite dimension. Within the two classes are the well-known DeepONet, PCA-Net, and Fourier Neural Operator architectures.

3.2.1. Encoder-decoder operator networks

A mapping $\Psi: \mathcal{X}_1 \rightarrow \mathcal{X}_2$ that takes the form

$$\Psi := \mathcal{D} \circ \mathcal{A} \circ \mathcal{E} \quad (3.8)$$

is said to have *encoder-decoder structure* if the encoder $\mathcal{E}: \mathcal{X}_1 \rightarrow \mathbb{R}^{d_1}$, approximator $\mathcal{A}: \mathbb{R}^{d_1} \rightarrow \mathbb{R}^{d_2}$, and decoder $\mathcal{D}: \mathbb{R}^{d_2} \rightarrow \mathcal{X}_2$ are all continuous maps [163, Sec. 2.4 and 4.1]. Encoder-decoder structure is a fundamental component of most universal approximation proofs for various operator learning methods [147, 172, 178, 179]. It can also be related to autoencoders on function spaces; see [163, Fig. 3] and [78, 180, 181]. Encoder-decoder networks are also the nonlinear architectures that enjoy the most comprehensive quantitative theory, including sharp approximate rates [179] and sample complexity bounds [182, 183].

The *DeepONet* architecture is a canonical encoder-decoder operator network [184]. Building off of earlier work in the shallow case [185], DeepONet constructs Ψ in (3.8) from traditional, finite-dimensional, deep feedforward neural networks [186, Chp. 2] as follows. Let $\mathcal{E} = L \in \mathcal{L}(\mathcal{X}_1; \mathbb{R}^{d_1})$ be a continuous linear map. For example, L could be represented by projections onto a finite number of basis functions if \mathcal{X}_1 is a Hilbert space, general linear functionals in \mathcal{X}_1^* if \mathcal{X}_1 is a Banach space, or point evaluations at d_1 fixed (or varying, see [187]) sensor points in Ω_1 if \mathcal{X}_1 embeds into the space of continuous functions. The approximator $\mathcal{A}: \mathbb{R}^{d_1} \rightarrow \mathbb{R}^{d_2}$ is a deep neural network with d_2 output components $a_j: \mathbb{R}^{d_1} \rightarrow \mathbb{R}$ called the “branch net”. For another deep neural network with d_2 output components $\varphi_j: \Omega_2 \rightarrow \mathbb{R}^{p_2}$ called the “trunk net”, the decoder is the linear map $\mathcal{D}: z \mapsto \sum_{j=1}^{d_2} z_j \varphi_j$. The $\{\varphi_j\}$ represent basis functions for the output space \mathcal{X}_2 . Putting together the pieces, we can write the DeepONet as

$$\Psi_{\text{DON}}(u; (\theta_{\mathcal{A}}, \theta_{\mathcal{D}}))(x) = \sum_{j=1}^{d_2} a_j(Lu; \theta_{\mathcal{A}}) \varphi_j(x; \theta_{\mathcal{D}}) \quad (3.9)$$

for all $u \in \mathcal{X}_1$ and $x \in \Omega_2$. Since both $\{a_j\}$ and $\{\varphi_j\}$ are parametrized as neural networks, we denote their parameter dependence explicitly in (3.9) by $\theta_{\mathcal{A}}$ and $\theta_{\mathcal{D}}$, respectively. Note that the encoder map L is fixed *a priori*, not learned.

A related architecture, called *PCA-Net* [181], is based on principal component analysis (PCA) [188]. This requires \mathcal{X}_1 and \mathcal{X}_2 to be separable Hilbert spaces, together with the conditions $\mathbb{E}_{u \sim \mu} \|u\|_{\mathcal{X}_1}^2 < \infty$ and $\mathbb{E}_{u \sim \mu} \|\mathsf{F}(u)\|_{\mathcal{X}_2}^2 < \infty$. Then μ and $\mathsf{F}_\# \mu$ (the pushforward of μ under F) have well-defined covariance operators $\text{Cov}(\mu) \in \mathcal{L}(\mathcal{X}_1; \mathcal{X}_1)$ and $\text{Cov}(\mathsf{F}_\# \mu) \in \mathcal{L}(\mathcal{X}_2; \mathcal{X}_2)$ whose eigenfunctions (i.e., the PCA bases) determine the encoder \mathcal{E} and decoder \mathcal{D} . The approximator \mathcal{A} is still a neural network. Letting $\{e_j\}_{j \in \mathbb{N}}$ be the PCA eigenbasis of $\text{Cov}(\mu)$, PCA-Net takes $\mathcal{E} = L: u \mapsto \{\langle e_j, u \rangle_{\mathcal{X}_1}\}_{j=1}^{d_1}$. Letting $\{\varphi_j\}_{j \in \mathbb{N}}$ be the PCA eigenbasis of $\text{Cov}(\mathsf{F}_\# \mu)$, PCA-Net is defined by

$$\Psi_{\text{PCA}}(u; \theta)(x) = \sum_{j=1}^{d_2} a_j(Lu; \theta) \varphi_j(x) \quad (3.10)$$

for all $u \in \mathcal{X}_1$ and $x \in \Omega_2$. Unlike DeepONet (3.9), which uses neural networks, the basis functions $\{\varphi_j\}$ in (3.10) are fixed by PCA and are parameter-free. Since μ and $\mathsf{F}_\# \mu$ are only accessible through the finite amount of training data $\{(u_n, \mathsf{F}(u_n))\}_{n=1}^N$, the inaccessible true PCA eigenfunctions $\{e_j\}$ and $\{\varphi_j\}$ are replaced by their empirical PCA counterparts in practice.

3.2.2. Neural operators

The encoder-decoder structure from (3.8) can be viewed as a form of dimension reduction. In contrast, *neural operator* architectures do not rely on dimension reduction into finite-dimensional latent spaces. They instead lift information into higher-dimensional latent function spaces. At their core, neural operators $\Psi_{\text{NO}}: \mathcal{X}_1 \rightarrow \mathcal{X}_2$ generalize the compositional feedforward structure of standard deep neural networks to function spaces [147].

To present the main ideas, we specialize to the setting that $\Omega := \Omega_1 = \Omega_2 \subset \mathbb{R}^d$. Let d_c be the so-called *channel dimension*, where we typically take $d_c \geq \max(p_1, p_2)$. Let $\mathcal{H} = \mathcal{H}(\Omega; \mathbb{R}^{d_c})$ be a latent function space. We define

$$\Psi_{\text{NO}}(u) := (\mathcal{Q} \circ \mathcal{L}_T \circ \mathcal{L}_{T-1} \circ \cdots \circ \mathcal{L}_2 \circ \mathcal{L}_1 \circ \mathcal{S})(u) \quad (3.11)$$

for all $u \in \mathcal{X}_1$. The number of hidden layers is denoted by T . The map $\mathcal{S}: \mathcal{X}_1 \rightarrow \mathcal{H}$ is a pointwise-defined local lifting operator given by

$$(\mathcal{S}(u))(x) := S(x, u(x)) \quad (3.12)$$

for some map $S: \mathbb{R}^d \times \mathbb{R}^{p_1} \rightarrow \mathbb{R}^{d_c}$ that is typically affine, but could also be a neural network.

Similarly, $\mathcal{Q}: \mathcal{H} \rightarrow \mathcal{X}_2$ is the pointwise-defined local projection operator

$$(\mathcal{Q}(h))(x) := Q(h(x)) \quad (3.13)$$

for a (typically shallow) neural network $Q: \mathbb{R}^{d_c} \rightarrow \mathbb{R}^{p_2}$. The nonlinearity of Q is crucial to ensure that Ψ_{NO} is a nonlinear method of approximation, which means that its

range $\Psi_{\text{NO}}(\mathcal{X}_1)$ is not a vector space [147]. In contrast, DeepONet and PCA-Net from Section 3.2.1 are linear approximators because their range is the linear span of the basis functions $\{\varphi_j\}_{j=1}^{d_2}$.

For each t , the hidden layers $\mathcal{L}_t: \mathcal{H} \rightarrow \mathcal{H}$ are the nonlinear operators

$$(\mathcal{L}_t(h))(x) = \sigma_t(W_t h(x) + (\mathcal{K}_t h)(x) + b_t(x)) \quad (3.14)$$

for every $h \in \mathcal{H}$ and $x \in \Omega$. In (3.14), $\sigma_t: \mathbb{R} \rightarrow \mathbb{R}$ is a nonlinear activation that acts pointwise on functions; usually σ_T is the identity map while the other activations σ_t for $t < T$ are taken to be the same non-polynomial nonlinearity (e.g., ReLU, GELU, etc). Moreover, $W_t \in \mathbb{R}^{d_c \times d_c}$ is a weight matrix, $b_t: \Omega \rightarrow \mathbb{R}^{d_c}$ is a bias function (usually parametrized as a constant vector), and $\mathcal{K}_t: \mathcal{H} \rightarrow \mathcal{H}$ is a linear kernel integral operator given by

$$(\mathcal{K}_t h)(x) := \int_{\Omega} \kappa_t(x, y) h(y) dy \quad (3.15)$$

for $h \in \mathcal{H}$ and $x \in \Omega$. The particular choice of parametrization of the matrix-valued kernel $\kappa_t: \Omega \times \Omega \rightarrow \mathbb{R}^{d_c \times d_c}$ determines the classification of the neural operator architecture. For example, choosing κ_t to be a neural network localized to patches defines the Graph Kernel Neural Operator, while choosing a low-rank kernel κ_t with learnable factors leads to the Low-Rank Neural Operator [147, Sec. 4]. There are generalizations to nonlinear \mathcal{K}_t in which its integral kernel κ_t depends on the input function h itself [147]. Regardless of the parametrization used, what is important is that \mathcal{K}_t is nonlocal [172].

This chapter emphasizes the use of the *Fourier Neural Operator* (FNO) [24, 189], which corresponds to a neural operator Ψ_{FNO} of the form (3.11) on the unit hypertorus $\Omega = \mathbb{T}^d \simeq [0, 1]_{\text{per}}^d$ with integral operator parametrization

$$(\mathcal{K}_t h)(x) := \left\{ \sum_{k \in \mathbb{Z}^d} \left(\sum_{j=1}^{d_c} (P_t^{(k)})_{\ell j} \langle e^{2\pi i \langle k, \cdot \rangle_{\mathbb{R}^d}}, h_j \rangle_{L^2(\mathbb{T}^d; \mathbb{C})} \right) e^{2\pi i \langle k, x \rangle_{\mathbb{R}^d}} \right\}_{\ell=1}^{d_c}. \quad (3.16)$$

This corresponds to enforcing that the matrix-valued function κ_t in (3.15) is a translation-invariant convolution kernel parametrized directly in Fourier space by its Fourier series coefficients $P_t^{(k)} \in \mathbb{C}^{d_c \times d_c}$ for each $k \in \mathbb{Z}^d$.

A practical discretization of the FNO is usually performed on equally-spaced grids with the Fast Fourier Transform algorithm after truncating the series in (3.16) to a maximum number of resolved Fourier modes [189, 190]. It is also possible to apply the FNO to functions on non-periodic domains [24, 25, 78, 172, 191, 192]. In addition to its vast practical success in scientific applications, theory for the FNO is also beginning to emerge [78, 172, 183, 190, 192].

4. Learning inverse problem solvers

To solve an inverse problem such as (2.1) is to recover the unknown input u from noisy observations $y = \mathcal{G}(u) + \eta$, thereby defining a solution operator $y \mapsto u$. Although traditional inverse solvers can approximate this data-to-parameter map with reasonable accuracy, evaluating $y \mapsto u$ even once can be computationally expensive due to the reliance on iterative or sequential algorithms. Direct solvers that are derived from first principles (e.g., the D-bar method for EIT [52]) can be more efficient, but they often must be handcrafted for each specific nonlinear inverse problem considered [54]. This naturally motivates the use of *operator learning* techniques to learn efficient inverse solvers directly from data.

However, a direct, off-the-shelf application of operator learning to inverse problems encounters several immediate challenges. Beyond the need for a sufficiently rich dataset to support the costly offline training step (3.2), the forward map \mathcal{G} is typically neither invertible nor well-conditioned. As a result, one cannot simply define the target operator to be $\mathbf{F} = \mathcal{G}^{-1}$ without carefully restricting the domain of \mathcal{G} to a sufficiently small set in order for a continuous inverse to be well-defined. Ensuring that the data distribution assigns probability one to such a set is itself a nontrivial challenge. Moreover, the additive noise model (3.1) commonly assumed in forward operator learning is inappropriate for the inverse setting. Here, the roles of input and output must be reversed: the inverse map is trained to recover noise-free ground-truth parameters, while the noisy outputs of the forward map now serve as inputs. This reversal leads to a challenging *errors-in-variables* learning problem [193–195].

Despite these challenges, there is growing theoretical and empirical evidence that estimating the inverse map with operator learning is both statistically principled and practically robust [25, 173, 196–198]. Neural operators can be trained using loss functions that explicitly target desired solution attributes, such as accurate parameter recovery or physical consistency with the forward model. In contrast, plug-in estimators that invert a learned forward map are not goal-oriented and therefore cannot achieve optimal performance; see [196, Eqn. (219), p. 58] for details. Moreover, even when the underlying inverse problem is severely ill-posed, the average-case nature of the training process tends to suppress the impact of worst-case instability: the extreme inputs and outputs responsible for instability are unlikely under realistic data distributions. End-to-end inverse map learning is especially advantageous in scenarios where data is plentiful and the forward or measurement processes are imperfect or only partially known.

A subset of the research on learning inverse solvers distinguishes itself by blending knowledge of the forward operator into the design of algorithms [6–8, 17, 25, 197, 199–201], as advocated by [202]. This could involve correcting errors in the forward model or inverse operator with learned postprocessing maps [26, 49]. Other work develops invertible network architectures that simultaneously learn approximate forward *and* inverse maps while incorporating physics information [9, 10, 203–207]. It is also possible to adopt a distribution-matching approach for the inverse map loss component [208], which lifts similar ideas [100–102, 209] to the operator learning setting.

This section concentrates on pure data-driven approaches for end-to-end operator learning in linear and nonlinear inverse problems. Section 4.1 formulates the problem of learning inverse maps from noisy paired training data. Section 4.2 introduces three neural operator architectures that are tailored to common forms of measurement data that arise in inverse problems. A theoretical analysis develops approximation theory for nonlinear inverse problems and convergence results for linear inverse problems in Section 4.3. A unifying theme of this theory is that of projection onto finite-dimensional spaces. Finally, Section 4.4 goes beyond the current emphasis on point estimation by using measure transport to learn the data dependence of posterior distributions.

4.1. Mathematical formulation

This subsection aims to make the inverse map learning problem more precise. We work under the model (2.1), that is, $y = \mathcal{G}(u) + \eta$. Suppose that $(\mathcal{U}, d_{\mathcal{U}})$ is a metric space of parameters and $(\mathcal{Y}, d_{\mathcal{Y}})$ is a metric space of data. Both spaces are assumed to be infinite-dimensional. We view

$$\mathcal{G}: \text{Dom}(\mathcal{G}) \subseteq \mathcal{U} \rightarrow \mathcal{Y} \quad (4.1)$$

as a mapping from its domain $(\text{Dom}(\mathcal{G}), d_{\mathcal{U}})$ into \mathcal{Y} . The introduction of the set $\text{Dom}(\mathcal{G}) \subseteq \mathcal{U}$ is necessary in many inverse problems because although \mathcal{G} may be well-defined on the whole of the metric space \mathcal{U} , often it is only injective on a smaller set (thus guaranteeing unique solutions of the noiseless inverse problem). This is the case for EIT from Example 1, where even smaller sets are identified such that the restriction of \mathcal{G} to these sets has a uniformly continuous inverse [210]. Thus, this subsection assumes that $\text{Dom}(\mathcal{G})$ is chosen such that the inverse map Ψ^* defined by

$$\begin{aligned} \Psi^*: \text{Dom}(\Psi^*) &\subseteq \mathcal{Y} \rightarrow \mathcal{U} \\ \mathcal{G}(u) &\mapsto u \end{aligned} \quad (4.2)$$

is uniformly continuous on its domain

$$\text{Dom}(\Psi^*) := \mathcal{G}(\text{Dom}(\mathcal{G})). \quad (4.3)$$

We denote the modulus of continuity of Ψ^* by ω^* . In Example 1 on EIT, ω^* is the logarithmic function on the right-hand side of (2.3). From (4.3), we see that $\text{Dom}(\Psi^*)$ equals the range $\text{Ran}(\mathcal{G})$ of the forward map \mathcal{G} in (4.1). For nonlinear inverse problems, identification of $\text{Dom}(\mathcal{G})$ and hence $\text{Dom}(\Psi^*)$ is often a challenging PDE analysis question in its own right.

The goal of end-to-end inverse map learning is to approximate the operator Ψ^* by some $\widehat{\Psi}$ in the sense that $\widehat{\Psi}(\mathcal{G}(u) + \eta) \approx u$ for (u, η) ranging over an appropriate set. An operator learning framework that seeks to achieve this goal is presented in Section 4.1.1. It is important to appreciate that the true inverse map Ψ^* in (4.2) is *only defined* on the range of \mathcal{G} . Section 4.1.2 explores the implications of this fact both in theory and in practice.

4.1.1. Training and evaluating learned inverse maps

We work in the setting of [Section 3.1](#), except here the noise plays a crucial role. The simplest training data generation model for inverse map learning is

$$\{(y_n, u_n)\}_{n=1}^N, \quad \text{where} \quad u_n \stackrel{\text{i.i.d.}}{\sim} \mu \quad \text{and} \quad y_n = \mathcal{G}(u_n) + \eta_n. \quad (4.4)$$

The $\{\eta_n\}$ are i.i.d. copies of a random variable η that models noise or errors. The roles of input and output are reversed from those in [Section 3.1](#). Now the y_n are inputs and the u_n are outputs. Choosing a hypothesis class \mathcal{H} consisting of operators mapping \mathcal{Y} into \mathcal{U} and a loss functional $\ell: \mathcal{U} \times \mathcal{U} \rightarrow \mathbb{R}$, we solve

$$\min_{\Psi \in \mathcal{H}} \frac{1}{N} \sum_{n=1}^N \ell(u_n, \Psi(y_n)) \quad (4.5)$$

to obtain an empirical risk minimizer $\widehat{\Psi}: \mathcal{Y} \rightarrow \mathcal{U}$. Notice that $\widehat{\Psi}$ is defined on all of \mathcal{Y} even though Ψ^* is only defined on $\text{Dom}(\Psi^*) \subseteq \mathcal{Y}$ (4.3). The hypothesis space \mathcal{H} could encompass the operator learning architectures from [Section 3.2](#), but also those neural operators tailored to inverse problems that will be introduced in [Section 4.2](#).

Similarly, the same losses ℓ from [Section 3.1](#) are valid here. However, there is considerably more freedom to choose ℓ in the present inverse problem setting. For example, one could choose an ℓ with dependence on the forward map \mathcal{G} to promote desirable problem-adapted structure in the estimator $\widehat{\Psi}$. Moreover, when reconstructing solutions to inverse problems that are discontinuous, such as piecewise constant conductivity fields in EIT or permeability fields in groundwater flow [25, 211, 212], it is beneficial to train in a metric on \mathcal{U} that penalizes sharp transitions less harshly. For instance, the TV norm and its variants are natural candidates, following on its successful introduction in the mathematical imaging community [213, 214]. Within the class of Lebesgue spaces L^p —whose norms are more efficient to compute in a deep learning training loop than TV norms—the L^1 distance is best adapted to discontinuous parameter fields [159, 166, 211, 212]. In analogy with the popular relative L^2 loss functions used in forward operator learning, this would involve choosing $X = L^1$ in (3.3).

A large amount of freedom also exists when choosing how to evaluate the performance of $\widehat{\Psi}$ as a learned inverse solver. In view of the ERM problem (4.5), the expected risk

$$\mathbb{E}_{(u,y)}[\ell(u, \widehat{\Psi}(y))] := \mathbb{E}_{(u,\eta)}[\ell(u, \widehat{\Psi}(\mathcal{G}(u) + \eta))] \quad (4.6)$$

is a natural notion of accuracy. However, we cannot expect (4.6) to be small unless the noise η is small in an appropriate sense. Other choices include the noise-free parameter reconstruction loss

$$\mathbb{E}_{u \sim \mu}[\ell(u, \widehat{\Psi}(\mathcal{G}(u)))] \quad (4.7)$$

or the data fitting losses

$$\mathbb{E}_y[\mathbf{d}_{\mathcal{Y}}(y, \mathcal{G}(\widehat{\Psi}(y)))] \quad \text{or} \quad \mathbb{E}_{(u,y)}[\mathbf{d}_{\mathcal{Y}}(\mathcal{G}(u), \mathcal{G}(\widehat{\Psi}(y)))] , \quad (4.8)$$

and variants thereof.

4.1.2. Noisy data and the range of the forward map

We have emphasized that the true inverse map Ψ^* from (4.2) is only defined on its domain $\text{Dom}(\Psi^*) = \text{Ran}(\mathcal{G})$. However, estimators of the inverse map, such as the empirical risk minimizer $\widehat{\Psi}$ of (4.5), must be defined on a larger set in order to handle perturbed measurement data as input. Indeed, we have that $\mathcal{G}(u) \in \text{Ran}(\mathcal{G})$, but in general $(\mathcal{G}(u) + \eta) \notin \text{Ran}(\mathcal{G})$. This challenge is not present in traditional forward operator learning. It is thus important to determine the actual operator that $\widehat{\Psi}$ is really trying to approximate.

Conceptually, an ideal approximation Ψ of Ψ^* would take the form $\Psi := \Psi^* \circ P_{\mathcal{G}}$, where $P_{\mathcal{G}}: \mathcal{Y} \rightarrow \text{Ran}(\mathcal{G})$ is some notion of projection onto $\text{Ran}(\mathcal{G})$. In this way, $\Psi: \mathcal{Y} \rightarrow \mathcal{U}$ extends Ψ^* : $\Psi(y) = \Psi^*(y)$ if $y \in \text{Ran}(\mathcal{G})$. If $y \notin \text{Ran}(\mathcal{G})$, then $P_{\mathcal{G}}(y)$ is a “denoised” version of y in a sense. However, it is practically problematic to construct $P_{\mathcal{G}}$ because for many infinite-dimensional nonlinear inverse problems, $\text{Ran}(\mathcal{G})$ is typically a complicated nonconvex set that is difficult to characterize [58]. Nonetheless, it is intuitively possible that by minimizing the end-to-end ERM training objective (4.5), $\widehat{\Psi}$ is *implicitly* approximating the extension Ψ even though Ψ is not accessible. An interesting research direction is to learn neural operators that *explicitly* project onto $\text{Ran}(\mathcal{G})$ by training on enough data from the range.

The intuition from the preceding thought experiment is instructive. Learned inverse maps $\widehat{\Psi}$ should approximate an *extension* $\widetilde{\Psi}^*$ of the true inverse Ψ^* . Figure 4 illustrates this idea. While we cannot expect the extension to exactly project onto the range of the forward map \mathcal{G} , we can hope that the extension inherits the stability of the true inverse map. Few works deliberately address these issues; the papers [196, 198, 211, 215] are exceptions. There are two main analysis strategies in this line of work. The first demands quantitative stability of the trained neural operator [198]. The second strategy puts the onus of stability only on the extended inverse map [211, 215].

Consider the setting of Fig. 4. Let $\widetilde{\Psi}^*: \mathcal{Y} \rightarrow \mathcal{U}$ extend Ψ^* . Suppose that $\widehat{\Psi}: \mathcal{Y} \rightarrow \mathcal{U}$ has modulus of continuity $\widehat{\omega}$. For a fixed $u \in \text{Dom}(\mathcal{G})$, we define $y := \mathcal{G}(u) \in \text{Dom}(\Psi^*)$ and $y^\delta = y + \eta$ with $\mathbf{d}_{\mathcal{Y}}(y^\delta, y) \leq \delta$. To control the approximation error of $\widehat{\Psi}$, the first analysis strategy rests on the following application of the triangle inequality:

$$\begin{aligned} \mathbf{d}_{\mathcal{U}}(\Psi^*(y), \widehat{\Psi}(y^\delta)) &\leq \mathbf{d}_{\mathcal{U}}(\Psi^*(y), \widehat{\Psi}(y)) + \mathbf{d}_{\mathcal{U}}(\widehat{\Psi}(y), \widehat{\Psi}(y^\delta)) \\ &\leq \sup_{v \in \text{Dom}(\Psi^*)} \mathbf{d}_{\mathcal{U}}(\widetilde{\Psi}^*(v), \widehat{\Psi}(v)) + \widehat{\omega}(\delta) . \end{aligned} \quad (4.9)$$

The first term in the upper bound (4.9) is controlled by how well $\widehat{\Psi}$ approximates $\widetilde{\Psi}^*$. The second error term is the modulus of continuity of the learned inverse map evaluated at the maximal noise level; this term tends to zero as $\delta \rightarrow 0$. While it is a hard

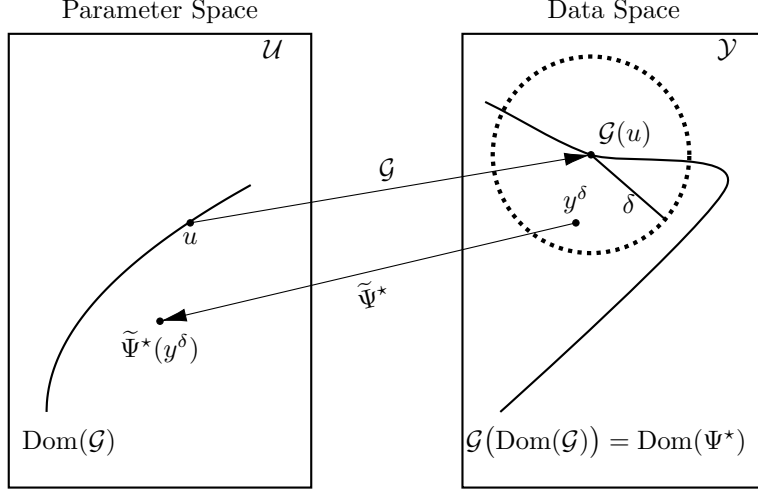


Fig. 4: Noisy data y^δ lives outside of the domain $\text{Dom}(\Psi^*)$ of the true inverse map $\Psi^* : \text{Dom}(\Psi^*) \rightarrow \mathcal{U}$. In the illustration, the distance between y^δ and $\text{Dom}(\Psi^*)$ is less than δ . A continuous extension $\tilde{\Psi}^* : \mathcal{Y} \rightarrow \mathcal{U}$ of Ψ^* is well-defined on noisy data y^δ . As $\delta \rightarrow 0$, it holds that $\tilde{\Psi}^*(y^\delta) \rightarrow \Psi^*(\mathcal{G}(u)) = u$ with a certain convergence rate. Learned inverse maps $\hat{\Psi} : \mathcal{Y} \rightarrow \mathcal{U}$ conceptually aim to approximate the extension $\tilde{\Psi}^*$.

problem to quantitatively control Lipschitz or other uniform continuity properties of trained neural networks and neural operators, there do exist specialized architectures that attempt this program [198, 216].

In contrast, the second analysis strategy demands that the extension $\tilde{\Psi}^*$ have a modulus of continuity $\tilde{\omega}^*$. Typically $\tilde{\omega}^*$ bounds ω^* from above. An alterative use of the triangle inequality delivers the bound

$$\begin{aligned} d_{\mathcal{U}}(\Psi^*(y), \hat{\Psi}(y^\delta)) &\leq d_{\mathcal{U}}(\tilde{\Psi}^*(y), \tilde{\Psi}^*(y^\delta)) + d_{\mathcal{U}}(\tilde{\Psi}^*(y^\delta), \hat{\Psi}(y^\delta)) \\ &\leq \tilde{\omega}^*(\delta) + \sup_{y' \in K_\delta} d_{\mathcal{U}}(\tilde{\Psi}^*(y'), \hat{\Psi}(y')) , \end{aligned} \quad (4.10)$$

where K_δ is a set of perturbed data with distance at most δ away from $\text{Dom}(\Psi^*)$. The advantage of this approach is that the stability of the learned map $\hat{\Psi}$ is never needed. However, finer properties of the extension are required [211].

One way to decouple the role of regularization from inverse map training is to build regularization into the training data itself [217]. This method trains approximate inverse maps on data consisting of regularized inverse problem solutions. These data are obtained from classical inverse solvers, e.g., Tikhonov or Bayesian regularization. The insight is that training on pre-regularized data corresponds to learning a regularized inverse map instead of Ψ^* [197, 217]. While this addresses the noisy data problem, the target regularized inverse no longer exactly solves the inverse problem on the range of \mathcal{G} . That is, it does not extend the true inverse. This reflects a tradeoff

between accuracy and regularization in the operator learning setting. Similar considerations arise when choosing to define the inverse map outside of its domain as a point estimator of a Bayesian posterior, such as the posterior mean [218].

The need to work with extensions does not arise in forward operator learning. Moreover, traditional inverse solvers handle data outside of the range of \mathcal{G} by explicitly prescribing regularization. In contrast, the minimization of (4.5) implicitly encodes regularization [129]. This regularization mechanism of learned inverse solvers is not well understood. Therefore, analyzing and interpreting the properties of regularization in end-to-end learned inverse maps is a vital direction for future research.

4.2. Architectures for data-to-parameter maps

The choice of machine learning architecture for end-to-end learning of inverse maps depends on the parameter space \mathcal{U} and data space \mathcal{Y} . If \mathcal{U} and \mathcal{Y} are both function spaces, then standard operator learning architectures such as FNO or DeepONet from Section 3.2 are appropriate. However, if the data-to-parameter solution operator of the inverse problem maps between more exotic spaces, then additional innovation is required. For simplicity, the current subsection assumes that the parameter of interest is a function belonging to $\mathcal{U} = \mathcal{U}(\Omega; \mathbb{R}^{d_p})$. Depending on the inverse problem, the observed data could be represented as a finite vector, a function, a functional, a (linear) operator, or even a probability measure. This subsection explores discretization-invariant architectures for vector-to-function maps in Section 4.2.1, operator-to-function maps in Section 4.2.2, and distribution-to-function maps in Section 4.2.3.

4.2.1. Fourier Neural Mappings

Although they might be modeled at a continuum level, finite-dimensional data $y \in \mathbb{R}^J$ for some $J \in \mathbb{N}$ are the actual quantities that are acquired by measurement devices in real applications. Thus, to approximate inverse maps $\Psi^*: \text{Dom}(\Psi^*) \subseteq \mathbb{R}^J \rightarrow \mathcal{U}(\Omega; \mathbb{R}^{d_p})$, we require architectures that map finite vectors to functions. In principle, any encoder–decoder model (3.8) can be turned into a vector-to-function (VtF) map by removing the encoder. This results in $\Psi = \mathcal{D} \circ \mathcal{A}: \mathbb{R}^J \rightarrow \mathcal{U}$ for the DeepONet (3.9) and PCA-Net (3.10) upon choosing the approximator \mathcal{A} to have input dimension J . Any other autoencoder method that uses a functional decoder \mathcal{D} also fits into this framework [180].

To produce VtF neural operators, one can append a functional decoder \mathcal{D} near the beginning of the iteration (3.11) from Section 3.2.2. This is the idea adopted by the Neural Mappings framework [78], which uses functional decoders \mathcal{D} of the form

$$(\mathcal{D}z)(x) := \kappa(x)z \quad (4.11)$$

for each input vector $z \in \mathbb{R}^{d_c}$ and point $x \in \Omega$ in the domain. In (4.11), $\kappa: \Omega \rightarrow \mathbb{R}^{d_c \times d_c}$ is a learnable matrix-valued function. Thus, $\mathcal{D}z: \Omega \rightarrow \mathbb{R}^{d_c}$ is a vector-valued function. In particular, Fourier Neural Mappings (FNMs) generalize FNOs—which only map functions to functions—by accommodating VtF or function-to-vector maps. In the

former case, these *Fourier Neural Decoders* parametrize the function κ in Fourier space by its conjugate symmetric Fourier coefficients $\{P^{(k)}\}_{k \in \mathbb{Z}^d} \subseteq \mathbb{C}^{d_c \times d_c}$. Letting $\Omega = \mathbb{T}^d$, this leads to the decoder

$$(\mathcal{D}z)(x) = \kappa(x)z = \sum_{k \in \mathbb{Z}^d} (P^{(k)}z) e^{2\pi i \langle k, x \rangle_{\mathbb{R}^d}} \quad (4.12)$$

for $z \in \mathbb{R}^{d_c}$ and $x \in \mathbb{T}^d$. Then the full VtF FNM $\Psi_{\text{FNM}}: \mathbb{R}^J \rightarrow \mathcal{U}$ is defined by

$$\Psi_{\text{FNM}}(z) := (\mathcal{Q} \circ \mathcal{L}_T \circ \mathcal{L}_{T-1} \circ \dots \circ \mathcal{L}_2 \circ \mathcal{D} \circ S)(z), \quad (4.13)$$

where \mathcal{D} is given in (4.12) and $S: \mathbb{R}^J \rightarrow \mathbb{R}^{d_c}$ is a shallow neural network; compare to (3.11), which uses \mathcal{L}_1 instead of \mathcal{D} and \mathcal{S} instead of S . The $\{\mathcal{L}_t\}$ are the usual Fourier integral operator layers as in (3.14) and (3.16). The map \mathcal{Q} is as in (3.13). FNMs retain the computational benefits and universal approximation properties of FNOs [78, Sec. 3].

If the measurements in the inverse problem are comprised of both functions and finite vectors, then the extension of FNMs introduced in [219] can be used to handle such multimodal data. The function-to-vector ideas from FNMs [78] are also useful when the dimension of the input and output spatial domains do not match, such as in inverse boundary value problems (IBVPs) [211]. Finally, we note that if J is allowed to vary, it could be more natural to model the inverse operator as a function-to-function map (Section 3.2), operator-to-function map (Section 4.2.2), or measure-to-function map (Section 4.2.3), depending on the nature of the limiting object as $J \rightarrow \infty$. This removes the need to re-train the model every time J changes, which would be the case for VtF architectures.

4.2.2. Operator Recurrent Neural Networks

Operator-to-function maps

$$\begin{aligned} \Psi^*: \text{Dom}(\Psi^*) \subseteq \mathcal{L}(\mathcal{X}; \mathcal{W}) &\rightarrow \mathcal{U}(\Omega; \mathbb{R}^{d_p}) \\ \Lambda &\mapsto \Psi^*(\Lambda) \end{aligned} \quad (4.14)$$

frequently arise as solution operators of IBVPs. Typically \mathcal{X} and \mathcal{W} are spaces of functions on the boundary $\partial\Omega$. The continuous linear operator $\Lambda \in \mathcal{L}(\mathcal{X}; \mathcal{W})$ is usually a mathematically idealized representation of all possible measurements that one can perform at the boundary. Several concrete IBVPs can be formulated as in (4.14), including EIT from Example 1, inverse wave scattering based on the Helmholtz equation, optical tomography based on the radiative transport equation, and seismic imaging based on the acoustic wave equation [212].

In practice, each single evaluation of the forward map $u \mapsto \Lambda_u$ requires tens, hundreds, or even thousands of PDE solves to probe the boundary and acquire measurements that lead to a discrete representation of $\Lambda = \Lambda_u$. Thus, repeated calls to the forward map can become prohibitively expensive, especially if wrapped around an

outer objective. An accurate learned inverse map can substantially reduce the time-to-solution when compared to PDE-constrained, optimization-based, iterative IVBP solvers. At the continuum level, it remains to define operator-to-function architectures.

If linear map Λ has a kernel integral operator representation, then viewing its kernel function as input data we return to the familiar function-to-function setting of Section 3.2; see [48, 211], where this approach is taken. A more novel deep learning architecture for representing nonlinear operator functions such as (4.14) is the *Operator Recurrent Neural Network* (ORN-Net) [196]. This architecture—and existing analysis for it—is currently restricted to a finite-dimensional discretized setting. However, it is straightforward to formally extend the idea of operator recurrence to function spaces by, e.g., following the principles outlined in [220]. We do so in the following description of the architecture.

To this end, we define $\Psi_{\text{ORN}}: \mathcal{L}(\mathcal{X}; \mathcal{W}) \rightarrow \mathcal{U}$, which is a neural operator version of ORN-Net, by

$$\Psi_{\text{ORN}}(\Lambda) := (\mathcal{Q} \circ \mathcal{L}_T(\cdot; \Lambda) \circ \mathcal{L}_{T-1}(\cdot; \Lambda) \circ \cdots \circ \mathcal{L}_1(\cdot; \Lambda) \circ \mathcal{S})(h_0). \quad (4.15)$$

Notice that because Ψ_{ORN} maps a linear operator to a function, the input linear operator $\Lambda \in \mathcal{L}(\mathcal{X}; \mathcal{W})$ does not appear as input to the first map \mathcal{S} in the chain of compositions (4.15), but instead *parametrizes* the function-to-function operators $\mathcal{L}_t(\cdot; \Lambda): \mathcal{H} \rightarrow \mathcal{H}$ acting on the hidden states. We used the notation $\mathcal{H} = \mathcal{H}(\Omega; \mathbb{R}^{d_c})$ from Section 3.2.2. The function h_0 is an initial hidden state function that serves as a tunable parameter of the architecture and does not depend on the input operator Λ . As usual, \mathcal{S} and \mathcal{Q} are pointwise lifting (3.12) and projection layers (3.13), respectively.

The key innovation of ORN-Net is the parametrization of the hidden layer operators $\mathcal{L}_t: \mathcal{H} \times \mathcal{L}(\mathcal{X}; \mathcal{W}) \rightarrow \mathcal{H}$. These are given by

$$\begin{aligned} \mathcal{L}_t(h; \Lambda) &:= u_t^{(0)} + \sigma_t(u_t^{(1)}), \quad \text{where} \\ u_t^{(j)}(x) &:= (\mathcal{K}_t^{(j)} \Lambda h)(x) + (\tilde{\mathcal{K}}_t^{(j)} h)(x) + W_t^{(j)} h(x) + b_t^{(j)}(x) \end{aligned} \quad (4.16)$$

for each $j \in \{0, 1\}$ and every h , Λ , t , and x . The $\{\mathcal{K}_t^{(j)}\}$ and $\{\tilde{\mathcal{K}}_t^{(j)}\}$ are nonlocal linear kernel integral operators of the form (3.15) or (3.16). Notice how Λ is introduced in the previous display via *operator composition*, i.e., matrix multiplication. If the activation functions $\{\sigma_t\}$ are set to the identity, then a deep ORN-Net computes operator polynomials and starts to resemble a truncated Neumann series expansion [196, Sec. 6]. Thus, the nonlinear version with non-polynomial activation functions generalizes the network's representation capacity to more complex operator functions.

Extensions to the core architecture include adding memory to the layers instead of settling for the Markovian evolution (4.15); see [196, Sec. 2.2–2.3]. The architecture design is further motivated by specific inverse problem structure such as the compositional or iterative nature of the ground truth inverse problem solution map. This leads to inductive biases that promote compactness, sparsity, and low-rankness in the model, which in turn lead to improved statistical generalization bounds. We refer to [196, Sec. 2–3, 7] for the details and an application to boundary control of the wave equation. We note that both the quantitative universal approximation and statistical

learning theory for ORN-Net [196] only handles target functions mapping $\mathbb{R}^{n \times n}$ to \mathbb{R}^m and does not carry over immediately to the infinite-dimensional case. This is an important avenue for future mathematical research. Numerical implementation of ORN-Nets in both finite- and infinite-dimensional settings is also an important future direction to determine the practical benefits of the architecture's multiplicative structure.

In practice, our access to the boundary data map Λ may only be through a finite collection of input-output pairs $\{(g_m, \Lambda g_m)\}_{m=1}^{M(\Lambda)}$ obtained by $M = M(\Lambda) \in \mathbb{N}$ operator-function products with some functions $\{g_m\}$. One could then perform a preprocessing step to obtain an integral kernel or matrix representation of Λ from the paired boundary data, e.g., via linear regression. Alternatively, one can adopt a measure-centric perspective to avoid the preprocessing step by viewing the paired data $\{(g_m, \Lambda g_m)\}_{m=1}^{M(\Lambda)}$ as a single empirical probability measure (Section 2.1.4). This is the subject of the next subsection.

4.2.3. Neural Inverse Operator

Inspired again by IBVPs in which a finite but varying number of function-valued boundary measurements serve as the observed data, we adopt the measure-centric perspective on inverse map learning from Section 2.1.4. In particular, we describe a general architecture called the *Neural Inverse Operator* (NIO) that is able to approximate measure-to-function maps in a discretization-invariant way [212]. We then instate the abstract NIO framework in the concrete IBVP of EIT from Example 1.

By now, there are several deep learning methods that can represent probability measure-to-vector operators of the form $\Psi: \mathcal{P}(\mathbb{R}^{d_1}) \rightarrow \mathbb{R}^{d_2}$. The attention mechanism in modern transformer architectures is known to define a mean-field transport map whose dependence on the underlying input measure leads to such a Ψ [92, 94, 95, 174]. Of more direct relevance to this subsection are the simpler and more computationally efficient DeepSet [221] and PointNet [97, 222] models. These architectures are originally formulated as acting on point clouds in \mathbb{R}^{d_1} . The basic idea is to encode the point clouds into a latent space \mathbb{R}^{d_c} by first pushing forward the points with a single neural network, followed by the application of a permutation-invariant aggregation or pooling operation, such as summation [221] or the entrywise maximum [97]. Another neural network is used to post-process the latent state into \mathbb{R}^{d_2} . For DeepSets, this gives

$$\Psi_{\text{DS}}(\mu) := \Psi^{(2)} \left(\int_{\mathbb{R}^{d_1}} \Psi^{(1)}(x) \mu(dx) \right), \quad (4.17)$$

where $\Psi^{(1)}: \mathbb{R}^{d_1} \rightarrow \mathbb{R}^{d_c}$ and $\Psi^{(2)}: \mathbb{R}^{d_c} \rightarrow \mathbb{R}^{d_2}$ are neural networks. In particular, (4.17) is valid for genuine probability measures $\mu \in \mathcal{P}(\mathbb{R}^{d_1})$ instead of just point clouds or, equivalently, empirical measures.

We now generalize DeepSets from finite to infinite dimensions. Let X be an abstract metric or Banach space and $\mu \in \mathcal{P}(X)$ be a probability measure over X . Consider our usual output function space $\mathcal{U} = \mathcal{U}(\Omega; \mathbb{R}^{d_p})$. In IBVPs, X is typically a space of functions defined on the boundary $\partial\Omega$. Let \mathcal{H} be a latent space. Choosing operators $\Psi^{(1)}: X \rightarrow \mathcal{H}$ and $\Psi^{(2)}: \mathcal{H} \rightarrow \mathcal{U}$ leads to an operator $\Psi: \mathcal{P}(X) \rightarrow \mathcal{U}$ of the form

(4.17). An abstract NIO [212] makes the more constrained choice

$$\Psi_{\text{NIO}}(\mu) := \Psi_{\text{FNO}}\left(\int_X \Psi_{\text{DON}}(f)\mu(df)\right), \quad (4.18)$$

where $\mathcal{H} := \mathcal{U}$, $\Psi^{(1)} := \Psi_{\text{DON}}: X \rightarrow \mathcal{U}$ is a DeepONet (3.9), and $\Psi^{(2)} := \Psi_{\text{FNO}}: \mathcal{U} \rightarrow \mathcal{U}$ is an FNO (3.11). The integral in (4.18) is a \mathcal{U} -valued Bochner integral that can equivalently be written as the expectation under μ .

Recent work has also proposed measure-to-function architectures by combining standard DeepSets with DeepONets [187, 223]. However, the NIO differs from these models because the input measures considered in [187, 223] are supported on finite-dimensional spaces. In contrast, the NIO (4.18) is the first operator learning architecture that accepts probability measures *supported on functions spaces* as input. Handling two levels of infinite-dimensionality, the first from X and the second from $\mathcal{P}(X)$, is a notable achievement. In principle, the transformer architecture could also be lifted to infinite-dimensional state spaces and used to solve IBVPs for PDEs, but so far it has been restricted to finite dimensions due to the quadratic complexity of the attention mechanism. Regardless, all such architectures lack strong theoretical guarantees aside from some universal approximation results.

For IBVPs like EIT, we only observe $M = M(\gamma)$ pairs (2.15) of Neumann and Dirichlet boundary values for each conductivity γ . The order of the pairs does not influence what the conductivity is; thus, the inverse map from the pairs to the conductivity is *permutation-invariant*. Modern techniques generalize this permutation-invariance by viewing such mappings as defined on the space of probability measures (Section 2.1.4). The practical discrete setting, where the data is an empirical measure centered at the pairs of Neumann and Dirichlet data, then becomes a special case of this more general framework.

When applied to IBVPs, the NIO (4.18) is called *A Measure-theoretic Inverse Neural Operator* (AMINO) [166]. The input to this architecture is a distribution over the joint space $\mathcal{X} \times \mathcal{W}$ of paired boundary samples, where $\mathcal{X} = \mathcal{X}(\partial\Omega)$ and $\mathcal{W} = \mathcal{W}(\partial\Omega)$ are boundary function spaces as in (4.14). Instead of working with operator-function products as in Section 4.2.2, AMINO processes paired samples from the input measure in a permutation-invariant manner. This results in one-shot inversion directly from the raw data. In contrast, ORN-Net (4.15) requires a pre-processing step to obtain the boundary operator Λ first.

Instate the EIT setting of Example 1. Then Λ is the NtD map Λ_γ . For a distribution $\rho \in \mathcal{P}(\mathcal{X})$ over Neumann boundary conditions, define a forward map

$$\begin{aligned} \mathsf{F}_\rho: \text{Dom}(\mathsf{F}_\rho) \subseteq \mathcal{U} &\rightarrow \mathcal{P}(\mathcal{X} \times \mathcal{W}) \\ \gamma &\mapsto (\text{Id}, \Lambda_\gamma)_\# \rho. \end{aligned} \quad (4.19)$$

Future work should aim to characterize the distributions ρ for which F_ρ is injective. We nevertheless proceed by formally defining an inverse map $\Psi^*: \mathsf{F}_\rho(\gamma) \mapsto \gamma$ for measure-centric EIT. AMINO approximates Ψ^* via the map $\Psi_{\text{AMINO}}: \mathcal{P}(\mathcal{X} \times \mathcal{W}) \rightarrow \mathcal{U}$ defined

by $\nu \mapsto \Psi_{\text{AMINO}}(\nu) := \Psi_{\text{NIO}}(\nu)$ as in (4.18). Thus, on $\text{Ran}(\mathsf{F}_\rho)$, we have

$$\Psi_{\text{AMINO}}(\mathsf{F}_\rho(\gamma)) = \Psi_{\text{FNO}}\left(\int_X \Psi_{\text{DON}}((g, \Lambda_\gamma g)) \rho(dg)\right). \quad (4.20)$$

Now consider a new realization of the finite collection $\{(g_m, y_m)\}_{m=1}^M$ of noisy input pairs. The $\{g_m\}$ are Neumann boundary values sampled from ρ . The $\{y_m\}$ are noisy Dirichlet boundary values as in (2.15). By identifying these data with the empirical measure on the left-hand side of (2.16), the action of AMINO on the empirical measure is

$$\Psi_{\text{AMINO}}\left(\frac{1}{M} \sum_{m=1}^M \delta_{(g_m, y_m)}\right) = \Psi_{\text{FNO}}\left(\frac{1}{M} \sum_{m=1}^M \Psi_{\text{DON}}((g_m, y_m))\right). \quad (4.21)$$

In particular, the trainable parameters of the FNO Ψ_{FNO} and DeepONet Ψ_{DNO} in (4.21) are *independent* of the number of atoms $M = M(\gamma)$, which may be viewed as a resolution hyperparameter in this measure-centric setting. During practical training of NIO and AMINO using ERM (4.5), additional ideas are used to improve computational cost and generalization accuracy by exploiting the atomic-invariance of the architecture. For example, one can subsample atoms uniformly at random from every input empirical measure in each minibatch of SGD. One can also evaluate the trained AMINO on new point clouds with any number of atoms. These features highlight the power of operator learning for IVPs.

4.3. Theoretical results

The theoretical analysis of end-to-end operator learning for approximating inverse problem solution maps remains a relatively new field. Although there are scattered results for specific nonlinear inverse problems, even the theory for linear inverse problems is far from complete. A key challenge lies in the fact that input data may not necessarily belong to the domain of the inverse map being studied (see Section 4.1.2). How to reconcile this issue with the training and optimization procedures used in learning remains an open question.

While new neural operator architectures tailored to the data structures arising in inverse problems have been developed (see Section 4.2), we currently lack a deep understanding of their theoretical properties. Moreover, end-to-end learning remains without a systematic regularization strategy to mitigate the inherent instability of the target inverse map. Current approaches have primarily relied on techniques such as dimension reduction [198, 205, 224, 225], implicit regularization through architecture design or optimizer-induced biases [196, 226], and training on pre-regularized solutions generated by traditional inverse solvers [217]. However, these strategies require further mathematical analysis to rigorously demonstrate their advantages, limitations, and tradeoffs.

This subsection examines theoretical results concerning the approximation of solution operators for inverse problems, highlighting this emerging but critical direction

of research. In Section 4.3.1, we explore the existence of neural operator approximations in the context of EIT from Example 1. Although the results are not necessarily constructive, they demonstrate that the specified architectures are well-suited for approximating inverse maps arising in IBVPs such as EIT. Notably, these existence results are general. They hold regardless of data availability or the specific choice of training procedure (e.g., physics-informed losses versus purely data-driven losses). This universality illustrates the flexibility of the theoretical framework. It is compatible with both current and future statistical analyses of different estimators and learning algorithms, as long as the hypothesis space is fixed.

In Section 4.3.2, we shift from EIT to a general deep learning framework for nonlinear inverse problems. This framework builds on the result that, even when the forward operator is infinite-dimensional and nonlinear, and the data are corrupted by noise, it is possible to restrict the forward operator to finite-dimensional subspaces in such a way that the inverse operator becomes Lipschitz continuous. Moreover, there exist neural networks that robustly approximate this projected inverse map in the presence of noise and can be effectively learned using suitably perturbed training data.

Finally, Section 4.3.3 investigates linear inverse problems in Hilbert spaces. It presents a data-driven regularization-by-projection framework that guarantees convergence of estimated solutions even when the forward operator is unknown or potentially ill-posed. This approach combines input-output training pairs with functional-analytic regularization techniques. By focusing on linear inverse problems, the framework goes beyond existence theorems by demonstrating convergence of estimators in the limit of infinite training data for both noise-free and noisy observations.

4.3.1. Neural operator approximation theory: A case study on EIT

We revisit the setting of Calderón’s problem, i.e., EIT, from Example 1. The goal is to recover the conductivity γ from knowledge of the NtD map Λ_γ , subject to the PDE (2.2). The extensive mathematical foundation underlying EIT makes it a natural testbed for developing and studying theoretical approximation results in the field of data-driven inverse problems. It is important to note, however, that existing statistical analysis of EIT solvers has largely been limited to the Bayesian framework, which assumes a fixed realization of observed boundary data [74]. Under this framework, computationally intensive Bayesian reconstructions must be re-computed for each new realization of observed data.

In contrast, the literature on approximation theory for EIT is significantly more developed [211, 215, 227]. The central theoretical approach consists of three main steps. First, one shows that the Calderón inversion operator maps between subsets of separable Hilbert spaces. This step often involves establishing fine-grained stability estimates for the inverse problem and applying results from PDE theory. Second, one extends the domain of the inverse map to the entire data space, while ideally preserving regularity properties. Third, one characterizes the compactness of the admissible sets of conductivities in suitable function spaces or their inclusion within the support of an appropriate probability measure. These three steps together enable the application of universal approximation theorems for neural operators. In the following, we provide

a more detailed discussion of the main results and insights arising from this line of research.

The papers [211, 215, 227] all formulate the inverse map Ψ^* of EIT as a mapping between two separable Hilbert spaces. This arises in [215, 227] due to a reliance on encoder-decoder architectures (3.8) that require use of Hilbert space concepts such as projection and expansion in orthogonal bases. However, the reformulation in Hilbert spaces involves significant effort because Ψ^* naturally maps a Banach space of continuous linear operators into $L^\infty(\Omega)$, neither of which are Hilbert spaces.

To elaborate further, [227] develops a generalization of DeepONets from function-to-function mappings to more general operators between separable Hilbert spaces \mathcal{H}_1 and \mathcal{H}_2 . This abstraction corresponds to PCA-Net (3.10), except with trunk functions $\{\varphi_j\}$ replaced by arbitrary vectors in the output separable Hilbert space \mathcal{H}_2 . The paper [227] constrains the architecture even more by enforcing that the encoder L , as defined in (3.10), projects onto an orthonormal basis (ONB) of the input Hilbert space \mathcal{H}_1 and that the trunk functions $\{\varphi_j\}$ form an ONB of the output Hilbert space \mathcal{H}_2 . With this structure, the approach can accommodate Hilbert–Schmidt operators as inputs or outputs while maintaining compatibility with the Hilbertian framework.

We slightly deviate from [Example 1](#) by working with Dirichlet-to-Neumann (DtN) maps as input data instead of NtD maps. This choice only affects the exponents of the boundary Sobolev spaces involved and leaves the central methodology unchanged. Define $\mathcal{H}_2 = L^2(\Omega)$ and $\mathcal{H}_1 = L^2_\mu(H^{1/2}(\partial\Omega); H^{-1/2}(\partial\Omega))$, where $\mu \in \mathcal{P}(H^{1/2}(\partial\Omega))$ is a probability measure. That is, the linear DtN maps, which belong to the Banach space $\mathcal{L}(H^{1/2}(\partial\Omega); H^{-1/2}(\partial\Omega))$ of continuous linear operators, are embedded into the larger Bochner Hilbert space \mathcal{H}_1 . We assume that \mathcal{H}_1 is separable. It is a large space and even contains nonlinear discontinuous maps.

Based on results for the encoder-decoder framework [178, 228], an approximation theorem for the inverse map Ψ^* , viewed as a mapping from a subset of \mathcal{H}_1 into \mathcal{H}_2 , holds [227, Thm. 4.4, p. 786]. This theorem asserts that for every $\varepsilon > 0$, there exists a generalized DeepONet $\Psi: \mathcal{H}_1 \rightarrow \mathcal{H}_2$ such that

$$\int_{\mathcal{H}_1} \mathbb{1}_{\text{Dom}(\Psi^*)}(\Lambda) \|\Psi^*(\Lambda) - \Psi(\Lambda)\|_{L^2(\Omega)}^2 \mathbb{Q}(d\Lambda) \leq \varepsilon^2. \quad (4.22)$$

Here $\mathbb{1}_A$ denotes the indicator function of the set A . The domain $\text{Dom}(\Psi^*)$ consists of DtN maps corresponding to sufficiently regular conductivities that are uniformly bounded above and below. The error is measured on average with respect to a probability measure \mathbb{Q} over the large Bochner space \mathcal{H}_1 . The result in (4.22) relies on a simple, discontinuous zero-extension of the inverse map Ψ^* outside its domain of definition (recall [Section 4.1.2](#)). The generalized DeepONet Ψ is then shown to approximate this extended inverse map. The proof only relies on the fact that Ψ^* is a measurable mapping between two separable Hilbert spaces, which simplifies the required analysis.

However, there remains an inherent modeling challenge in defining a probability measure supported on the range of the forward map. This range is a highly intricate set that is neither easily parametrized nor straightforwardly related to a distribution over conductivities. Furthermore, the current approach offers no mechanisms to control the approximation when faced with noisy input data. This limitation is somewhat

artificial because the map Ψ^* is uniformly continuous on its domain. Incorporating such finer-grained continuity information could improve the treatment of data outside of the range of the forward map $\gamma \mapsto \Lambda_\gamma$.

To this end, we turn our attention to a quantitative extension approach that does use detailed stability information about the inverse map [211]. To simplify the presentation, we restrict to a setting in which $d = 2$ and $\Omega \subset \mathbb{R}^2$ is the open unit disk. Thus, we identify the boundary $\partial\Omega$ with the unit torus \mathbb{T} . This aligns with Fig. 2 from Example 1. Next, we consider an infinite-dimensional set $\Gamma \subset L^\infty(\Omega)$ of conductivities identically equal to one outside of a compact subset of Ω , uniformly bounded above and below pointwise a.e., and that have uniformly bounded $L^1(\Omega)$ and TV norms. This set is compact in $L^2(\Omega)$ and contains discontinuous conductivities of practical relevance [211, Sec. 4]. The compactness of Γ enables us to work with uniformly accurate approximations, which interact with stability more favorably than average error estimates such as (4.22).

For any $\gamma \in \Gamma$, one can show that the NtD map $\Lambda_\gamma \in \text{HS}(L^2(\mathbb{T}); L^2(\mathbb{T}))$ is a Hilbert–Schmidt operator on $L^2(\mathbb{T})$ and hence a kernel integral operator. This implies that we can identify Λ_γ with its integral kernel function $\kappa_\gamma \in L^2(\mathbb{T} \times \mathbb{T})$. Writing $\text{Dom}(\Psi^*) := \{\kappa_\gamma \mid \gamma \in \Gamma\}$, we seek an approximation to the inverse map $\Psi^* : \text{Dom}(\Psi^*) \subseteq L^2(\mathbb{T} \times \mathbb{T}) \rightarrow L^2(\Omega)$ defined by $\Psi^*(\kappa_\gamma) := \gamma$. By the Benyamin–Lindenstrauss extension theorem [229, Theorem 1.12, p. 18], the fact that Ψ^* maps between two Hilbert spaces and (2.3) allow us to deduce the existence of a continuous extension with log stability *outside* of $\text{Dom}(\Psi^*)$ [211, Sec. 3]; recall Figs. 3 and 4. Specifically, there exists $C > 0$, $\alpha > 0$, and $\tilde{\Psi}^* : L^2(\mathbb{T} \times \mathbb{T}) \rightarrow L^2(\Omega)$ such that $\tilde{\Psi}^*$ extends Ψ^* and

$$\|\tilde{\Psi}^*(\kappa_0) - \tilde{\Psi}^*(\kappa_1)\|_{L^2(\Omega)} \leq C \left(\frac{1}{\log\left(\|\kappa_0 - \kappa_1\|_{L^2(\mathbb{T} \times \mathbb{T})}^{-1}\right)} \right)^\alpha \quad (4.23)$$

for all $\kappa_0 \in L^2(\mathbb{T} \times \mathbb{T})$ sufficiently close to $\kappa_1 \in L^2(\mathbb{T} \times \mathbb{T})$.

The stability estimate (4.23) shows that $\tilde{\Psi}^*$ is a continuous function-to-function map and hence is amenable to universal approximation theorems for neural operators (Section 3.2). We chose to work with the FNO from (3.11), (3.14), and (3.16); other architectures would also be valid. Let E_σ be a compact subset of $L^2(\mathbb{T} \times \mathbb{T})$ with the property that $\sup_{\eta \in E_\sigma} \|\eta\|_{L^2(\mathbb{T} \times \mathbb{T})} \leq \sigma$. Then by following the approach (4.10) from Section 4.1.2, we can establish a noise-robust approximation result [211, Sec. 4] which states that for every $\varepsilon > 0$, there exists an FNO $\Psi : L^2(\mathbb{T} \times \mathbb{T}) \rightarrow L^2(\Omega)$ such that

$$\sup_{(\gamma, \eta) \in \Gamma \times E_\sigma} \|\gamma - \Psi(\kappa_\gamma + \eta)\|_{L^2(\Omega)} \leq \varepsilon + C \left(\frac{1}{\log(\sigma^{-1})} \right)^\alpha. \quad (4.24)$$

Although this result demonstrates robustness to noise in the sense that the second term on the right-hand side of (4.24) goes to zero as $\sigma \rightarrow 0$, *it converges slowly*. In other words, the inherent instability of EIT is still present. In particular, it is sufficient

to take the noise level $\sigma = O(\exp(-\varepsilon^{-1/\alpha}))$ exponentially small to match the size of the FNO approximation error ε .

Related work [215] exploits quantitative continuity properties of Ψ^* in the more practical complete electrode model (CEM) of EIT [54, 109]. In the CEM model, measurements are limited to voltages corresponding to currents injected at a fixed finite number M of electrodes located along the boundary. This results in a discretized NtD map $\Lambda_\gamma^M \in \mathbb{R}^{M \times M}$. Instead of working with infinite-dimensional sets of admissible conductivities as in [211, 227], another option is to restrict attention to a finite-dimensional manifold $\Gamma \subset L^\infty(\Omega)$ of piecewise analytic conductivities. These conductivities are assumed to be identically equal to one outside of a compact subset of the domain Ω and uniformly bounded above and below pointwise a.e. [215]. Crucially, the finite-dimensionality of this set permits the derivation of *Lipschitz stability* results for the inverse map [210, 230, 231], as opposed to logarithmic stability results [55].

By approximating the EIT inverse map using a DeepONet (3.9) adapted to linear operator inputs, the following result holds [215, Thm. 3.1, p. 7]. Let L_M be the map $L_M: \Lambda_\gamma \mapsto \Lambda_\gamma^M - \Lambda_1^M$. For any $\varepsilon > 0$, there exists a number of electrodes M and a DeepONet Ψ of the form (3.9) (with $L = L_M$, viewed as a function of $L_M(\Lambda_\gamma)$ instead of Λ_γ) such that

$$\sup_{\gamma \in \Gamma} \|\gamma - \Psi(\Lambda_\gamma^M - \Lambda_1^M)\|_{L^2(\Omega)} \leq \varepsilon. \quad (4.25)$$

The proof relies on formulating Ψ^* as a mapping from a space of Hilbert–Schmidt operators into $L^2(\Omega)$, using Dugundji’s extension theorem [232] to continuously extend the domain of the map to the entire Hilbert space, and leveraging forward and inverse stability estimates to argue that the image of Γ under the parameter-to-data forward map is a compact set.

The DeepONet Ψ in (4.25) receives as input the raw measurements $\Lambda_\gamma^M \in \mathbb{R}^{M \times M}$ shifted by the background NtD map Λ_1^M corresponding to $\gamma \equiv 1$. The use of shifted NtD maps is for technical convenience but is not fundamentally necessary, as demonstrated in [211]. Regardless, these matrix inputs are treated as vectors in an M^2 -dimensional Euclidean space rather than matrices in a Banach algebra of linear operators. It would be interesting to replace fully connected neural networks with ORN-Nets (4.15) in the branch net of Ψ , as these may be better suited for matrix-based data [196]; recall Section 4.2.

Due to Lipschitz stability arising from the finite dimensionality of Γ , it should further be possible to prove Lipschitz robustness to noisy NtD maps in (4.25) by adapting the ideas in [211]. However, this favorable robustness will degrade as the dimensionality of Γ —and hence the number of measurements M —increases [231, Sec. 4.1, Thm. 5]. One would expect to only recover the logarithmic robustness shown in (4.24).

To summarize, the three preceding lines of research critically rely on inverse stability estimates for Ψ^* when viewed as a map between subsets of two separable Hilbert spaces [211, 215, 227]. Achieving such bounds requires leveraging the PDE structure inherent to EIT. Extending this framework beyond EIT entails developing appropriate stability estimates and extensions for the particular inverse map under consideration. However, these results must be carefully verified on a case-by-case basis; not all

PDE models possess the necessary structure to enable such analysis. Consequently, an important direction for future research is to apply the current approximation theory framework to other PDE-based nonlinear inverse problems, such as inverse wave scattering, optical tomography, or seismic imaging [212].

4.3.2. Finite-dimensionalizing nonlinear inverse problems

Although most analysis of deep learning for nonlinear inverse problems proceeds on a case-by-case basis, one notable exception is the work of Pineda and Petersen [198]. By transforming the conceptually infinite-dimensional nonlinear inverse problem into a finite-dimensional one, it is possible to reduce the setting to that of finite-dimensional unknown parameters and Lipschitz continuous inverse maps defined on a finite-dimensional data manifold. This transformation relies on ideas from [231]. The precise connection between the finite and infinite problems is explained in [198, Sec. 1.2.1 and Sec. 2]. A key point is that this procedure is valid for a broad class of nonlinear inverse problems. The main ingredients involve restricting the forward map to an *a priori* finite-dimensional set of admissible parameters and then composing a family of finite-rank “measurement” linear operators with the restricted forward map.

By carrying out this program, the original problem reduces to one about function approximation in finite dimensions. The following notable result holds true [198, Thm. 1.1]. Write d_m for manifold dimension and d_a for ambient dimension. Let $J \in \mathbb{N}$ and let $\psi^* : \text{Dom}(\psi^*) \subset \mathbb{R}^{d_a} \rightarrow \mathbb{R}^J$ be a bounded Lipschitz mapping such that $\text{Dom}(\psi^*)$ is a d_m -dimensional relatively compact manifold satisfying certain technical conditions [198, Thm. 3.9]. There exists $\sigma_0 > 0$ such that the following holds. If $\sigma^2 \leq \sigma_0^2$, then for every $\varepsilon > 0$, there exists a ReLU neural network ψ with $O(\varepsilon^{-d_m})$ parameters such that

$$\mathbb{E}_{\eta \sim \mathcal{N}(0, \sigma^2 I_{d_a})} \left[\sup_{y \in \text{Dom}(\psi^*)} \|\psi^*(y) - \psi(y + \eta)\|_{\mathbb{R}^J}^2 \right] \leq \varepsilon^2 + C^* d_m \sigma^2. \quad (4.26)$$

The constant C^* depends on the Lipschitz constant $\text{Lip}(\psi^*)$ of ψ^* , the manifold $\text{Dom}(\psi^*)$, and the maximal variance σ_0^2 , but not on the error tolerance ε . The result as stated in (4.26) follows from [198, Thm. 3.9] and the first choice of triangle inequality (4.9) mentioned in Section 4.1.2; compare to (4.24), which uses the second triangle inequality (4.10). As usual, the proof involves extending ψ^* away from its domain and approximating the extension instead. The extra Lipschitz-type robustness of the network to Gaussian noise is due in part to its construction based on ideas from finite element approximation.

We observe from (4.26) that the network approximation ψ has a favorable noise-damping property in the following sense. First notice that $d_m \sigma^2 = (d_m/d_a) \mathbb{E} \|\eta\|_{\mathbb{R}^{d_a}}^2$. A Lipschitz estimate for a general function on \mathbb{R}^{d_a} would only provide an average-case bound of order $\mathbb{E} \|\eta\|_{\mathbb{R}^{d_a}}^2$ for the perturbation η . Here, we instead see that the fine properties of the particular data manifold produce the dampening factor $d_m/d_a \leq 1$. This factor could be significantly smaller than 1 if the manifold is low-dimensional compared to the ambient space. Although (4.26) corresponds only to a quantitative existence theorem, it is shown that a neural network approximation can actually be

found through ERM (4.5) over noisy training pairs generated from the forward map [198, Thm. 4.3]. This trained network is accurate on average and further enjoys Lipschitz stability properties similar to those of the idealized, unattainable network ψ from (4.26).

To connect back to the motivation of inverse problem solvers, it is instructive to interpret the map ψ^* as a finite-dimensional representation of an underlying infinite-dimensional inverse map Ψ^* : $\text{Dom}(\Psi^*) \subseteq \mathcal{Y} \rightarrow \mathcal{U}$ between Banach spaces [231, Cor. 1]. Indeed, it is shown that the preceding theory applies to several nonlinear inverse problems corresponding to Darcy flow, Euler–Bernoulli beam, and nonlinear Volterra integral models [198, Sec. 2]. One limitation of the general approach put forth by [198] is that much of the infinite-dimensional structure, including instability as manifested by a generally non-Lipschitz modulus of continuity of Ψ^* , is hidden in the finite-dimensionalization procedure and associated Lipschitz constants. Indeed, the neural network approximation is intertwined with the number of measurements d_m . The estimation becomes harder as the parameter dimension J grows because $\text{Lip}(\psi^*)$ —and hence the number of measurements d_m —tends to infinity in this limit [231]. The network also must change each time J or d_m changes, which violates the desirable discretization invariance principles of operator learning. Adding additional encoder-decoder structure to the approximation could reinstate consistency (see Section 3.2.1). Moreover, since the theory is only valid for finite-dimensional parameters, this precludes natural infinite-dimensional parameter models such as bounded transformations of Gaussian random fields [57, 109]. Overcoming such challenges while maintaining the wide applicability of [198] would be a substantial contribution to the field of data-driven inverse problems.

4.3.3. Finite-dimensionalizing linear inverse problems

It is fruitful to analyze operator learning for linear inverse maps because linearity enables the uncovering of deep theoretical insights that are widely applicable to a whole family of inverse problems, unlike the nonlinear setting of the previous subsections. Such a program was carried out successfully for linear forward operator learning [148, 149]. Analogous results for linear inverse problems are still missing, possibly due to the difficulty of handling the unboundedness of the inverse operator in conjunction with the training data and noise models.

One exception where analysis can be pushed through is the method of data-driven regularization-by-projection [224, 225]. The analysis adopts the framework of functional-analytic regularization [233] and works in the setting that the forward operator is unknown. Instead, the forward map is only accessible through input-output training data. The theory establishes convergence guarantees in the limit of infinite training data, both for noise-free and noisy observations. We now survey such results.

Let \mathcal{U} and \mathcal{Y} be real separable Hilbert spaces. Let $\mathcal{A} \in \mathcal{L}(\mathcal{U}; \mathcal{Y})$ be an injective compact linear operator. For example, \mathcal{A} could represent the Radon transform from the imaging sciences or a (possibly non-symmetric) linear solution operator of a linear PDE. Suppose we are given a training dataset of noiseless labeled input-output pairs

$$(u_n, y_n), \quad \text{where } y_n = \mathcal{A}u_n \quad \text{for } n \in \{1, \dots, N\}. \quad (4.27)$$

Based on the N pairs from (4.27), our goal is to find an estimator $\mathcal{R}_N: \mathcal{Y} \rightarrow \mathcal{U}$ of the unbounded operator $\mathcal{A}^{-1}: \text{Ran}(\mathcal{A}) \subset \mathcal{Y} \rightarrow \mathcal{U}$ such that for any $y \in \text{Ran}(\mathcal{A})$ and any $y^\delta \in \mathcal{Y}$ such that $\|y - y^\delta\|_{\mathcal{Y}} \leq \delta$, it holds that the reconstruction error

$$\|\mathcal{A}^{-1}y - \mathcal{R}_N y^\delta\|_{\mathcal{U}} \quad (4.28)$$

is small if the noise level $\delta > 0$ is sufficiently small. That is, we have *learned to solve* the inverse problem of finding u from imperfect observations $y^\delta \approx \mathcal{A}u$. Of course, we must choose $N = N(\delta)$ as a function of δ in order for the display in (4.28) to converge to zero as $\delta \rightarrow 0$ [233, 234]. Thus, the sample size N plays the role of a regularization hyperparameter.

To define our choice of learned inverse map $\mathcal{R}_N \in \mathcal{L}(\mathcal{Y}; \mathcal{U})$, let the linear span of the training data be written as

$$\mathcal{U}_N := \text{span}\{u_n\}_{n=1}^N \quad \text{and} \quad \mathcal{Y}_N := \text{span}\{y_n\}_{n=1}^N. \quad (4.29)$$

Further define $P_{\mathcal{U}_N}: \mathcal{U} \rightarrow \mathcal{U}_N$ to be the orthogonal projection operator onto \mathcal{U}_N . Similarly, define $P_{\mathcal{Y}_N}: \mathcal{Y} \rightarrow \mathcal{Y}_N$ to be the orthogonal projection operator onto \mathcal{Y}_N . The *data-driven regularization-by-projection estimator* is defined by

$$\mathcal{R}_N := \mathcal{A}^{-1}P_{\mathcal{Y}_N}. \quad (4.30)$$

The motivation for the formula (4.30) is that the action of the forward map \mathcal{A} on the span \mathcal{U}_N of the input training data is completely determined by the data. It is then possible to deduce that $\mathcal{R}_N y$ corresponds to the minimum norm solution of the *input-projected* linear operator equation $y = \mathcal{A}P_{\mathcal{U}_N}u$. Then \mathcal{R}_N in (4.30) is seen to be the Moore–Penrose pseudoinverse of $\mathcal{A}P_{\mathcal{U}_N}$ [225, Thm. 4, p. 5].

To evaluate the map $y \mapsto \mathcal{R}_N y$ only using the training data (4.27) and not \mathcal{A} itself, we appeal to the Gram–Schmidt orthonormalization procedure. Let $\{\varphi_j\}_{j=1}^N$ be the orthonormal basis of \mathcal{Y}_N obtained from the Gram–Schmidt algorithm applied to $\{y_n\}_{n=1}^N$ (already assumed to be linearly independent). Then

$$P_{\mathcal{Y}_N} = \sum_{j=1}^N \varphi_j \otimes_{\mathcal{Y}} \varphi_j, \quad (4.31)$$

where $(a \otimes_{\mathcal{Y}} b)h := \langle b, h \rangle_{\mathcal{Y}} a$ is the outer product operator on \mathcal{Y} . It follows that

$$\mathcal{R}_N = \sum_{j=1}^N (\mathcal{A}^{-1}\varphi_j) \otimes_{\mathcal{Y}} \varphi_j =: \sum_{j=1}^N v_j \otimes_{\mathcal{Y}} \varphi_j. \quad (4.32)$$

The vectors $\{v_j\}_{j=1}^N$ can be computed offline using $v_1 := u_1 / \|y_1\|_{\mathcal{Y}}$ and the iteration

$$v_j = \frac{u_j - \sum_{k=1}^{j-1} \langle \varphi_k, y_j \rangle_{\mathcal{Y}} v_k}{\|y_j - P_{\mathcal{Y}_{j-1}}y_j\|_{\mathcal{Y}}} \quad \text{for all } j > 1. \quad (4.33)$$

Thus, we can compute $y \mapsto \mathcal{R}_N y = \sum_{j=1}^N \langle \varphi_j, y \rangle_{\mathcal{Y}} v_j$ in linear time complexity without access to \mathcal{A} or its inverse. These expensive offline steps are similar to the ones used in PCA-Net (3.10) and other model reduction methods [181].

To obtain convergence guarantees for \mathcal{R}_N , we require some assumptions on the training data (4.27). Assume that the sequence $\{\|u_n\|_{\mathcal{U}}\}$ is bounded away from zero and infinity. For all N , suppose that the vectors $\{u_n\}_{n=1}^N$ are linearly independent. Furthermore, assume that

$$\{(u_n, y_n)\}_{n=1}^{N+1} = \{(u_n, y_n)\}_{n=1}^N \cup \{(u_{N+1}, y_{N+1})\} \quad (4.34)$$

are nested and that $\overline{\cup_{N \in \mathbb{N}} \mathcal{U}_N} = \mathcal{U}$. Notice that the training data need not be generated according to a probability distribution; they could be deterministic and highly correlated. For example, one could select the $\{u_n\}$ to be a problem-adapted orthonormal basis or construct them according to some greedy algorithm. Under further technical assumptions on the compatibility between \mathcal{A} , the linear span \mathcal{U}_N , and a fixed $y \in \text{Ran}(\mathcal{A})$ [224, Sec. 2.2.1], it holds that $\mathcal{R}_N y$ converges both weakly and strongly to $\mathcal{A}^{-1}y$ in the Hilbert space \mathcal{U} as $N \rightarrow \infty$ [225, Thms. 9, 11, 15]. We can also handle the noisy data case $y^\delta \notin \text{Ran}(\mathcal{A})$. Optimizing a standard bias-variance tradeoff [234, Thm. 46, p. 33] by choosing $N = N(\delta) \rightarrow \infty$ according to the requirement

$$\delta \sqrt{N(\delta)} \sup_{n \in \{1, \dots, N(\delta)\}} \frac{1}{|\langle \varphi_n, y_n \rangle_{\mathcal{Y}}|} \rightarrow 0 \quad \text{as } \delta \rightarrow 0, \quad (4.35)$$

it then holds under the aforementioned technical assumptions that

$$\lim_{\delta \rightarrow 0} \sup_{\tilde{y} \in B_\delta(y)} \|\mathcal{A}^{-1}y - \mathcal{R}_{N(\delta)}\tilde{y}\|_{\mathcal{U}} = 0 \quad \text{for all } y \in \text{Ran}(\mathcal{A}) \quad (4.36)$$

by [225, Thm. 17, p. 17]. In (4.36), we write $B_\delta(y) := \{z \in \mathcal{Y} \mid \|y - z\| \leq \delta\}$.

The convergence result (4.36) is pointwise in the “input space” $\text{Ran}(\mathcal{A})$ and uniform over perturbations. Because \mathcal{A}^{-1} is not continuous, we cannot expect a version of (4.36) that is uniform over the unit ball of $\text{Ran}(\mathcal{A})$ to be valid [234, Thm. 4.9, p. 36]. However, comparing to Eqs. (4.22), (4.24) and (4.26) which are *uniform* over the domain of a nonlinear inverse map, it is of interest to determine meaningful compact source sets or probability measures over parameter space that lead to uniform or average case convergence, respectively, of $\mathcal{R}_{N(\delta)}$ at the level of operators, possibly with respect to new accuracy metrics.

The data-driven regularization-by-projection method can be viewed both as learning the forward operator—via $\mathcal{A} \approx \mathcal{A}P_{\mathcal{U}_N}$ —or as learning the inverse operator—via $\mathcal{A}^{-1} \approx \mathcal{A}^{-1}P_{\mathcal{Y}_N}$. Both viewpoints can be unified in the special case that the training data arise from the SVD of \mathcal{A} [225, Remark 6, p. 6]. The current approach is but one of many ways to finite-dimensionalize linear inverse problems by discretizing parameters or data [235]. Dual least squares and explicitly regularized variational problems also enjoy convergence guarantees [225, Secs. 4–5]. Beyond deterministic data with span-increasing and linear independence constraints, other choices of projection sets

could include the leading eigenspaces of convenient ‘‘prior’’ operators that are compatible with \mathcal{A} [177]. This could help circumvent the technical difficulties associated with the Gram–Schmidt procedure.

The preceding methodologies can all be viewed as simple ways to actively select training data [11, 165–168]. Nevertheless, the development of a theoretical foundation for the i.i.d. random training data setting is still essential. A natural counterpart to deterministic regularization-by-projection in this stochastic setting is an empirical PCA projection-based inversion method. A sharp comparative analysis could help clarify the benefits of active versus passive data design strategies for linear inverse operator learning.

4.4. Beyond point estimation: Data-to-posterior maps

Compared to data-to-parameter map learning, the literature on learning data-to-posterior maps in the context of infinite-dimensional Bayesian inverse problems (Section 2.1.1) is much sparser [34, Chp. 6]. For a fixed observation y , there is abundant work on how to compute the posterior probability measure μ^y given by (2.4), e.g., by sampling or density estimation methods. However, such traditional inference methods are relatively slow. This cost is magnified if the application requires the repeated calculation of the posterior for many different measurements, which is the case in sequential data assimilation [236] or Bayesian optimal experimental design [106]. By *data-to-posterior operator learning*, we refer to the problem of approximating the map $y \mapsto \mu^y$. This approach effectively solves entire families of Bayesian inverse problems parametrized by the observed data without the need for re-training or repeated optimization solves. Although the upfront training or data generation cost may be high, this offline cost is amortized if the trained map is evaluated multiple times and each evaluation is fast (e.g., near real-time). Similar considerations hold for the prior-to-posterior map $\mu \mapsto \mu^y$, or even the combined Bayesian solution map $(\mu, y) \mapsto \mu^y$, although these are outside the scope of the present chapter.

Some work within the fields of likelihood-free [237] and simulation-based inference [238] can be interpreted within the amortized data-to-posterior framework. For instance, one can build efficient surrogate models for the forward map simulator appearing in the likelihood function to accelerate the Bayesian inference loop. There is other research on data-amortized conditional score-based diffusion models for infinite-dimensional linear inverse problems [239, 240]. Instead, this subsection focuses on *measure transport* methods that directly target the parametric dependence of the posterior on the observed data.

To this end, one approach is to learn data-to-posterior maps with a hypernetwork [241]. The hypernetwork Ψ maps the data y to the parameters $\theta = \Psi(y)$ of another neural network F . We view F as an approximate transport map from the prior μ to the posterior μ^y . That is, $\mu^y \approx F(\cdot; \theta) \# \mu$. The map F only depends on y through its parameters $\theta = \Psi(y)$. The training of Ψ can be performed in an unsupervised way by optimizing the Kullback–Leibler (KL) divergence, but this requires knowledge of the likelihood to evaluate the loss. The overall method is a ‘‘meta’’ conditional normalizing flow and has been applied to inverse problems on function spaces [241]. Since the

hypernetwork training task is difficult in practice, one should later fine tune the meta-conditional model or use it as a preconditioner for a fixed data realization if higher accuracy is required.

An alternative methodology is that of triangular transport maps [119]. This approach falls under the broader purview of computational measure transport [79], as described in Section 2.1.2. In (2.5), which we recall is the minimization problem $\min_{T \in \mathcal{T}} d(\nu, T \# \rho)$, the triangular framework takes d to be the KL divergence and \mathcal{T} to be a class of triangular maps with a particular parametrization (e.g., polynomial or wavelet expansions) and structural constraints such as monotonicity [118]. This construction is inherently finite-dimensional, which precludes its scalability to infinite-dimensional inverse problems. One solution involves a relaxation to *block triangular transport maps*, which are well-defined between infinite-dimensional Banach spaces and naturally amortize posterior sampling with respect to the observation data [82]. Our discussion is restricted to a useful but specific case of a more general setup [81].

Let \mathcal{U} be the parameter state space and \mathcal{Y} the data space, both assumed to be separable Banach spaces. Suppose there is an unknown joint probability measure $\nu \in \mathcal{P}(\mathcal{Y} \times \mathcal{U})$ over the joint data-parameter space. For instance, the data likelihood model (2.1) and the prior measure $\mu \in \mathcal{P}(\mathcal{U})$ together define such a ν . We wish to solve the minimum divergence estimation problem (2.5) such that the class \mathcal{T} consists of block triangular maps of the form

$$T(y, u) = \begin{pmatrix} y \\ \Psi(y, u) \end{pmatrix} \quad (4.37)$$

for $(y, u) \in \mathcal{Y} \times \mathcal{U}$ and $\Psi: \mathcal{Y} \times \mathcal{U} \rightarrow \mathcal{U}$. The map Ψ parametrizes the class \mathcal{T} . The nonlinear function (4.37) is called block triangular due to the variable dependence in each block coordinate that ensures the derivative of T takes values as a block lower-triangular linear operator. We further take $\rho := \nu_{\mathcal{Y}} \otimes \rho_{\mathcal{U}} \in \mathcal{P}(\mathcal{Y} \times \mathcal{U})$ to be an independent product reference measure, where $\nu_{\mathcal{Y}}$ is the \mathcal{Y} -marginal of ν and $\rho_{\mathcal{U}}$ is arbitrary. A typical choice is $\rho_{\mathcal{U}} = \mu$ for a Bayesian inverse problem with prior μ [81, Sec. 4]. The form (4.37) is useful for the following reason. If $T \# \rho = \nu$, then

$$\Psi(y, \cdot) \# \rho_{\mathcal{U}} = \nu(\cdot | y) \quad (4.38)$$

for $\nu_{\mathcal{Y}}$ -a.e. $y \in \mathcal{Y}$ [82, Thm. 2.4, p. 875]. That is, we can extract the desired conditional distribution $\nu(\cdot | y)$ from the subcomponent Ψ of the full transport map T . Moreover, global minimizers T^* to (2.5) over the class (4.37) exist and achieve $T^* \rho = \nu$ [82, Remark 2.11, p. 878].

These theoretical underpinnings help motivate the monotone generative adversarial network (M-GAN) architecture [82, Sec. 3], which is a powerful amortized solver for Bayesian inverse problems. M-GAN takes d to be a min-max approximation of the Wasserstein-1 distance. For PDE-based inverse problems such as Darcy flow, the transport map Ψ is parametrized using PCA-Net (3.10). Practically, we only have access to ν through a finite training dataset of N pairs of i.i.d. joint samples. Then ν in (2.5) is replaced by the empirical measure ν^N corresponding to these samples.

To avoid overfitting to the training data, the reference ρ is also replaced by its M -sample approximation, with M possibly different from N . After training, the M-GAN estimator $\widehat{\Psi}$ satisfies

$$\widehat{\Psi}(y, \cdot) \# \mu \approx \mu^y. \quad (4.39)$$

Numerical experiments demonstrate the excellent performance of M-GAN on a wide range of Bayesian inverse problems [81, 82].

Although there are sample complexity bounds [242] and some approximation theory for measure transport [243], at least for fixed y , a general error analysis for the performance of learned data-to-posterior operators is still missing. In the block triangular transport setting where training is done at the level of joints (2.5), one important open question is to understand how errors in joint distribution approximation propagate to errors in the desired conditionals or posteriors. A satisfactory answer will be highly dependent on the choice of statistical divergence \mathbf{d} used to quantify such errors.

5. Learning prior distributions and regularizers

Learning prior information or regularization terms directly from data has become a powerful alternative to hand-crafted regularization in solving inverse problems [137, 244–251]. Traditionally, priors were imposed using explicit penalty terms or probabilistic assumptions; however, modern approaches instead learn these priors from examples of signals or measurements. This allows one to capture complex structures or statistical correlations in data that are difficult to express analytically, especially in high-dimensional or ill-posed settings. The learned prior can be used either in variational inference or to guide iterative algorithms. This section focuses on two complementary paradigms for learning prior distributions and regularizers: approaches based on Bayesian variational inference in Section 5.1 and denoising-based regularization (e.g., plug-and-play methods) in Section 5.2.

5.1. Prior learning and Bayesian variational inference

In the Bayesian formulation, solving an inverse problem involves specifying a prior distribution μ over the unknown parameter u and a likelihood function $\mathbf{L}^y(u) = \exp(-\Phi(u; y))$, which models the relationship between the data y and the parameter u (Section 2.1.1). The likelihood represents the forward and measurement processes as well as uncertainties, while the prior encodes our assumptions or background knowledge about u before observing the data.

Bayesian inference combines the prior μ and likelihood \mathbf{L}^y using Bayes' theorem to obtain the posterior distribution μ^y :

$$\mu^y(u) \propto \mathbf{L}^y(u) \mu(u), \quad (5.1)$$

where, for convenience in this section, we abuse notation by writing $\mu^y(u)$ and $\mu(u)$ for the density of the posterior and the prior measures, respectively. The posterior represents the updated distribution of u after incorporating the data y . However, Bayesian

inference is expensive. From a computational efficiency perspective, one goal that does not require probing the full posterior distribution is to extract a point estimate of u that best aligns with the posterior. A common approach is MAP estimation [62], which maximizes the posterior probability via

$$u_{\text{MAP}} := \arg \max_{u \in \mathcal{U}} \mu^y(u). \quad (5.2)$$

Equivalently, using the negative log likelihood potential Φ , MAP estimation minimizes the energy functional given by:

$$\mathcal{E}(u | y) := -\log \mathcal{L}^y(u) - \log \mu(u) = \Phi(u; y) - \log \mu(u). \quad (5.3)$$

From this optimization perspective, regularization can be interpreted as imposing a prior through the term $R(u) := -\log \mu(u)$. In classical inverse problems, handcrafted regularizers such as quadratic penalties for smoothness or sparsity-promoting norms play the role of R . For example, Gaussian priors lead to Tikhonov-type regularizers, while a Laplace prior aligns with sparsity-promoting regularizers. Note that in infinite dimensions, the densities appearing in the preceding formulas (5.1), (5.2), and (5.3) require careful interpretation [60].

The fact that the prior acts like a regularization term can also be seen from the variational form of Bayes' theorem [34, 252]. Rather than viewing Bayes' rule as a formula for conditioning, one can interpret the posterior μ^y as the minimizer of a variational problem over the metric space of probability measures. Specifically, the posterior distribution minimizes the functional

$$\mu^y = \arg \min_{\nu \in \mathcal{P}(\mathcal{U})} \left\{ \mathbb{E}_{u \sim \nu} [\Phi(u; y)] + \text{KL}(\nu \| \mu) \right\}, \quad (5.4)$$

where $\text{KL}(\nu \| \mu)$ is the KL divergence between ν and the prior μ . In this formulation, the KL divergence serves as a regularization term that penalizes deviations from the prior, while the expected negative log-likelihood promotes fidelity with the observed data. The choice of prior μ directly determines the structure and strength of the regularization term $\text{KL}(\nu \| \mu)$.

In modern settings, data-driven approaches aim to learn the prior μ directly from training samples. By modeling complex, high-dimensional distributions of real-world data, these methods offer greater flexibility compared to traditional handcrafted priors. Machine learning techniques, particularly deep generative models [253], have been particularly effective in capturing such distributions. Examples include energy-based models, generative adversarial networks (GANs), variational autoencoders (VAEs), and score-based diffusion models [140, 254–258]. These learned priors provide a data-driven means to enforce regularization in the Bayesian framework and provide state-of-the-art reconstructions in many inverse problems.

Section 5.1.1 introduces popular regularizers arising from the combination of variational inference with deep learning. To state concrete theoretical results, Section 5.1.2 first develops an analysis of the effect that learned priors have on downstream posteriors. Specializing to infinite-dimensional linear inverse problems, the subsection

then presents an analysis of optimal Tikhonov and spectral regularizers within the nonparametric statistical framework of [Section 2.1.3](#).

5.1.1. Mathematical formulation and architecture choices

This subsection focuses on unsupervised neural network-based regularization techniques. In this setting, one assumes access to an i.i.d. dataset

$$\{u_n\}_{n=1}^N \sim \mu_{\text{data}}^{\otimes N}, \quad (5.5)$$

but not paired observation data. The goal is to learn a prior μ or its parametric representation from this collection of representative “ground-truth” samples distributed according to the inaccessible data distribution μ_{data} . The measure μ_{data} is rarely Gaussian. But if it is Gaussian, then the problem becomes equivalent to *covariance estimation* [259], which is one of the simplest examples of unsupervised operator learning. Even in the non-Gaussian case, estimating the covariance operator of μ_{data} from samples (5.5) is a nontrivial task in high or infinite dimensions. We focus on finding μ_{data} itself. It is also possible, but more challenging, to handle the case when only indirect observations of the model (5.5) are available [107, 207]; see also [Section 2.1.4](#) for a measure-centric approach to this distributional inversion problem.

Let \mathcal{Z} be a finite-dimensional latent space. Most state-of-the-art methods represent the prior as the pushforward under a neural network or neural operator

$$\mathsf{T}_\theta: \mathcal{Z} \rightarrow \mathcal{U} \quad (5.6)$$

that maps samples z from a latent distribution ρ —typically a standard isotropic Gaussian—to the parameter space. That is,

$$u = \mathsf{T}_\theta(z) \sim \mu \quad \text{and} \quad \mu = \mu_\theta = (\mathsf{T}_\theta)_\# \rho. \quad (5.7)$$

Once an appropriate T_θ is trained, this transport map framework ([Section 2.1.2](#)) converts the inverse problem $y = \mathcal{G}(u)$ from (2.18) into that of finding z from

$$y = \mathcal{G}(\mathsf{T}_\theta(z)). \quad (5.8)$$

Thus, the inference is now over the latent space \mathcal{Z} . Different methods vary in the choice of architecture for T_θ and the design of the loss function, which together determine the learning preferences for encoding the prior. We now survey several possible options.

Maximum likelihood and invertible transport maps

When T_θ is invertible (e.g., a normalizing flow), the density of the prior μ_θ is

$$\mu_\theta(u) = \rho(\mathsf{T}_\theta^{-1}(u)) |\det(\nabla \mathsf{T}_\theta^{-1}(u))|. \quad (5.9)$$

The parameters $\theta \in \Theta$ can be optimized using maximum likelihood estimation

$$\max_{\theta \in \Theta} \frac{1}{N} \sum_{n=1}^N \log \mu_\theta(u_n) \quad (5.10)$$

by plugging in the density formula (5.9).

Autoencoders

Architectures based on *autoencoders* consist of an encoder-decoder pair

$$E_\vartheta: \mathcal{U} \rightarrow \mathcal{Z} \quad \text{and} \quad \mathsf{T}_\vartheta: \mathcal{Z} \rightarrow \mathcal{U} \quad (5.11)$$

that are trained to reconstruct input data. This amounts to the optimization problem

$$\min_{(\theta, \vartheta)} \frac{1}{N} \sum_{n=1}^N \|\mathsf{T}_\vartheta(E_\vartheta(u_n)) - u_n\|_{\mathcal{U}}^2. \quad (5.12)$$

After training, the prior over the space \mathcal{U} is implicitly defined by pushing forward a simple distribution $\rho \in \mathcal{P}(\mathcal{Z})$. The decoder T_ϑ maps this latent distribution to the parameter space. This induces a trained prior distribution $\mu_\theta = (\mathsf{T}_\vartheta)_\# \rho$ as before.

Evidence lower bound and variational autoencoders

Variational autoencoders (VAEs) are generative models that represent the prior by introducing a latent random variable $z \in \mathcal{Z}$, which is typically drawn from a standard Gaussian $\rho = \mathcal{N}(0, I)$ [260, 261]. The conditional likelihood of the parameter u given a latent variable z is modeled as

$$u \sim p_\theta(\cdot | z). \quad (5.13)$$

The probability measure $p_\theta(\cdot | z)$ is parametrized by $z \in \mathcal{Z}$ and is known as a decoder network. It is common to take

$$p_\theta(\cdot | z) = \mathcal{N}(m_\theta(z), \Sigma_\theta(z)) \quad (5.14)$$

to be a Gaussian distribution. The mean $m_\theta: \mathcal{Z} \rightarrow \mathcal{U}$ and covariance $\Sigma_\theta: \mathcal{Z} \rightarrow \mathcal{L}(\mathcal{U}; \mathcal{U})$ are parametrized by neural networks or neural operators. The covariance is usually constrained to be diagonal.

Since the marginal likelihood

$$p_\theta(du) := \mathbb{E}_{z \sim \rho}[p_\theta(du | z)] \quad (5.15)$$

can be intractable to compute, we approximate the posterior $p_\theta(dz | u)$ with a variational distribution $q_\vartheta(dz | u)$. This is often a Gaussian encoder

$$q_\vartheta(\cdot | u) = \mathcal{N}(\tilde{m}_\vartheta(u), \tilde{\Sigma}_\vartheta(u)). \quad (5.16)$$

Just as for the decoder, the mean $\tilde{m}_\vartheta: \mathcal{U} \rightarrow \mathcal{Z}$ and covariance $\tilde{\Sigma}_\vartheta: \mathcal{U} \rightarrow \mathcal{L}(\mathcal{Z}; \mathcal{Z})$ of the encoder are parametrized by neural networks or neural operators. The covariance is typically enforced to be diagonal.

VAE training maximizes the *evidence lower bound* (ELBO). The ELBO is a tractable lower bound on $\log p_\theta(u)$, given by

$$\begin{aligned} \log p_\theta(u) &\geq \text{ELBO}(\theta, \vartheta; u) \\ &:= \mathbb{E}_{z \sim q_\vartheta(\cdot | u)} [\log p_\theta(u | z)] - \mathsf{KL}(q_\vartheta(\cdot | u) \| \rho). \end{aligned} \quad (5.17)$$

The first term of the ELBO encourages accurate reconstruction of u . The second term regularizes the encoder by keeping it close to the latent prior distribution ρ . The mean of the decoder, m_θ , can be used as a generator. This means that after training, samples from the prior $z \sim \rho$ are mapped to the parameter space with $u = m_\theta(z)$. This induces a learned prior distribution $\mu_\theta := (m_\theta)_\# \rho$ over u .

Generative adversarial networks

Generative Adversarial Networks (GANs) are trained to learn a generator

$$\mathsf{T}_\theta: \mathcal{Z} \rightarrow \mathcal{U} \quad (5.18)$$

that induces a distribution

$$\mu_\theta := (\mathsf{T}_\theta)_\# \rho \quad (5.19)$$

given a known latent distribution $\rho \in \mathcal{P}(\mathcal{Z})$. This is the same setup as before. The point of departure is the training procedure. GANs are trained with an adversarial loss, where the adversary is a discriminator

$$D_\vartheta: \mathcal{U} \rightarrow [0, 1]. \quad (5.20)$$

The original GAN objective is a *minimax game* between the generator and discriminator. This game reads

$$\min_\theta \max_\vartheta \left\{ \mathbb{E}_{u \sim \mu_{\text{data}}} [\log D_\vartheta(u)] + \mathbb{E}_{z \sim \rho} [\log (1 - D_\vartheta(\mathsf{T}_\theta(z)))] \right\}, \quad (5.21)$$

where μ_{data} is the training data distribution (5.5). The discriminator tries to assign 1 to real data samples and 0 to generated ones, while the generator attempts to fool the discriminator by producing samples for which $D_\vartheta(\mathsf{T}_\theta(z)) \approx 1$. Variants such as the *Wasserstein GAN* [262] replace the Jensen–Shannon divergence in the GAN loss with an approximation of the dual form of the Wasserstein-1 distance. This leads to the minimax game

$$\min_\theta \max_{\{\vartheta \mid \text{Lip}(D_\vartheta) \leq 1\}} \left\{ \mathbb{E}_{u \sim \mu_{\text{data}}} [D_\vartheta(u)] - \mathbb{E}_{z \sim \rho} [D_\vartheta(\mathsf{T}_\theta(z))] \right\}. \quad (5.22)$$

The 1-Lipschitz constraint $\text{Lip}(D_\theta) \leq 1$ can be enforced using a gradient penalty or weight clipping [216]. The Wasserstein GAN tends to exhibit improved stability. The expectations in the preceding displays (5.21) and (5.22) are replaced by empirical averages during training in practice. After training, the generator T_θ induces a prior that approximates μ_{data} .

Explicit prior or score learning

Finally, some methods seek to learn an explicit, parametrized regularization functional $R_\theta : \mathcal{U} \rightarrow \mathbb{R}$ that approximates the negative log prior density from (5.3). In approaches based on maximum likelihood estimation, one fits a model of the form

$$\mu_\theta(u) \propto \exp(-R_\theta(u)) \quad (5.23)$$

to a dataset $\{u_n\}_{n=1}^N \sim \mu_{\text{data}}^{\otimes N}$ by solving

$$\max_{\theta \in \Theta} \frac{1}{N} \sum_{n=1}^N \log \mu_\theta(u_n) = \min_{\theta} \frac{1}{N} \sum_{n=1}^N \left[R_\theta(u_n) + \log Z_\theta \right], \quad (5.24)$$

where Z_θ is the normalization constant implied in (5.23). In practice, computing Z_θ is often intractable, which necessitates approximate training schemes such as contrastive divergence [263] or score matching [264]. Once trained, the resulting R_θ provides an explicit regularizer suitable for use in downstream inverse problem solvers.

Alternatively, score-based models, such as denoising score matching and diffusion models [36, 254], bypass the need to evaluate or approximate the normalizing constant Z_θ by instead learning the score function

$$u \mapsto (\nabla \log \mu)(u) \quad (5.25)$$

directly with neural networks or neural operators [239, 240]. While these models do not yield an explicit density for μ , they enable sampling and approximate inference through stochastic dynamics. Consequently, they define the prior implicitly through its score or generative process rather than an explicit functional form.

5.1.2. Theoretical results

Mathematical guarantees for the *accuracy* of data-driven priors and regularizers in the infinite-dimensional setting, which is the primary focus of this chapter, remain somewhat limited [140]. For instance, in the variational framework of (2.20), much of the existing literature focuses on analyzing the convergence or computational complexity of optimization schemes used to find the regularizer or solve the inverse problem, rather than directly addressing the quality of the inversion itself [250, 251, 265]. Furthermore, there is a strong preference in existing work for the functional-analytic regularization framework, which combines worst-case analysis with deterministic, bounded noise models [124].

In contrast, this subsection surveys theoretical work that has a more probabilistic flavor. In the context of prior learning for Bayesian inverse problems, we study the stability of the posterior distribution with respect to perturbations in the prior. By developing quantitative estimates for the modulus of continuity of the prior-to-posterior map, we can control posterior accuracy—that is, the accuracy of the Bayesian inverse problem solution—by the error incurred by the approximate prior. Due to its generality, this stability approach is widely applicable to various choices of data-driven prior learning architectures or algorithms, including those highlighted in Section 5.1.1. However, from the perspective of accuracy, such prior-to-posterior bounds can be quite crude because all of the dependence on the likelihood (i.e., the forward map, observed data, and noise level) is hidden in the stability constants.

To achieve possibly sharper results, we then turn our attention to the concrete *average-case* analysis of learned regularization in infinite-dimensional linear inverse problems. The statistical aspects of this problem setting—primarily the training data distribution and noise distribution—are seen to greatly impact inversion accuracy.

Stability of prior learning

The quantitative robustness of Bayesian inference has been a subject of extensive study for several decades [266–269]. Recent advancements in the theoretical analysis of Bayesian inverse problems and generative modeling have reignited interest in this topic [270–273]. A key question of relevance to this chapter is the robustness of the posterior distribution with respect to perturbations in the prior distribution. Such prior perturbations can arise from randomized approximations [176, 274] or finite element approximations [275] of Gaussian process priors, for example. To present the results, we adopt the compact linear functional notation $\pi(f) := \mathbb{E}_{u \sim \pi}[f(u)]$, which represents the integral of a function f with respect to a measure π .

Recall the setting of Bayesian inverse problems from Section 2.1.1. We are concerned with stability estimates for the nonlinear prior-to-posterior map $\mu \mapsto \mu^y$ from (2.4) for some fixed y . The results we cover are of the type

$$d(\mu^y, \nu^y) \leq \frac{C(\mu, \nu; y)}{\min(Z_\mu^y, Z_\nu^y)} d_0(\mu, \nu), \quad (5.26)$$

where d quantifies closeness of posteriors μ^y and ν^y , d_0 quantifies closeness of priors μ and ν , Z_μ^y and Z_ν^y are the posterior normalizing constants, and $C(\mu, \nu; y)$ is a constant that depends on the priors (typically only through their moments) and the data y . See Figure 5 for an illustration. Most works take $d = d_0$ as the TV, Hellinger, or Wasserstein-1 distances [270]. There are generalizations to the case $d \neq d_0 \equiv d_0^y$, where d_0^y is a *data-dependent* distance function [271]. With respect to the local Lipschitz constants, slightly tighter upper bounds than (5.26) exist, depending on the choice of d . Recently, the sharpness of (5.26) has been studied from the perspective of lower bounds [273]. These results reveal that the increasing sensitivity as the posterior becomes more concentrated, i.e., as the evidence Z_μ^y from (2.4) approaches zero, is inevitable under certain statistical divergences.

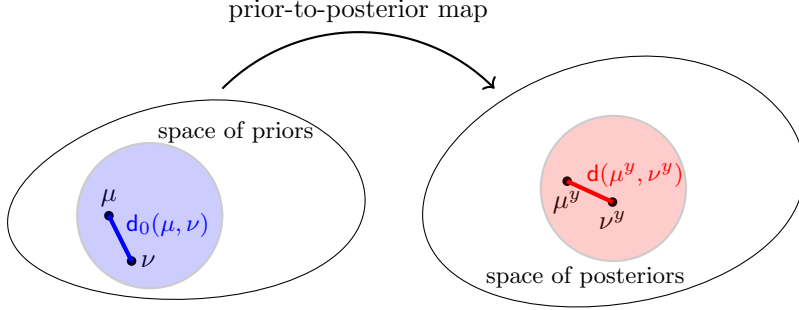


Fig. 5: The stability of prior learning concerns the relationship between the closeness of the posteriors, measured by $d(\mu^y, \nu^y)$, and the closeness of the priors, measured by $d_0(\mu, \nu)$.

When $d = W_1$, the Wasserstein-1 distance [80], it holds that

$$W_1(\mu^y, \nu^y) \leq \frac{C_p(\mu, \nu; y)}{\min(Z_\mu^y, Z_\nu^y)} W_p(\mu, \nu) \quad (5.27)$$

for any $p \in [1, \infty]$; see [272, Lem. 5.1, p. 38]. The constant $C_p(\mu, \nu; y)$ depends on the $p/(p-1)$ -th moment of the priors and is known explicitly [272]. In particular, the limit $p \rightarrow 1$ requires one of the priors to have compact support, which excludes popular unbounded priors such as Gaussian measures. As a result, the scenario $d = d_0 = W_1$ is relatively uncommon.

A result similar to (5.27) can be derived using more sophisticated techniques, particularly in the case $p = 2$ [271]. Both proofs rely on Kantorovich–Rubinstein duality formulas for W_1 . Thus, it remains an open problem to establish stability estimates for the prior-to-posterior map using the stronger Wasserstein-2 distance, $d = W_2$. There has been some recent progress addressing this issue for the data-to-posterior map [276]. Yet, stability bounds in the Wasserstein-2 distance for the prior-to-posterior map would hold particular relevance for uncertainty quantification because $W_2(\mu^y, \nu^y)$ also controls the distance between the posterior covariance operators.

Although $d = d_0 = W_1$ is challenging to satisfy, there are many settings in which we nonetheless wish for $d = d_0$ in (5.26) to hold. For example, this assumption is especially useful when applying the stability estimate iteratively to a time-indexed sequence of Bayesian inverse problems [62, 236]. By relaxing W_1 to the *Dudley metric*, also referred to as the bounded Lipschitz distance, we show that $d = d_0$ becomes achievable under minimal assumptions.

The bounded Lipschitz distance is an integral probability metric defined as

$$d_{BL}(\mu, \nu) := \sup_{\|f\|_{BL} \leq 1} |\mu(f) - \nu(f)|, \quad \text{where } \|f\|_{BL} := \max(\|f\|_{L^\infty}, \text{Lip}(f)) \quad (5.28)$$

for any probability measures μ and ν . We recall that $\text{Lip}(f) = \sup_{u \neq v} |f(u) - f(v)| / \|u - v\|$. The distance d_{BL} metrizes the topology of weak convergence [80]. Local Lipschitz

stability in Dudley's metric has been established in previous work [266, 267]. However, we present a more quantitative version tailored for inverse problems that is inspired by prior work [272, Remark 5.2, p. 39].

For brevity, we define $\mathsf{L}^y(u) := \exp(-\Phi(u; y))$ from (2.4). We now state the following local Lipschitz continuity result.

Proposition 1 (prior-to-posterior local Lipschitz stability in Dudley metric). *Fix y and let μ^y and ν^y be posteriors corresponding to priors μ and ν , respectively, according to (2.4). If the likelihood function L^y is globally Lipschitz continuous and there exists a constant $b^y > 0$ such that $0 \leq \mathsf{L}^y \leq b^y$ everywhere, then*

$$\mathsf{d}_{\text{BL}}(\mu^y, \nu^y) \leq \left(\frac{2b^y + 2 \text{Lip}(\mathsf{L}^y)}{\max(Z_\mu^y, Z_\nu^y)} \right) \mathsf{d}_{\text{BL}}(\mu, \nu). \quad (5.29)$$

We provide the proof of Proposition 1 below, which is prototypical of how other basic results of the prior-to-posterior type (5.26) are established (see, e.g., [34, Thm. 4.6, p. 43] or [270, Thm. 8, p. 11]).

Proof. Except where required, we ignore all dependence on y for notational convenience. Let f satisfy $\|f\|_{\text{BL}} \leq 1$. By the definition (2.4) of posterior,

$$\begin{aligned} \mu^y(f) - \nu^y(f) &= \frac{\mu(f\mathsf{L})}{\mu(\mathsf{L})} - \frac{\nu(f\mathsf{L})}{\nu(\mathsf{L})} \\ &= \frac{\mu(f\mathsf{L}) - \nu(f\mathsf{L})}{\mu(\mathsf{L})} + \nu^y(f) \left(\frac{\nu(\mathsf{L}) - \mu(\mathsf{L})}{\mu(\mathsf{L})} \right) \\ &\leq \frac{1}{\mu(\mathsf{L})} \left[|\mu(f\mathsf{L}) - \nu(f\mathsf{L})| + |\mu(\mathsf{L}) - \nu(\mathsf{L})| \right] \end{aligned}$$

because $|f| \leq 1$ everywhere and ν^y is a probability measure. Next, since $\|f\|_{\text{BL}} \leq 1$, it holds that $|f\mathsf{L}| \leq b$ and

$$\begin{aligned} |f(u)\mathsf{L}(u) - f(v)\mathsf{L}(v)| &\leq |f(u)\mathsf{L}(u) - f(u)\mathsf{L}(v)| + |f(u)\mathsf{L}(v) - f(v)\mathsf{L}(v)| \\ &\leq |\mathsf{L}(u) - \mathsf{L}(v)| + b|f(u) - f(v)| \\ &\leq (\text{Lip}(\mathsf{L}) + b)\|u - v\|. \end{aligned}$$

Thus, $\|f\mathsf{L}\|_{\text{BL}} \leq \max(b, b + \text{Lip}(\mathsf{L})) = b + \text{Lip}(\mathsf{L})$. We also have $\|\mathsf{L}\|_{\text{BL}} \leq \max(b, \text{Lip}(\mathsf{L}))$. We deduce using (5.28) that

$$\begin{aligned} |\mu^y(f) - \nu^y(f)| &\leq \frac{(b + \text{Lip}(\mathsf{L}))\mathsf{d}_{\text{BL}}(\mu, \nu) + \max(b, \text{Lip}(\mathsf{L}))\mathsf{d}_{\text{BL}}(\mu, \nu)}{\mu(\mathsf{L})} \\ &\leq \frac{2b + 2\text{Lip}(\mathsf{L})}{\mu(\mathsf{L})} \mathsf{d}_{\text{BL}}(\mu, \nu) \end{aligned}$$

uniformly in f . Since $\mu(\mathsf{L}) = Z_\mu^y$, the assertion (5.29) follows by symmetry. \square

Remark 1. The hypotheses of [Proposition 1](#) are quite mild. For example, if \mathcal{Y} is finite-dimensional, then a Gaussian likelihood satisfies the assumptions on \mathcal{L}^y . Moreover, it is easy to generalize the proof of [Proposition 1](#) if the likelihood functional \mathcal{L}^y is only Hölder continuous instead of Lipschitz continuous.

Weak metrics such as d_{BL} and W_p are particularly well-suited for data-driven prior learning because these distances remain meaningful even when the two input distributions are mutually singular. In contrast, statistical divergences such as TV, KL, and Hellinger attain their maximum value when the measures are mutually singular. This issue often arises in practice because a finite training dataset can lead to an approximate prior that is mutually singular with respect to the reference prior. For instance, using the empirical measure as an estimator results in discrete mismatched support, while employing the closest Gaussian approximation to the reference prior yields a degenerate covariance operator. More fundamentally, in infinite-dimensional spaces, probability measures tend to be mutually singular. As an illustrative example, we refer to the Feldman–Hajek equivalence theorem for Gaussian measures [57, Thm. 6.13, p. 531].

Results such as [Proposition 1](#) provide *consistency* in the following sense. Suppose that the observed data samples are drawn from a “true” prior and that we can consistently estimate this prior using a data-driven method. Consequently, [Proposition 1](#) shows that we can achieve consistency in the resulting posteriors, even if the estimated prior is mutually singular with respect to the true prior.

Insights from linear regularization analysis

Theoretical analyses of regularizer learning for linear inverse problems in infinite dimensions have recently gained attention, with notable developments presented in [138, 277–280]. This line of research is more naturally situated within the nonparametric statistical setting described in [Section 2.1.3](#), as opposed to the functional-analytic viewpoint of [Section 2.2](#) or the Bayesian perspective in [Section 2.1.1](#). However, the research in this direction can still be related to Bayesian inference by interpreting variational point estimators as either the mean or MAP point of an underlying posterior distribution. Such a connection will be made clear in the following discussions. Regardless of viewpoint, the probabilistic models for the parameters and observed data in the inverse problem play a major role in the theoretical insights that are unveiled, as we now explain.

To fix the notation, let \mathcal{U} and \mathcal{Y} be real separable Hilbert spaces. Consider the inverse problem of finding an unknown parameter $u \in \mathcal{U}$ from observed data y , where u and y are related by

$$y = \mathcal{A}u + \eta. \quad (5.30)$$

Here, η denotes additive noise corrupting the observation, as in [\(2.1\)](#), except now the forward operator $\mathcal{A}: \mathcal{U} \rightarrow \mathcal{Y}$ is assumed to be linear, continuous, injective, and *fully known*. Now departing from the setting of [Section 4.3.3](#), we provide a description of the statistical structure of [\(5.30\)](#). We model u as a \mathcal{U} -valued random vector with mean

and covariance denoted by

$$\bar{u} := \mathbb{E} u \quad \text{and} \quad \Sigma := \mathbb{E}[(u - \bar{u}) \otimes_{\mathcal{U}} (u - \bar{u})], \quad (5.31)$$

respectively. Similarly, we model η as a zero-mean \mathcal{Y} -indexed stochastic process with a continuous covariance operator $\Gamma: \mathcal{Y} \rightarrow \mathcal{Y}$, independent of u . We assume that Σ and Γ are both strictly positive definite for simplicity.

One can associate to (5.30) the *generalized Tikhonov reconstruction operator* $\mathcal{R}_{h,B}^{\Gamma}: \mathcal{Y} \rightarrow \mathcal{U}$ defined by

$$y \mapsto \mathcal{R}_{h,B}^{\Gamma}(y) := \arg \min_{u \in \mathcal{U}} \{d_{\Gamma}^2(y, \mathcal{A}u) + \|B^{-1}(u - h)\|_{\mathcal{U}}^2\}. \quad (5.32)$$

The element $h \in \mathcal{U}$ is a centering parameter for u . The continuous linear operator $B \in \mathcal{L}(\mathcal{U}; \mathcal{U})$ penalizes the smoothness of u . We interpret the second term on the right-hand side of (5.32) as being equal to $+\infty$ if $(u - h) \notin \text{Ran}(B)$. The first term can be interpreted formally as $\|\Gamma^{-1/2}(y - \mathcal{A}u)\|_{\mathcal{Y}}^2$, but such an expression is infinite almost surely if \mathcal{Y} is infinite-dimensional. To address this, the actual discrepancy function d_{Γ} captures the technical modifications needed to ensure that (5.32) is well-defined [277, Sec. 2]. We emphasize that d_{Γ} depends on the covariance operator Γ of the noise, which is assumed known. Thus, $\mathcal{R}_{h,B}^{\Gamma}$ itself depends on the inherent noise level in the observations.

Due to the possibility of a nonzero h , the map $\mathcal{R}_{h,B}^{\Gamma}$ is affine rather than linear. Its closed-form expression is provided in [277, Sec. 2, p. 5]. The associated calculations are similar to those used to establish that the posterior distribution for a linear Gaussian Bayesian inverse problem in an infinite-dimensional setting (for both data and parameters) is well-defined [67]. However, it is important to emphasize that no Gaussian assumptions are made in the current context.

Alberti et al. [277] rigorously characterize the average-case optimal generalized Tikhonov regularizer in terms of the covariance structure assumed on the unknown parameter u . To this end, let (h^*, B^*) be the optimal pair minimizing the expected squared reconstruction error

$$\mathbb{E}_{(u,y) \sim \nu} \|u - \mathcal{R}_{h,B}^{\Gamma}(y)\|_{\mathcal{U}}^2. \quad (5.33)$$

The expectation is taken with respect to the joint distribution $\nu := \text{Law}(u, y)$ of the random variable (u, y) under (5.30). Under minor technical assumptions, the unique global minimizer of (5.33) is $(h^*, B^*) = (\bar{u}, \Sigma^{1/2})$ [277, Thm. 3.1, p. 6]. Notably, even though (5.33) depends on the full joint distribution ν —and hence the forward map \mathcal{A} —the optimal solution *only depends* on the first two moments of the marginal law of u . The technical contributions leading to this result are substantial, as they require careful analysis to handle the infinite-dimensional noise process η and regularized inverses of compact operators.

It is also possible to develop finite-sample estimators for the problem (5.33) if only a dataset of i.i.d. pairs $\{(u_n, y_n)\}_{n=1}^N$ from ν is available. Because the optimal Tikhonov regularizer (h^*, B^*) is known to be the mean and square root covariance of the random

variable u , a natural *unsupervised* strategy is first to compute the empirical mean \hat{u} and empirical covariance $\hat{\Sigma}$ from the training data, then define the plug-in estimator $(\hat{h}, \hat{B}) := (\hat{u}, \hat{\Sigma}^{1/2})$. Assuming that u is strongly-subgaussian, application of tools from covariance estimation [277, Thm. 4.2, p. 8, and p. 29] deliver the nonasymptotic error bound

$$\mathbb{E} \left[\mathbb{E}_{(u,y) \sim \nu} \|u - R_{\hat{h}, \hat{B}}^{\Gamma}(y)\|_{\mathcal{U}}^2 \right] \leq \mathbb{E}_{(u,y) \sim \nu} \|u - R_{h^*, B^*}^{\Gamma}(y)\|_{\mathcal{U}}^2 + \frac{C}{\sqrt{N}} \quad (5.34)$$

for some $C > 0$. The first expectation on the left-hand side of (5.34) is taken with respect to the randomness in the finite sample set $\{(u_n, y_n)\}_{n=1}^N$. The C/\sqrt{N} term corresponds to a “slow” nonparametric rate for the excess error because a fast rate for squared error would instead approach $1/N$. It would be interesting to explore the optimality of the derived rate in (5.34).

Alternatively, a fully supervised training strategy based on minimizing an empirical approximation to (5.33) gives similar convergence guarantees in theory [277, Thm. 4.1, p. 7], but empirically demonstrates worse performance than the unsupervised approach. However, suppose the Tikhonov regularizer is replaced by a more general regularizer, such as a sparsity-promoting one [278]. In that case, the supervised learning strategy becomes necessary because closed-form expressions for the optimal (h^*, B^*) are no longer available. The resulting finite-sample analysis also becomes more difficult, requiring advanced tools from statistical learning theory [280].

Although the preceding discussion characterizes the optimal Tikhonov regularizer (h^*, B^*) from a linear operator learning perspective, it does not comment on the *accuracy* of the corresponding reconstruction map $\mathcal{R}_{h^*, B^*}^{\Gamma}$. This requires understanding under what conditions $\|u - R_{h^*, B^*}^{\Gamma}(\mathcal{A}u + \eta)\|_{\mathcal{U}} \rightarrow 0$ as $\Gamma \rightarrow 0$ in an appropriate sense. Combined with (5.34), such a result would also imply convergence for the estimator $\mathcal{R}_{\hat{h}, \hat{B}}^{\Gamma}$. To carry out this consistency analysis, it is instructive to work in a setup in which $\mathcal{A}^* \mathcal{A}$ and Σ , together with $\mathcal{A} \mathcal{A}^*$ and Γ , are simultaneously diagonalizable. This should be compared to a similar approach used to develop sharp convergence rates for forward operator learning [148].

At the center of the analysis is the SVD of the compact injective forward operator \mathcal{A} , which we expand as

$$\mathcal{A} = \sum_{j=1}^{\infty} \sigma_j e_j \otimes_{\mathcal{U}} \phi_j. \quad (5.35)$$

The singular values $\{\sigma_j\}_{j \in \mathbb{N}} \subset \mathbb{R}_{>0}$ of \mathcal{A} are ordered to be nonincreasing and assumed to each have multiplicity one. The $\{\phi_j\}_{j \in \mathbb{N}}$ form an ONB of \mathcal{U} and $\{e_j\}_{j \in \mathbb{N}}$ form an ONB of \mathcal{Y} . Using these SVD bases, we further assume that

$$\Sigma = \sum_{j=1}^{\infty} \varsigma_j \phi_j \otimes_{\mathcal{U}} \phi_j \quad \text{and} \quad \Gamma = \delta^2 \sum_{j=1}^{\infty} \gamma_j e_j \otimes_{\mathcal{Y}} e_j, \quad (5.36)$$

which delivers simultaneous diagonalizability with the normal operators corresponding to \mathcal{A} . The eigenvalues $\{\varsigma_j\}_{j \in \mathbb{N}}$ and $\{\delta^2 \gamma_j\}_{j \in \mathbb{N}}$ from (5.36) are nonincreasing sequences. We assume that $\gamma_1 = 1$ [138, Sec. 2.2]. The parameter $\delta > 0$ in (5.36) serves as a noise level. It will be convenient to define $\xi := \eta/\delta$. The covariance operator of ξ is $\sum_{j=1}^{\infty} \gamma_j e_j \otimes_{\mathcal{Y}} e_j$. We also assume that $\mathbb{E} u = \bar{u} = 0$.

Based on the SVD from (5.35), *spectral reconstruction operators* regularize the pseudoinverse of \mathcal{A} by only approximately inverting the singular values. Define the spectral reconstruction operator $\mathcal{R}_{\psi}: \mathcal{Y} \rightarrow \mathcal{U}$ by

$$\mathcal{R}_{\psi} := \sum_{j=1}^{\infty} \psi_j \phi_j \otimes_{\mathcal{Y}} e_j, \quad (5.37)$$

where $\psi := \{\psi_j\}_{j \in \mathbb{N}} \subset \mathbb{R}_{\geq 0}$ is a sequence of filtering coefficients—allowed to depend on \mathcal{A} —such that $\psi_j \approx 1/\sigma_j$ [138]. One can then ask what the optimal choice of ψ is with respect to the expected squared error (5.33) [279].

To answer this question, we adopt the common approach of diagonalizing the equation (5.30) into a sequence space model in the SVD bases of \mathcal{A} [67, 83, 148]. This delivers the sequence of decoupled scalar linear inverse problems

$$\langle y, e_j \rangle = \sigma_j \langle u, \phi_j \rangle + \delta \langle \xi, e_j \rangle \quad \text{for all } j \in \mathbb{N}. \quad (5.38)$$

Due to (5.38) and the definitions in (5.36), it holds that

$$\mathbb{E}_{(u,y) \sim \nu} \|u - \mathcal{R}_{\psi} y\|_{\mathcal{U}}^2 = \sum_{j=1}^{\infty} \left[(1 - \sigma_j \psi_j)^2 \varsigma_j + \delta^2 \gamma_j \psi_j^2 \right]. \quad (5.39)$$

Thus, the minimization of (5.39) over the whole sequence $\{\psi_j\}_{j \in \mathbb{N}}$ decouples into scalar minimization problems for each individual ψ_j . The minimizers are

$$\psi_j(\delta) := \frac{\sigma_j}{\sigma_j^2 + \frac{\delta^2 \gamma_j}{\varsigma_j}} \quad \text{for all } j \in \mathbb{N}, \quad (5.40)$$

which is seen by explicitly solving the quadratic program. Writing $\psi(\delta) := \{\psi_j(\delta)\}_{j \in \mathbb{N}}$, the optimal spectral regularizer is then $\mathcal{R}_{\psi(\delta)}$.

Under the simultaneous diagonalizability assumption (5.36) and the condition $\bar{u} = h^* = 0$, by comparing to [277, Eqn. (12), p. 5] when written in the SVD bases (5.35) of \mathcal{A} , we find that $\mathcal{R}_{\psi(\delta)} = \mathcal{R}_{h^*, B^*}^{\Gamma}$ [138, Remark 2, p. 49]. That is, the optimal spectral regularizer—which did not enforce an explicit smoothness penalization—is *identical to* the optimal Tikhonov regularizer, which does enforce a quadratic penalty. It is interesting that Tikhonov structure *emerges* in the optimal spectral reconstruction as a consequence of the additive noise model (5.30) and the expected squared reconstruction error objective function (5.39). This finding is consistent with known results for finite-dimensional nonlinear regression [129, 281].

A heuristic explanation for this phenomenon in the current linear infinite-dimensional setup is as follows. The optimal generalized Tikhonov reconstruction

(5.32) implicitly computes the MAP point of a Gaussian posterior μ^y determined by a Gaussian likelihood $\mathcal{N}(\mathcal{A}u, \Gamma)$ and Gaussian prior $\mathcal{N}(0, \Sigma)$, which match the first two moments of $\text{Law}(y | u)$ and $\text{Law}(u)$, respectively. This immediately shows that the optimal Tikhonov reconstruction is the posterior mean $\mathbb{E}_{u \sim \mu^y}[u]$ of μ^y , agreeing with known formulas [67, Prop. 3.1, p. 2630]. To relate back to the optimal spectral regularizer, one would have to argue that since \mathcal{R}_ψ is linear in ψ and y is linearly related to u in expectation, the minimizer of (5.39) over ψ (i.e., linear maps) should equal the Gaussian posterior mean instead of the Bayes estimator $\mathbb{E}[u | y]$. However, a proper proof based on this intuition in the present infinite-dimensional setting is beyond the scope of the chapter.

We close this subsection by summarizing accuracy guarantees for the optimal spectral regularizer $\mathcal{R}_{\psi(\delta)}$. The preceding discussion implies that consistency of learned spectral regularization is equivalent to consistency of the Gaussian posterior mean estimator. Consistency of the latter is well known [67, 69]. Under mild distributional assumptions, more direct arguments [279, Thm. 1, p. 1351] establish the pointwise average-case convergence

$$\lim_{\delta \rightarrow 0} \mathbb{E}_{\xi \sim \text{Law}(\xi)} \|\mathcal{A}^{-1}y - \mathcal{R}_{\psi(\delta)}(y + \delta\xi)\|_{\mathcal{U}}^2 = 0 \quad \text{for all } y \in \text{Ran}(\mathcal{A}). \quad (5.41)$$

Compare this result with (4.36), which gives pointwise worst-case convergence. The convergence in (5.41) is actually uniform over certain bounded sets of noise distributions with noise level at most δ and covariance Γ ; see [138, Eqn. (2.8), p. 48]. Going beyond pointwise error, we also have the full mean square convergence

$$\lim_{\delta \rightarrow 0} \mathbb{E}_{(u, \xi) \sim \text{Law}(u, \xi)} \|u - \mathcal{R}_{\psi(\delta)}(\mathcal{A}u + \delta\xi)\|_{\mathcal{U}}^2 = 0. \quad (5.42)$$

By using well-established Bayesian theory, it should also be possible to obtain *quantitative* convergence rates as $\delta \rightarrow 0$ under suitable decay conditions on the singular values of all the involved operators [67]. The misspecified case, in which the noise distribution in the training data possibly differs from the one used to compute the squared reconstruction error, has also been handled [138]. In all cases, the diagonal analysis suggests that choosing the training data to be corrupted by white noise (i.e., $\gamma_j = 1$ for all j) leads to better convergence properties for solving the inverse problem. This message is consistent with a related insight for forward linear operator learning in the following sense. In [148, Corollary 3.6, pp. 17–18], it was observed that training data $\{y_n\}$ corrupted with white noise worsens convergence rates for learning the forward operator. Since the forward problem becomes harder, the inverse problem intuitively becomes easier as claimed.

Beyond the mean square optimal estimator (5.40), the preceding spectral regularization framework has also been combined with plug-and-play estimators [138, Sec. 4]. We will overview such plug-and-play methods next.

5.2. Denoising networks and plug-and-play methods

A major breakthrough in bridging model-based and learning-based approaches to inverse problems was the realization that powerful denoisers—including neural networks trained to denoise corrupted signals—implicitly encode high-quality priors. Plug-and-play (PnP) methods capitalize on this insight by integrating pre-trained image denoising networks into iterative optimization algorithms as implicit regularizers. Instead of explicitly specifying a prior through a regularization functional R , PnP methods replace the proximal step in classical algorithms such as the alternating direction method of multipliers (ADMM) or proximal gradient descent with a learned denoiser \mathcal{D} . In the following, we briefly review the latest developments in PnP. [Section 5.2.1](#) introduces the PnP framework and [Section 5.2.2](#) surveys existing theoretical guarantees for the framework.

5.2.1. Motivation for PnP

To motivate PnP, consider a composite objective function

$$\mathcal{J}(u) = f(u) + R(u), \quad (5.43)$$

where f represents a data-fidelity term and R is a possibly non-smooth regularizer. In classical variational approaches, proximal methods play a central role in handling non-smooth regularization. The proximal operator associated with R is defined by

$$y \mapsto \text{prox}_R(y) = \arg \min_{u \in \mathcal{U}} \left\{ \frac{1}{2} \|y - u\|_{\mathcal{U}}^2 + R(u) \right\}. \quad (5.44)$$

Comparing (5.44) to (2.20), we observe that $\text{prox}_R(y)$ precisely computes the variational regularization solution of a linear inverse problem with identity forward map, i.e., denoising, under a least-squares misfit and regularizer R . The proximal operation also has a natural Bayesian interpretation: it computes the MAP estimate under a Gaussian likelihood centered at y and a prior distribution with density proportional to $\exp(-R)$.

In proximal gradient descent (PGD), the iteration for minimizing \mathcal{J} takes the form

$$u_{k+1} = \text{prox}_R(u_k - s_k \nabla f(u_k)) \quad (5.45)$$

for each k , where $s_k > 0$ is a step size. PnP methods modify this framework by replacing the proximal operator with a denoising operator $\mathcal{D}: \mathcal{U} \rightarrow \mathcal{U}$, which implicitly encodes prior knowledge. That is, the update rule becomes

$$u_{k+1} = \mathcal{D}(u_k - s_k \nabla f(u_k)), \quad (5.46)$$

where \mathcal{D} may be a pre-trained convolutional neural network (CNN), neural operator, or any other denoiser. In this formulation, \mathcal{D} implicitly serves as a *learned proximal operator* that regularizes the solution to lie on a manifold of natural images or signals learned from the training data.

The original formulation of PnP was introduced by Venkatakrishnan et al. [282] in the context of ADMM and using the classical BM3D denoiser. This idea was later extended to incorporate deep learning-based denoisers, including CNNs [283]. More generally, each PnP iteration computes the fixed point of an operator that combines the forward model—appearing in the data-fidelity term f —with the denoiser, which acts as a prior. This has close connections to deep equilibrium architectures that are also based on fixed-point iterations [284].

In the language of operator learning, the denoiser is viewed as a learned nonlinear map $\mathcal{D}: \mathcal{U} \rightarrow \mathcal{U}$ that is trained to model the structure of realistic signals. For example, in the case of a linear forward map $\mathcal{G}(u) = \mathcal{A}u$ and quadratic data fidelity $f(u) := \frac{1}{2}\|\mathcal{A}u - y\|_2^2$, the PnP iteration becomes

$$u_{k+1} = \mathcal{D}(u_k - s_k \mathcal{A}^*(\mathcal{A}u_k - y)) . \quad (5.47)$$

This formulation embeds a learned operator into an iterative algorithm that solves an inverse problem governed by the forward operator \mathcal{A} .

Subsequent developments in the PnP framework have focused on theoretical analysis (including fixed-point convergence), stability, and the implicit regularization properties of the denoiser. These investigations aim to understand the conditions under which such iterations are well-posed and whether they yield solutions consistent with the underlying inverse problem in the limit of vanishing noise.

5.2.2. Theoretical analysis of PnP

The theoretical understanding of PnP methods has advanced considerably. There is a growing focus on identifying conditions under which a learned denoiser \mathcal{D} can be reliably embedded into iterative optimization or sampling algorithms for solving inverse problems. Broadly, these developments can be categorized into four areas: convergence analysis, proximal structure, probabilistic interpretations, and control of regularization strength.

Convergence via nonexpansiveness and monotonicity

A foundational line of work views the denoiser \mathcal{D} as a nonexpansive Lipschitz-continuous operator. Ryu et al. [285] proves that if \mathcal{D} is strictly nonexpansive, i.e., $\text{Lip}(\mathcal{D}) < 1$, then PnP-ADMM and PnP-FBS (forward-backward splitting) converge to a fixed point without requiring vanishing step sizes. The key idea is that the overall update becomes a contraction under suitable step-size conditions. Belkouchi et al. [286] employ monotone operator theory to analyze PnP iterations. They show that if \mathcal{D} is the resolvent of a monotone operator, then fixed-point iterations converge under Tseng's splitting scheme. This analysis links learned operators to classical monotone inclusions, which broadens the class of denoisers for which convergence guarantees hold.

Learned proximal structure

Another direction seeks to design denoisers that are explicit proximal operators. Fang et al. [287] introduce Learned Proximal Networks (LPNs), in which \mathcal{D} is trained to

be the gradient of a convex function, i.e., $\mathcal{D} = \nabla\phi$ for some convex ϕ . This implies that $\mathcal{D} = \text{prox}_R$ is a proximal map of a convex regularizer R . It further allows PnP iterations to be interpreted as classical PGD or ADMM updates whose convergence is inherited from convex optimization theory. Pesquet et al. [288] propose learning resolvent operators directly. In this setting, a universal approximation theorem holds: any nonexpansive neural network can approximate the resolvent of a maximally monotone operator. This result connects learned denoisers to variational analysis by showing that even when the underlying regularizer is unknown, a denoiser with resolvent structure ensures convergence and interpretability.

Probabilistic and sampling-based extensions

A complementary line of work reframes PnP as a probabilistic inference method. Bouman et al. [289] introduce Generative PnP (GPnP), which transforms deterministic PnP iterations into a Markov chain by replacing each update with a stochastic proximal generator. The resulting dynamics sample from the Bayesian posterior distribution, thus providing both point estimates and uncertainty quantification. Wu et al. [38] demonstrate that any inverse problem can be reformulated as a Gaussian image denoising task. This allows one to embed pretrained diffusion models within lightweight MCMC schemes, thereby integrating score-based generative models into the PnP framework. In this setting, denoisers serve as approximations to the score function. They enable posterior sampling via Langevin dynamics or stochastic proximal steps.

Regularization control and stability

Recent theoretical contributions establish that PnP methods can serve as convergent regularization schemes in the classical sense: reconstructions remain stable in the presence of noise and converge to the true solution of the inverse problem as the noise level decreases [124, 125]. Ebner and Haltmeier [290] prove this result for a family of PnP methods with denoisers tailored to the noise level. Hauptmann et al. [265] provide the first complete regularization theory for PnP with linear denoisers. By introducing a tunable spectral filter into the denoiser, it is shown that the resulting iterations form a Tikhonov-type regularization scheme. As the measurement noise δ goes to zero, the iterates converge to the exact minimizer of a well-defined variational problem and classical convergence rates are recovered under realistic assumptions. Khelifa et al. [291] propose Tweedie scaling, which introduces a single tunable parameter to rescale any pretrained denoiser. This parameter allows precise control over the strength of the implicit regularization, guarantees convergence of PnP-PGD, and improves empirical performance on tasks such as inpainting and denoising. The Tweedie scaling approach provides a systematic mechanism for adjusting the influence of the prior.

6. Conclusion and outlook

This chapter surveys recent advances in the use of operator learning as a tool to solve inverse problems. The intersection of these two fields is particularly powerful when unknown parameters are infinite-dimensional and the forward map requires solving

a partial differential equation. Two complementary paradigms emerge in this subject area. The first is an end-to-end approach that uses operator learning to directly invert for unknown parameters or Bayesian posteriors given new observations. This strategy replaces traditional inverse problem solvers with neural operator models that are trained on noisy data-parameter pairs. The most popular operator learning architectures enjoy theoretical approximation guarantees for a few specific inverse problems. New architectures that are more adapted to the ill-posed character of inverse problems have been proposed, but are less established theoretically. The second framework is more modular. Instead of emulating the entire inverse map, this approach invokes operator learning to selectively estimate priors, regularizers, or denoisers within conventional inversion algorithms. This results in a principled blending of data-driven components with structure encoded by the forward map. Consequently, the nature of the regularization introduced by these hybrid data-driven methods is better understood than that of fully learned inverse maps. By adopting a probabilistic perspective, the chapter unifies both paradigms and invites further mathematical development in this rapidly evolving field.

A distinctive feature of this chapter is its emphasis on measure-centric formulations of inverse problems and their compatibility with operator learning. Although the chapter takes a first step in merging both ideas, for example, by connecting DeepSets to Neural Inverse Operators for inverse boundary value problems, there is still a need for basic theoretical development. Core well-posedness questions regarding existence, uniqueness, and stability largely remain unanswered for inverse problems in the space of probability measures. Novel distribution-based operator learning architectures lack guarantees when applied to measure-valued data. Just as importantly, the deployment of measure-based operator learning in scientific inverse problems involving noisy, real-world experimental data would greatly elevate the impact and relevance of the field.

Sequential Bayesian inverse problems in data assimilation [62, 236] are an application where the probabilistic and measure-centric principles advocated by this chapter are highly relevant. Existing accurate algorithms are hindered in practice by the computational expense of repeatedly applying Bayes' rule to update prior to posterior. Recent work shows the promise of combining operator learning with measure transport to capture complex mean-field distribution dependence in filtering problems [34, 95, 241, 292–294]. Despite this encouraging progress toward overcoming the computational barriers associated with sequential Bayesian inference in dynamical systems, the underlying mathematical theory and design of measure-based architectures demand further investigation.

Recent cautionary work draws attention to adversarial instabilities, poor interpretability, and overfitting in learned inverse solvers, particularly in high-dimensional imaging tasks [295–299]. These limitations underscore the need for theory that clarifies when and why operator learning can deliver both accurate and stable solutions to ill-posed problems. To be more impactful, such a theory will have to go beyond the current approach of performing a case-by-case analysis for each individual inverse problem. As advocated by [300], methodological innovation in out-of-distribution detection and uncertainty quantification (UQ) will bolster trust of data-driven inversion methods.

Regarding the former, preliminary work shows that a careful design of the training data distribution can make learned maps robust to distribution shifts [166]. For the latter, probabilistic inversion methods already deliver UQ. However, the modeling uncertainty inherent in learned inverse maps or regularizers must also be accounted for in the UQ framework. One possible way to achieve this is to use the uncertainty from operator learning to improve the quality of Bayesian inversion [274, 301].

Funding. N.H.N. is supported by the U.S. National Science Foundation (NSF) under award DMS-2402036 and by a Klarman Fellowship through Cornell University’s College of Arts & Sciences. Y.Y. is partially supported by NSF award DMS-2409855.

Acknowledgments. The authors thank Maarten de Hoop, Bamdad Hosseini, Matti Lassas, Youssef Marzouk, Richard Nickl, and Andrew Stuart for numerous discussions that helped to shape this chapter. The authors are also grateful to Nicolas Guerra for helpful comments on a previous version of the manuscript.

References

- [1] Hadamard, J.: Sur les problèmes aux dérivées partielles et leur signification physique. *Princeton University Bulletin*, 49–52 (1902) (cited on pp. 3 and 5)
- [2] Lucas, A., Iliadis, M., Molina, R., Katsaggelos, A.K.: Using deep neural networks for inverse problems in imaging: beyond analytical methods. *IEEE Signal Processing Magazine* **35**(1), 20–36 (2018) (cited on p. 3)
- [3] McCann, M.T., Jin, K.H., Unser, M.: Convolutional neural networks for inverse problems in imaging: A review. *IEEE Signal Processing Magazine* **34**(6), 85–95 (2017) (not cited)
- [4] Ongie, G., Jalal, A., Metzler, C.A., Baraniuk, R.G., Dimakis, A.G., Willett, R.: Deep learning techniques for inverse problems in imaging. *IEEE Journal on Selected Areas in Information Theory* **1**(1), 39–56 (2020) (cited on p. 3)
- [5] Ovadia, O., Kahana, A., Stinis, P., Turkel, E., Givoli, D., Karniadakis, G.E.: ViTP: Vision transformer-operator. *Computer Methods in Applied Mechanics and Engineering* **428** (2024) (cited on pp. 3 and 20)
- [6] Cho, S.W., Son, H.: Physics-informed deep inverse operator networks for solving PDE inverse problems. In: The Thirteenth International Conference on Learning Representations (2025) (cited on p. 23)
- [7] Jiang, X., Wang, X., Wen, Z., Wang, H.: Resolution-independent generative models based on operator learning for physics-constrained Bayesian inverse problems. *Computer Methods in Applied Mechanics and Engineering* **420** (2024) (not cited)

[8] Jiao, A., Yan, Q., Harlim, J., Lu, L.: Solving forward and inverse PDE problems on unknown manifolds via physics-informed neural operators. preprint arXiv:2407.05477 (2024) (cited on p. 23)

[9] Kaltenbach, S., Perdikaris, P., Koutsourelakis, P.-S.: Semi-supervised invertible neural operators for Bayesian inverse problems. *Computational Mechanics* **72**(3), 451–470 (2023) (cited on p. 23)

[10] Long, D., Xu, Z., Yuan, Q., Yang, Y., Zhe, S.: Invertible Fourier neural operators for tackling both forward and inverse problems. In: *International Conference on Artificial Intelligence and Statistics*, pp. 3043–3051 (2025). PMLR (cited on p. 23)

[11] Gao, Z., Yan, L., Zhou, T.: Adaptive operator learning for infinite-dimensional Bayesian inverse problems. *SIAM/ASA Journal on Uncertainty Quantification* **12**(4), 1389–1423 (2024) (cited on pp. 18 and 42)

[12] Guo, R., Jiang, J.: Construct deep neural networks based on direct sampling methods for solving electrical impedance tomography. *SIAM Journal on Scientific Computing* **43**(3), 678–711 (2021) (cited on p. 6)

[13] Guo, R., Cao, S., Chen, L.: Transformer meets boundary value inverse problems. In: *The Eleventh International Conference on Learning Representations* (2023) (cited on pp. 6 and 20)

[14] Wang, T., Wang, C.: Latent neural operator for solving forward and inverse PDE problems. In: *Advances in Neural Information Processing Systems*, vol. 37, pp. 33085–33107 (2024) (not cited)

[15] Yang, Y., Gao, A.F., Castellanos, J.C., Ross, Z.E., Azizzadenesheli, K., Clayton, R.W.: Seismic wave propagation and inversion with neural operators. *The Seismic Record* **1**(3), 126–134 (2021) (not cited)

[16] Yang, Y., Gao, A.F., Azizzadenesheli, K., Clayton, R.W., Ross, Z.E.: Rapid seismic waveform modeling and inversion with neural operators. *IEEE Transactions on Geoscience and Remote Sensing* **61**, 1–12 (2023) (not cited)

[17] Zhang, R.Z., Xie, X., Lowengrub, J.S.: BiLO: Bilevel local operator learning for PDE inverse problems. preprint arXiv:2404.17789 (2024) (cited on p. 23)

[18] Zhang, Z., Liu, H., Liao, W., Lin, G.: Coefficient-to-basis network: A fine-tunable operator learning framework for inverse problems with adaptive discretizations and theoretical guarantees. preprint arXiv:2503.08642 (2025) (cited on p. 3)

[19] Chen, Y., Hosseini, B., Owhadi, H., Stuart, A.M.: Solving and learning nonlinear PDEs with Gaussian processes. *Journal of Computational Physics* **447** (2021) (cited on p. 3)

[20] Raissi, M., Perdikaris, P., Karniadakis, G.: Physics-informed neural networks: A deep learning framework for solving forward and inverse problems involving nonlinear partial differential equations. *Journal of Computational physics* **378**, 686–707 (2019) (cited on p. 3)

[21] Burman, E., Larson, M.G., Larsson, K., Lundholm, C.: Stabilizing and solving inverse problems using data and machine learning. preprint arXiv:2412.04409 (2024) (cited on p. 3)

[22] Cao, L., O’Leary-Roseberry, T., Ghattas, O.: Derivative-informed neural operator acceleration of geometric MCMC for infinite-dimensional Bayesian inverse problems. *Journal of Machine Learning Research* **26**(78), 1–68 (2025) (not cited)

[23] Herrmann, L., Schwab, C., Zech, J.: Deep neural network expression of posterior expectations in bayesian PDE inversion. *Inverse Problems* **36**(12) (2020) (not cited)

[24] Li, Z., Kovachki, N.B., Azizzadenesheli, K., Liu, B., Bhattacharya, K., Stuart, A.M., Anandkumar, A.: Fourier neural operator for parametric partial differential equations. *International Conference on Learning Representations* (2021) (cited on p. 22)

[25] Li, Z., Zheng, H., Kovachki, N.B., Jin, D., Chen, H., Liu, B., Azizzadenesheli, K., Anandkumar, A.: Physics-informed neural operator for learning partial differential equations. *ACM/JMS Journal of Data Science* **1**(3), 1–27 (2024) (cited on pp. 22, 23, and 25)

[26] Lunz, S., Hauptmann, A., Tarvainen, T., Schönlieb, C.-B., Arridge, S.: On learned operator correction in inverse problems. *SIAM Journal on Imaging Sciences* **14**(1), 92–127 (2021) (cited on p. 23)

[27] Wu, K., O’Leary-Roseberry, T., Chen, P., Ghattas, O.: Large-scale Bayesian optimal experimental design with derivative-informed projected neural network. *Journal of Scientific Computing* **95**(1) (2023) (not cited)

[28] Zhou, T., Wan, X., Huang, D.Z., Li, Z., Peng, Z., Anandkumar, A., Brady, J.F., Sternberg, P.W., Daraio, C.: AI-aided geometric design of anti-infection catheters. *Science Advances* **10**(1) (2024) (cited on p. 3)

[29] Helin, T., Stuart, A.M., Teckentrup, A.L., Zygalakis, K.C.: Introduction to gaussian process regression in bayesian inverse problems, with new results on experimental design for weighted error measures. In: Hinrichs, A., Kritzer, P., Pillichshammer, F. (eds.) *Monte Carlo and Quasi-Monte Carlo Methods*, pp. 49–79. Springer (2024) (cited on p. 4)

[30] Lie, H.C., Sullivan, T.J., Teckentrup, A.L.: Random forward models and log-likelihoods in Bayesian inverse problems. *SIAM/ASA Journal on Uncertainty*

Quantification **6**(4), 1600–1629 (2018) (not cited)

- [31] Stuart, A., Teckentrup, A.: Posterior consistency for Gaussian process approximations of Bayesian posterior distributions. *Mathematics of Computation* **87**(310), 721–753 (2018) (not cited)
- [32] Cao, L., O’Leary-Roseberry, T., Jha, P.K., Oden, J.T., Ghattas, O.: Residual-based error correction for neural operator accelerated infinite-dimensional Bayesian inverse problems. *Journal of Computational Physics* **486** (2023) (not cited)
- [33] Cao, L., Chen, J., Brennan, M., O’Leary-Roseberry, T., Marzouk, Y., Ghattas, O.: LazyDINO: Fast, scalable, and efficiently amortized Bayesian inversion via structure-exploiting and surrogate-driven measure transport. preprint arXiv:2411.12726 (2024) (cited on p. 4)
- [34] Bach, E., Baptista, R., Sanz-Alonso, D., Stuart, A.M.: Inverse problems and data assimilation: A machine learning approach. preprint arXiv:2410.10523 (2024) (cited on pp. 4, 10, 42, 45, 52, and 61)
- [35] Ho, J., Jain, A., Abbeel, P.: Denoising diffusion probabilistic models. In: *Advances in Neural Information Processing Systems*, vol. 33, pp. 6840–6851 (2020) (cited on p. 4)
- [36] Song, Y., Sohl-Dickstein, J., Kingma, D.P., Kumar, A., Ermon, S., Poole, B.: Score-based generative modeling through stochastic differential equations. In: *International Conference on Learning Representations* (2021) (cited on p. 49)
- [37] Sun, Y., Wu, Z., Chen, Y., Feng, B.T., Bouman, K.L.: Provable probabilistic imaging using score-based generative priors. *IEEE Transactions on Computational Imaging* (2024) (not cited)
- [38] Wu, Z., Sun, Y., Chen, Y., Zhang, B., Yue, Y., Bouman, K.: Principled probabilistic imaging using diffusion models as plug-and-play priors. In: *Advances in Neural Information Processing Systems*, vol. 37, pp. 118389–118427 (2024) (cited on pp. 4 and 60)
- [39] Lipman, Y., Chen, R.T., Ben-Hamu, H., Nickel, M., Le, M.: Flow matching for generative modeling. In: *The Eleventh International Conference on Learning Representations* (2022) (cited on p. 4)
- [40] Albergo, M.S., Vanden-Eijnden, E.: Building normalizing flows with stochastic interpolants. In: *The Eleventh International Conference on Learning Representations* (2023) (cited on p. 4)
- [41] Albergo, M.S., Boffi, N.M., Vanden-Eijnden, E.: Stochastic interpolants: A unifying framework for flows and diffusions. preprint arXiv:2303.08797 (2023) (not cited)

cited)

- [42] Chen, Y., Goldstein, M., Hua, M., Albergo, M.S., Boffi, N.M., Vanden-Eijnden, E.: Probabilistic Forecasting with Stochastic Interpolants and Föllmer Processes. In: International Conference on Machine Learning, pp. 6728–6756 (2024). PMLR (cited on p. 4)
- [43] Cheney, M., Isaacson, D., Newell, J.C.: Electrical impedance tomography. SIAM Review **41**(1), 85–101 (1999) (cited on p. 5)
- [44] Agnelli, J.P., Cöl, A., Lassas, M., Murthy, R., Santacesaria, M., Siltanen, S.: Classification of stroke using neural networks in electrical impedance tomography. Inverse Problems **36**(11) (2020) (cited on p. 6)
- [45] Bui-Thanh, T., Li, Q., Zepeda-Núñez, L.: Bridging and improving theoretical and computational electrical impedance tomography via data completion. SIAM Journal on Scientific Computing **44**(3), 668–693 (2022) (cited on p. 6)
- [46] Beretta, E., Deng, M., Gandolfi, A., Jin, B.: The discrete inverse conductivity problem solved by the weights of an interpretable neural network. Journal of Computational Physics (2025) (not cited)
- [47] Colibazzi, F., Lazzaro, D., Morigi, S., Samoré, A.: Learning nonlinear electrical impedance tomography. Journal of Scientific Computing **90**(1) (2022) (not cited)
- [48] Fan, Y., Ying, L.: Solving electrical impedance tomography with deep learning. Journal of Computational Physics **404** (2020) (cited on p. 30)
- [49] Hamilton, S.J., Hauptmann, A.: Deep D-bar: Real-time electrical impedance tomography imaging with deep neural networks. IEEE Transactions on Medical Imaging **37**(10), 2367–2377 (2018) (cited on p. 23)
- [50] Hamilton, S.J., Hänninen, A., Hauptmann, A., Kolehmainen, V.: Beltrami-net: domain-independent deep D-bar learning for absolute imaging with electrical impedance tomography (a-EIT). Physiological Measurement **40**(7) (2019) (not cited)
- [51] Tanyu, D.N., Ning, J., Hauptmann, A., Jin, B., Maass, P.: Electrical impedance tomography: A fair comparative study on deep learning and analytic-based approaches. In: Bubba, T.A. (ed.) Data-driven Models in Inverse Problems, pp. 437–470. Walter de Gruyter GmbH & Co KG (2024). Chap. 13 (not cited)
- [52] Knudsen, K., Lassas, M., Mueller, J.L., Siltanen, S.: Regularized D-bar method for the inverse conductivity problem. Inverse Problems and Imaging **35**(4) (2009) (cited on pp. 6 and 23)
- [53] Calderón, A.P.: On an inverse boundary value problem. Computational &

Applied Mathematics **25**, 133–138 (2006) (cited on p. 6)

- [54] Mueller, J.L., Siltanen, S.: Linear and Nonlinear Inverse Problems with Practical Applications. SIAM (2012) (cited on pp. 6, 14, 23, and 37)
- [55] Alessandrini, G.: Stable determination of conductivity by boundary measurements. *Applicable Analysis* **27**(1-3), 153–172 (1988) (cited on pp. 7 and 37)
- [56] Calvetti, D., Somersalo, E.: Inverse problems: From regularization to Bayesian inference. *Wiley Interdisciplinary Reviews: Computational Statistics* **10**(3) (2018) (cited on p. 7)
- [57] Stuart, A.M.: Inverse problems: a Bayesian perspective. *Acta Numerica* **19**, 451–559 (2010) (cited on pp. 8, 9, 39, and 53)
- [58] Nickl, R.: Bayesian Non-linear Statistical Inverse Problems. EMS Press Berlin (2023) (cited on pp. 8, 9, and 26)
- [59] Agapiou, S., Larsson, S., Stuart, A.M.: Posterior contraction rates for the Bayesian approach to linear ill-posed inverse problems. *Stochastic Processes and Their Applications* **123**(10), 3828–3860 (2013) (cited on pp. 8 and 9)
- [60] Dashti, M., Stuart, A.M.: The Bayesian approach to inverse problems. In: Ghanem, R., Higdon, D., Owhadi, H. (eds.) *Handbook of Uncertainty Quantification*, pp. 311–428. Springer (2017) (cited on pp. 8, 9, and 45)
- [61] Cotter, S.L., Roberts, G.O., Stuart, A.M., White, D.: MCMC methods for functions: modifying old algorithms to make them faster. *Statistical Science*, 424–446 (2013) (cited on p. 8)
- [62] Sanz-Alonso, D., Stuart, A.M., Taeb, A.: Inverse Problems and Data Assimilation vol. 107. Cambridge University Press (2023) (cited on pp. 8, 12, 45, 51, and 61)
- [63] Nickl, R., Wang, S.: On polynomial-time computation of high-dimensional posterior measures by Langevin-type algorithms. *Journal of the European Mathematical Society* **26**(3), 1031–1112 (2022) (cited on p. 9)
- [64] Agapiou, S., Stuart, A.M., Zhang, Y.-X.: Bayesian posterior contraction rates for linear severely ill-posed inverse problems. *Journal of Inverse and Ill-posed Problems* **22**(3), 297–321 (2014) (cited on pp. 9 and 10)
- [65] Agapiou, S., Castillo, I.: Heavy-tailed Bayesian nonparametric adaptation. *The Annals of Statistics* **52**(4), 1433–1459 (2024) (not cited)
- [66] Gugushvili, S., Vaart, A., Yan, D.: Bayesian linear inverse problems in regularity scales. *Annales de l’Institut Henri Poincaré-Probabilités et Statistiques* **56**(3), 2081–2107 (2020) (not cited)

[67] Knapik, B.T., Van Der Vaart, A.W., Zanten, J.H.: Bayesian inverse problems with Gaussian priors. *Annals of Statistics* **39**(5), 2626–2657 (2011) (cited on pp. 54, 56, and 57)

[68] Knapik, B.T., Szabó, B.T., Van Der Vaart, A.W., Zanten, J.H.: Bayes procedures for adaptive inference in inverse problems for the white noise model. *Probability Theory and Related Fields* **164**, 771–813 (2016) (not cited)

[69] Knapik, B., Salomond, J.-B.: A general approach to posterior contraction in nonparametric inverse problems. *Bernoulli* **24**(3), 2091–2121 (2018) (cited on p. 57)

[70] Ray, K.: Bayesian inverse problems with non-conjugate priors. *Electronic Journal of Statistics* **7**, 2516–2549 (2013) (not cited)

[71] Trabs, M.: Bayesian inverse problems with unknown operators. *Inverse Problems* **34**(8) (2018) (cited on p. 9)

[72] Monard, F., Nickl, R., Paternain, G.P.: Statistical guarantees for Bayesian uncertainty quantification in nonlinear inverse problems with Gaussian process priors. *The Annals of Statistics* **49**(6), 3255–3298 (2021) (cited on p. 9)

[73] Nickl, R., Pavliotis, G.A., Ray, K.: Bayesian nonparametric inference in McKean–Vlasov models. *The Annals of Statistics* **53**(1), 170–193 (2025) (cited on p. 9)

[74] Abraham, K., Nickl, R.: On statistical Calderón problems. *Mathematical Statistics and Learning* **2**(2), 165–216 (2020) (cited on pp. 9, 11, and 34)

[75] Giordano, M., Nickl, R.: Consistency of Bayesian inference with Gaussian process priors in an elliptic inverse problem. *Inverse Problems* **36**(8) (2020) (not cited)

[76] Nickl, R., Geer, S., Wang, S.: Convergence rates for penalized least squares estimators in PDE constrained regression problems. *SIAM/ASA Journal on Uncertainty Quantification* **8**(1), 374–413 (2020) (cited on p. 11)

[77] Nickl, R.: Bernstein–von Mises theorems for statistical inverse problems I: Schrödinger equation. *Journal of the European Mathematical Society* **22**(8), 2697–2750 (2020) (cited on p. 9)

[78] Huang, D.Z., Nelsen, N.H., Trautner, M.: An operator learning perspective on parameter-to-observable maps. *Foundations of Data Science* **7**(1), 163–225 (2025) (cited on pp. 9, 20, 22, 28, and 29)

[79] Marzouk, Y.M., Moseley, T., Parno, M., Spantini, A.: Sampling via measure transport: An introduction. In: *Handbook of Uncertainty Quantification*, pp.

1–41. Springer (2016) (cited on pp. 10, 15, and 43)

[80] Villani, C.: Optimal Transport: Old and New vol. 338. Springer (2009) (cited on pp. 10 and 51)

[81] Hosseini, B., Hsu, A.W., Taghvaei, A.: Conditional optimal transport on function spaces. *SIAM/ASA Journal on Uncertainty Quantification* **13**(1), 304–338 (2025) (cited on pp. 10, 43, and 44)

[82] Baptista, R., Hosseini, B., Kovachki, N.B., Marzouk, Y.M.: Conditional sampling with monotone GANs: From generative models to likelihood-free inference. *SIAM/ASA Journal on Uncertainty Quantification* **12**(3), 868–900 (2024) (cited on pp. 10, 43, and 44)

[83] Cavalier, L.: Nonparametric statistical inverse problems. *Inverse Problems* **24**(3) (2008) (cited on pp. 10, 11, and 56)

[84] Bissantz, N., Hohage, T., Munk, A., Ruymgaart, F.: Convergence rates of general regularization methods for statistical inverse problems and applications. *SIAM Journal on Numerical Analysis* **45**(6), 2610–2636 (2007) (not cited)

[85] Kaipio, J.P., Somersalo, E.: Statistical and Computational Inverse Problems. Springer (2005) (not cited)

[86] Kaipio, J., Somersalo, E.: Statistical inverse problems: discretization, model reduction and inverse crimes. *Journal of Computational and Applied Mathematics* **198**(2), 493–504 (2007) (cited on p. 10)

[87] Bissantz, N., Hohage, T., Munk, A.: Consistency and rates of convergence of nonlinear Tikhonov regularization with random noise. *Inverse Problems* **20**(6), 1773 (2004) (cited on p. 11)

[88] Blanchard, G., Mücke, N.: Optimal rates for regularization of statistical inverse learning problems. *Foundations of Computational Mathematics* **18**(4), 971–1013 (2018) (cited on p. 11)

[89] Helin, T.: Least squares approximations in linear statistical inverse learning problems. *SIAM Journal on Numerical Analysis* **62**(4), 2025–2047 (2024) (cited on p. 11)

[90] Panaretos, V.M., Zemel, Y.: An Invitation to Statistics in Wasserstein Space. Springer (2020) (cited on p. 11)

[91] Khurana, V.: Learning on the space of probability measures. PhD thesis, University of California, San Diego (2024) (not cited)

[92] Geshkovski, B., Letrouit, C., Polyanskiy, Y., Rigollet, P.: A mathematical perspective on transformers. *Bulletin of the American Mathematical Society* **62**(3),

427–479 (2025) (cited on p. 31)

- [93] Oprea, M., Townsend, A., Yang, Y.: The distributional Koopman operator for random dynamical systems. preprint arXiv:2504.11643 (2025) (not cited)
- [94] Huang, H., Lai, R.: Unsupervised solution operator learning for mean-field games. *Journal of Computational Physics* **537** (2025) (cited on pp. 11 and 31)
- [95] Bach, E., Baptista, R., Calvello, E., Chen, B., Stuart, A.M.: Learning enhanced ensemble filters. preprint arXiv:2504.17836 (2025) (cited on pp. 11, 20, 31, and 61)
- [96] Haviv, D., Pooladian, A.-A., Pe'er, D., Amos, B.: Wasserstein flow matching: Generative modeling over families of distributions. In: *Forty-second International Conference on Machine Learning* (2025) (cited on p. 11)
- [97] Qi, C.R., Su, H., Mo, K., Guibas, L.J.: PointNet: Deep learning on point sets for 3D classification and segmentation. In: *Proceedings of the IEEE Conference on Computer Vision and Pattern Recognition*, pp. 652–660 (2017) (cited on pp. 11 and 31)
- [98] Bredies, K., Pikkarainen, H.K.: Inverse problems in spaces of measures. *ESAIM: Control, Optimisation and Calculus of Variations* **19**(1), 190–218 (2013) (cited on p. 11)
- [99] Botvinick-Greenhouse, J.: Invariant measures for data-driven dynamical system identification: Analysis and application. preprint arXiv:2502.05204 (2025) (not cited)
- [100] Li, Q., Wang, L., Yang, Y.: Differential equation–constrained optimization with stochasticity. *SIAM/ASA Journal on Uncertainty Quantification* **12**(2), 549–578 (2024) (cited on pp. 15 and 23)
- [101] Yang, Y., Nurbekyan, L., Negrini, E., Martin, R., Pasha, M.: Optimal transport for parameter identification of chaotic dynamics via invariant measures. *SIAM Journal on Applied Dynamical Systems* **22**(1), 269–310 (2023) (not cited)
- [102] Li, Q., Oprea, M., Wang, L., Yang, Y.: Inverse problems over probability measure space. preprint arXiv:2504.18999 (2025) (cited on pp. 15 and 23)
- [103] Butler, T., Estep, D., Sandelin, J.: A computational measure theoretic approach to inverse sensitivity problems II: A posteriori error analysis. *SIAM Journal on Numerical Analysis* **50**(1), 22–45 (2012) (cited on pp. 11 and 14)
- [104] Jin, R., Guerra, M., Li, Q., Wright, S.: Optimal design for linear models via gradient flow. preprint arXiv:2401.07806 (2024) (cited on p. 11)
- [105] Jin, R., Li, Q., Mussmann, S.O., Wright, S.J.: Continuous nonlinear adaptive experimental design with gradient flow. preprint arXiv:2411.14332 (2024) (not cited)

cited)

- [106] Huan, X., Jagalur, J., Marzouk, Y.: Optimal experimental design: Formulations and computations. *Acta Numerica* **33**, 715–840 (2024) (cited on pp. 11 and 42)
- [107] Akyildiz, O.D., Girolami, M., Stuart, A.M., Vadeboncoeur, A.: Efficient prior calibration from indirect data. *SIAM Journal on Scientific Computing* **47**(4), 932–958 (2025) (cited on pp. 11, 12, 13, 15, and 46)
- [108] Vadeboncoeur, A., Girolami, M., Stuart, A.M.: Efficient deconvolution in populational inverse problems. preprint arXiv:2505.19841 (2025) (cited on pp. 11, 12, 13, and 15)
- [109] Dunlop, M.M., Stuart, A.M.: The Bayesian formulation of EIT: Analysis and algorithms. *Inverse Problems and Imaging* **10**(4), 1007–1036 (2016) (cited on pp. 14, 37, and 39)
- [110] Breidt, J., Butler, T., Estep, D.: A measure-theoretic computational method for inverse sensitivity problems I: Method and analysis. *SIAM Journal on Numerical Analysis* **49**(5), 1836–1859 (2011) (cited on p. 14)
- [111] Butler, T., Estep, D., Tavener, S., Dawson, C., Westerink, J.J.: A measure-theoretic computational method for inverse sensitivity problems III: Multiple quantities of interest. *SIAM/ASA Journal on Uncertainty Quantification* **2**(1), 174–202 (2014) (cited on p. 14)
- [112] Butler, T., Jakeman, J., Wildey, T.: Combining push-forward measures and Bayes’ rule to construct consistent solutions to stochastic inverse problems. *SIAM Journal on Scientific Computing* **40**(2), 984–1011 (2018) (cited on p. 14)
- [113] Butler, T., Yen, T.Y.: Data-consistent inversion for stochastic input-to-output maps. *Inverse Problems* **36**(8) (2020) (not cited)
- [114] Butler, T., Jakeman, J., Pilosov, M., Walsh, S., Wildey, T.: Optimal experimental design criteria for data-consistent inversion. preprint arXiv:2506.12157 (2025) (not cited)
- [115] Bergstrom, K.O., Butler, T.D., Wildey, T.M.: A distributions-based approach for data-consistent inversion. *SIAM Journal on Scientific Computing* **46**(5), 3124–3150 (2024) (cited on p. 14)
- [116] Li, Q., Oprea, M., Wang, L., Yang, Y.: Stochastic Inverse Problem: stability, regularization and Wasserstein gradient flow. preprint arXiv:2410.00229 (2024) (cited on p. 15)
- [117] Bingham, D., Butler, T., Estep, D.: Inverse problems for physics-based process models. *Annual Review of Statistics and Its Application* **11** (2024) (cited on

p. 15)

- [118] Baptista, R., Marzouk, Y., Zahm, O.: On the representation and learning of monotone triangular transport maps. *Foundations of Computational Mathematics* **24**(6), 2063–2108 (2024) (cited on pp. 15 and 43)
- [119] El Moselhy, T.A., Marzouk, Y.M.: Bayesian inference with optimal maps. *Journal of Computational Physics* **231**(23), 7815–7850 (2012) (cited on pp. 15 and 43)
- [120] Chewi, S., Niles-Weed, J., Rigollet, P.: Wasserstein gradient flows: Applications. In: *Statistical Optimal Transport: École d’Été de Probabilités de Saint-Flour XLIX–2019*, pp. 151–186. Springer (2025) (cited on p. 15)
- [121] Chewi, S., Niles-Weed, J., Rigollet, P.: Wasserstein gradient flows: Theory. In: *Statistical Optimal Transport: École d’Été de Probabilités de Saint-Flour XLIX–2019*, pp. 121–149. Springer (2025) (cited on p. 15)
- [122] White, R.D., Jakeman, J.D., Wildey, T., Butler, T.: Building population-informed priors for Bayesian inference using data-consistent stochastic inversion. preprint arXiv:2407.13814 (2024) (cited on p. 15)
- [123] Espinosa, D.S., Thiede, E.H., Yang, Y.: Cryo-EM as a Stochastic Inverse Problem. Forthcoming (2025) (cited on p. 15)
- [124] Engl, H.W., Hanke, M., Neubauer, A.: *Regularization of Inverse Problems* vol. 375. Springer (1996) (cited on pp. 15, 49, and 60)
- [125] Benning, M., Burger, M.: Modern regularization methods for inverse problems. *Acta Numerica* **27**, 1–111 (2018) (cited on pp. 15 and 60)
- [126] Haber, E., Ascher, U.M., Oldenburg, D.: On optimization techniques for solving nonlinear inverse problems. *Inverse Problems* **16**(5) (2000) (cited on p. 15)
- [127] Groetsch, C.: The theory of Tikhonov regularization for Fredholm equations. Boston Pitman Publication **104** (1984) (cited on p. 16)
- [128] Golub, G.H., Hansen, P.C., O’Leary, D.P.: Tikhonov regularization and total least squares. *SIAM Journal on Matrix Analysis and Applications* **21**(1), 185–194 (1999) (not cited)
- [129] Bishop, C.M.: Training with noise is equivalent to Tikhonov regularization. *Neural Computation* **7**(1), 108–116 (1995) (cited on pp. 16, 28, and 56)
- [130] Rudin, L.I., Osher, S., Fatemi, E.: Nonlinear total variation based noise removal algorithms. *Physica D: Nonlinear Phenomena* **60**(1-4), 259–268 (1992) (cited on p. 16)

- [131] Osher, S., Burger, M., Goldfarb, D., Xu, J., Yin, W.: An iterative regularization method for total variation-based image restoration. *Multiscale Modeling & Simulation* **4**(2), 460–489 (2005) (not cited)
- [132] Chan, T.F., Esedoglu, S.: Aspects of total variation regularized l^1 function approximation. *SIAM Journal on Applied Mathematics* **65**(5), 1817–1837 (2005) (cited on p. 16)
- [133] Bredies, K., Kunisch, K., Pock, T.: Total generalized variation. *SIAM Journal on Imaging Sciences* **3**(3), 492–526 (2010) (cited on p. 16)
- [134] Lou, Y., Zhang, X., Osher, S., Bertozzi, A.: Image recovery via nonlocal operators. *Journal of Scientific Computing* **42**(2), 185–197 (2010) (not cited)
- [135] Zhang, X., Burger, M., Bresson, X., Osher, S.: Bregmanized nonlocal regularization for deconvolution and sparse reconstruction. *SIAM Journal on Imaging Sciences* **3**(3), 253–276 (2010) (not cited)
- [136] Zhang, J., Chen, K.: A total fractional-order variation model for image restoration with nonhomogeneous boundary conditions and its numerical solution. *SIAM Journal on Imaging Sciences* **8**(4), 2487–2518 (2015) (cited on p. 16)
- [137] Chirinos-Rodríguez, J., De Vito, E., Molinari, C., Rosasco, L., Villa, S.: On learning the optimal regularization parameter in inverse problems. *Inverse Problems* **40**(12) (2024) (cited on pp. 16 and 44)
- [138] Burger, M., Kabri, S.: Learned regularization for inverse problems: insights from a spectral model. In: Bubba, T.A. (ed.) *Data-driven Models in Inverse Problems*, pp. 39–72. Walter de Gruyter GmbH & Co KG (2024). Chap. 2 (cited on pp. 16, 53, 56, and 57)
- [139] Duff, M., Campbell, N.D., Ehrhardt, M.J.: Regularising inverse problems with generative machine learning models. *Journal of Mathematical Imaging and Vision* **66**(1), 37–56 (2024) (not cited)
- [140] Arridge, S., Maass, P., Öktem, O., Schönlieb, C.-B.: Solving inverse problems using data-driven models. *Acta Numerica* **28**, 1–174 (2019) (cited on pp. 16, 45, and 49)
- [141] Habring, A., Holler, M.: Neural-network-based regularization methods for inverse problems in imaging. *GAMM-Mitteilungen* **47**(4) (2024) (cited on p. 16)
- [142] Ulyanov, D., Vedaldi, A., Lempitsky, V.: Deep image prior. In: *Proceedings of the IEEE Conference on Computer Vision and Pattern Recognition*, pp. 9446–9454 (2018) (cited on p. 16)
- [143] Feng, B.T., Smith, J., Rubinstein, M., Chang, H., Bouman, K.L., Freeman,

W.T.: Score-based diffusion models as principled priors for inverse imaging. In: Proceedings of the IEEE/CVF International Conference on Computer Vision, pp. 10520–10531 (2023) (cited on p. 16)

[144] Chung, H., Kim, J., McCann, M.T., Klasky, M.L., Ye, J.C.: Diffusion posterior sampling for general noisy inverse problems. In: 11th International Conference on Learning Representations (2023) (not cited)

[145] Daras, G., Chung, H., Lai, C.-H., Mitsufuji, Y., Ye, J.C., Milanfar, P., Dimakis, A.G., Delbracio, M.: A survey on diffusion models for inverse problems. preprint arXiv:2410.00083 (2024) (not cited)

[146] Tolooshams, B., Chandrashekhar, A., Zirvi, R., Mammadov, A., Yao, J., Wang, C., Anandkumar, A.: EquiReg: Equivariance Regularized Diffusion for Inverse Problems. preprint arXiv:2505.22973 (2025) (cited on p. 16)

[147] Kovachki, N.B., Li, Z., Liu, B., Azizzadenesheli, K., Bhattacharya, K., Stuart, A.M., Anandkumar, A.: Neural operator: Learning maps between function spaces with applications to PDEs. *Journal of Machine Learning Research* **24**(89), 1–97 (2023) (cited on pp. 17, 20, 21, and 22)

[148] Hoop, M.V., Kovachki, N.B., Nelsen, N.H., Stuart, A.M.: Convergence rates for learning linear operators from noisy data. *SIAM/ASA Journal on Uncertainty Quantification* **11**(2), 480–513 (2023) (cited on pp. 17, 19, 20, 39, 55, 56, and 57)

[149] Mollenhauer, M., Mücke, N., Sullivan, T.: Learning linear operators: Infinite-dimensional regression as a well-behaved non-compact inverse problem. preprint arXiv:2211.08875 (2022) (cited on pp. 20 and 39)

[150] Lu, F., Lang, Q., An, Q.: Data adaptive RKHS Tikhonov regularization for learning kernels in operators. In: Mathematical and Scientific Machine Learning, pp. 158–172 (2022). PMLR (cited on p. 17)

[151] Nelsen, N.H.: Statistical foundations of operator learning. PhD thesis, California Institute of Technology (2024) (cited on pp. 17 and 19)

[152] De Vito, E., Rosasco, L., Caponnetto, A., De Giovannini, U., Odone, F., Bartlett, P.: Learning from examples as an inverse problem. *Journal of Machine Learning Research* **6**(5) (2005) (cited on p. 17)

[153] Caponnetto, A., De Vito, E.: Optimal rates for the regularized least-squares algorithm. *Foundations of Computational Mathematics* **7**, 331–368 (2007) (cited on p. 17)

[154] Rosasco, L., Belkin, M., De Vito, E.: On learning with integral operators. *Journal of Machine Learning Research* **11**(2), 905–934 (2010) (not cited)

[155] Smale, S., Zhou, D.-X.: Learning theory estimates via integral operators and their approximations. *Constructive Approximation* **26**(2), 153–172 (2007) (cited on p. 17)

[156] Boullé, N., Earls, C.J., Townsend, A.: Data-driven discovery of Green's functions with human-understandable deep learning. *Scientific Reports* **12**(1) (2022) (cited on pp. 17 and 20)

[157] Boullé, N., Kim, S., Shi, T., Townsend, A.: Learning Green's functions associated with time-dependent partial differential equations. *Journal of Machine Learning Research* **23**(218), 1–34 (2022) (not cited)

[158] Boullé, N., Townsend, A.: Learning elliptic partial differential equations with randomized linear algebra. *Foundations of Computational Mathematics* **23**(2), 709–739 (2023) (cited on p. 20)

[159] Boullé, N., Townsend, A.: A mathematical guide to operator learning. In: *Handbook of Numerical Analysis* vol. 25, pp. 83–125. Elsevier (2024) (cited on pp. 17, 18, 19, and 25)

[160] Chada, N.K., Lang, Q., Lu, F., Wang, X.: A data-adaptive RKHS prior for Bayesian learning of kernels in operators. *Journal of Machine Learning Research* **25**(317), 1–37 (2024) (cited on p. 17)

[161] Lu, F., An, Q., Yu, Y.: Nonparametric learning of kernels in nonlocal operators. *Journal of Peridynamics and Nonlocal Modeling* **6**(3), 347–370 (2024) (not cited)

[162] Zhang, S., Wang, X., Lu, F.: Minimax rate for learning kernels in operators. preprint arXiv:2502.20368 (2025) (cited on p. 17)

[163] Kovachki, N.B., Lanthaler, S., Stuart, A.M.: Operator learning: Algorithms and analysis. *Handbook of Numerical Analysis* **25**, 419–467 (2024) (cited on pp. 17, 19, and 20)

[164] Subedi, U., Tewari, A.: Operator learning: A statistical perspective. preprint arXiv:2504.03503 (2025) (cited on pp. 17 and 19)

[165] Boullé, N., Halikias, D., Townsend, A.: Elliptic PDE learning is provably data-efficient. *Proceedings of the National Academy of Sciences* **120**(39) (2023) (cited on pp. 18, 20, and 42)

[166] Guerra, N., Nelsen, N.H., Yang, Y.: Learning where to learn: Training distribution selection for provable OOD performance. preprint arXiv:2505.21626 (2025) (cited on pp. 19, 25, 32, and 62)

[167] Subedi, U., Tewari, A.: On the benefits of active data collection in operator learning. In: *Forty-Second International Conference on Machine Learning* (2025)

(not cited)

- [168] Satheesh, A., Khandelwal, A., Ding, M., Balan, R.: PICore: Physics-Informed Unsupervised Coreset Selection for Data Efficient Neural Operator Training. preprint arXiv:2507.17151 (2025) (cited on pp. 18 and 42)
- [169] Nelsen, N.H., Stuart, A.M.: Operator learning using random features: A tool for scientific computing. *SIAM Review* **66**(3), 535–571 (2024) (cited on pp. 19 and 20)
- [170] Schäfer, F., Owhadi, H.: Sparse recovery of elliptic solvers from matrix-vector products. *SIAM Journal on Scientific Computing* **46**(2), 998–1025 (2024) (cited on p. 20)
- [171] Batlle, P., Darcy, M., Hosseini, B., Owhadi, H.: Kernel methods are competitive for operator learning. *Journal of Computational Physics* **496** (2024) (cited on pp. 19 and 20)
- [172] Lanthaler, S., Li, Z., Stuart, A.M.: Nonlocality and nonlinearity implies universality in operator learning. *Constructive Approximation*, 1–43 (2025) (cited on pp. 19, 20, and 22)
- [173] Cao, S.: Choose a transformer: Fourier or Galerkin. In: *Advances in Neural Information Processing Systems*, vol. 34, pp. 24924–24940 (2021) (cited on pp. 20 and 23)
- [174] Geshkovski, B., Rigollet, P., Ruiz-Balet, D.: Measure-to-measure interpolation using transformers. preprint arXiv:2411.04551 (2024) (cited on p. 31)
- [175] Calvello, E., Kovachki, N.B., Levine, M.E., Stuart, A.M.: Continuum attention for neural operators. preprint arXiv:2406.06486 (2024) (cited on p. 20)
- [176] Nelsen, N.H., Stuart, A.M.: The random feature model for input-output maps between Banach spaces. *SIAM Journal on Scientific Computing* **43**(5), 3212–3243 (2021) (cited on pp. 20 and 50)
- [177] Boullé, N., Halikias, D., Otto, S.E., Townsend, A.: Operator learning without the adjoint. *Journal of Machine Learning Research* **25**(364), 1–54 (2024) (cited on pp. 20 and 42)
- [178] Lanthaler, S., Mishra, S., Karniadakis, G.E.: Error estimates for DeepONets: A deep learning framework in infinite dimensions. *Transactions of Mathematics and Its Applications* **6**(1) (2022) (cited on pp. 20 and 35)
- [179] Lanthaler, S.: Operator learning with PCA-Net: upper and lower complexity bounds. *Journal of Machine Learning Research* **24**(318), 1–67 (2023) (cited on p. 20)

[180] Bunker, J., Girolami, M., Lambley, H., Stuart, A.M., Sullivan, T.: Autoencoders in function space. preprint arXiv:2408.01362 (2024) (cited on pp. 20 and 28)

[181] Bhattacharya, K., Hosseini, B., Kovachki, N.B., Stuart, A.M.: Model reduction and neural networks for parametric PDEs. *The SMAI Journal of Computational Mathematics* **7**, 121–157 (2021) (cited on pp. 20, 21, and 41)

[182] Liu, H., Yang, H., Chen, M., Zhao, T., Liao, W.: Deep nonparametric estimation of operators between infinite dimensional spaces. *Journal of Machine Learning Research* **25**(24), 1–67 (2024) (cited on p. 20)

[183] Kovachki, N.B., Lanthaler, S., Mhaskar, H.: Data complexity estimates for operator learning. preprint arXiv:2405.15992 (2024) (cited on pp. 20 and 22)

[184] Lu, L., Jin, P., Pang, G., Zhang, Z., Karniadakis, G.E.: Learning nonlinear operators via DeepONet based on the universal approximation theorem of operators. *Nature Machine Intelligence* **3**(3), 218–229 (2021) (cited on p. 20)

[185] Chen, T., Chen, H.: Universal approximation to nonlinear operators by neural networks with arbitrary activation functions and its application to dynamical systems. *IEEE Transactions on Neural Networks* **6**(4), 911–917 (1995) (cited on p. 20)

[186] Petersen, P., Zech, J.: Mathematical theory of deep learning. preprint arXiv:2407.18384 (2024) (cited on p. 20)

[187] Tretiakov, S., Li, X., Kumar, K.: SetONet: A Deep Set-based Operator Network for Solving PDEs with permutation invariant variable input sampling. preprint arXiv:2505.04738 (2025) (cited on pp. 20 and 32)

[188] Reiss, M., Wahl, M.: Nonasymptotic upper bounds for the reconstruction error of PCA. *The Annals of Statistics* **48**(2), 1098–1123 (2020) (cited on p. 21)

[189] Kossaifi, J., Kovachki, N.B., Azizzadenesheli, K., Anandkumar, A.: Multi-grid tensorized Fourier neural operator for high- resolution PDEs. *Transactions on Machine Learning Research*, 1–27 (2024) (cited on p. 22)

[190] Lanthaler, S., Stuart, A.M., Trautner, M.: Discretization error of Fourier neural operators. preprint arXiv:2405.02221 (2024) (cited on p. 22)

[191] Li, Z., Huang, D.Z., Liu, B., Anandkumar, A.: Fourier neural operator with learned deformations for PDEs on general geometries. *Journal of Machine Learning Research* **24**(388), 1–26 (2023) (cited on p. 22)

[192] Kovachki, N.B., Lanthaler, S., Mishra, S.: On universal approximation and error bounds for Fourier neural operators. *Journal of Machine Learning Research* **22**(290), 1–76 (2021) (cited on p. 22)

- [193] Cardot, H., Crambes, C., Kneip, A., Sarda, P.: Smoothing splines estimators in functional linear regression with errors-in-variables. *Computational Statistics & Data Analysis* **51**(10), 4832–4848 (2007) (cited on p. 23)
- [194] Patel, R., Manickam, I., Lee, M., Gulian, M.: Error-in-variables modelling for operator learning. In: *Mathematical and Scientific Machine Learning*, pp. 142–157 (2022). PMLR (not cited)
- [195] Zhou, S., Pati, D., Wang, T., Yang, Y., Carroll, R.J.: Gaussian processes with errors in variables: Theory and computation. preprint arXiv:1910.06235 (2019) (cited on p. 23)
- [196] de Hoop, M.V., Lassas, M., Wong, C.A.: Deep learning architectures for non-linear operator functions and nonlinear inverse problems. *Mathematical Statistics and Learning* **4**(1), 1–86 (2022) (cited on pp. 23, 26, 30, 31, 33, and 37)
- [197] Nguyen, H.V., Bui-Thanh, T.: TNet: A model-constrained Tikhonov network approach for inverse problems. *SIAM Journal on Scientific Computing* **46**(1), 77–100 (2024) (cited on pp. 23 and 27)
- [198] Pineda, A.F.L., Petersen, P.C.: Deep neural networks can stably solve high-dimensional, noisy, non-linear inverse problems. *Analysis and Applications* **21**(1), 49–91 (2023) (cited on pp. 23, 26, 27, 33, 38, and 39)
- [199] Ren, K., Zhang, L.: A model-consistent data-driven computational strategy for PDE joint inversion problems. *Journal of Computational Physics* (2025) (cited on p. 23)
- [200] Ding, W., Ren, K., Zhang, L.: Coupling deep learning with full waveform inversion. preprint arXiv:2203.01799 (2022) (not cited)
- [201] Jin, P., Zhang, X., Chen, Y., Huang, S.X., Liu, Z., Lin, Y.: Unsupervised learning of full-waveform inversion: Connecting CNN and partial differential equation in a loop. In: *10th International Conference on Learning Representations* (2022) (cited on p. 23)
- [202] Ghattas, O., Willcox, K.: Learning physics-based models from data: perspectives from inverse problems and model reduction. *Acta Numerica* **30**, 445–554 (2021) (cited on p. 23)
- [203] Ardizzone, L., Kruse, J., Rother, C., Köthe, U.: Analyzing inverse problems with invertible neural networks. In: *International Conference on Learning Representations* (2019) (cited on p. 23)
- [204] Arndt, C., Denker, A., Dittmer, S., Heilenkötter, N., Iske, M., Kluth, T., Maass, P., Nickel, J.: Invertible residual networks in the context of regularization theory for linear inverse problems. *Inverse Problems* **39**(12) (2023) (not cited)

[205] Chung, M., Peters, B., Solomon, M.: Good things come in pairs: Paired autoencoders for inverse problems. preprint arXiv:2505.06549 (2025) (cited on p. 33)

[206] Furuya, T., Puthawala, M., Lassas, M., de Hoop, M.V.: Globally injective and bijective neural operators. In: Advances in Neural Information Processing Systems, vol. 36, pp. 57713–57753 (2023) (not cited)

[207] Vadeboncoeur, A., Akyildiz, Ö.D., Kazlauskaitė, I., Girolami, M., Cirak, F.: Fully probabilistic deep models for forward and inverse problems in parametric PDEs. *Journal of Computational Physics* **491** (2023) (cited on pp. 23 and 46)

[208] Lingsch, L., Grund, D., Mishra, S., Kissas, G.: FUSE: Fast unified simulation and estimation for PDEs. In: Advances in Neural Information Processing Systems, vol. 37, pp. 21656–21698 (2024) (cited on p. 23)

[209] Dunlop, M.M., Yang, Y.: Stability of Gibbs posteriors from the Wasserstein loss for Bayesian full waveform inversion. *SIAM/ASA Journal on Uncertainty Quantification* **9**(4), 1499–1526 (2021) (cited on p. 23)

[210] Harrach, B.: Uniqueness and Lipschitz stability in electrical impedance tomography with finitely many electrodes. *Inverse Problems* **35**(2) (2019) (cited on pp. 24 and 37)

[211] de Hoop, M.V., Kovachki, N.B., Lassas, M., Nelsen, N.H.: Extension and approximation of the electrical impedance tomography inversion operator. Forthcoming (2025) (cited on pp. 25, 26, 27, 29, 30, 34, 35, 36, and 37)

[212] Molinaro, R., Yang, Y., Engquist, B., Mishra, S.: Neural inverse operators for solving PDE inverse problems. In: International Conference on Machine Learning, pp. 25105–25139 (2023). PMLR (cited on pp. 25, 29, 31, 32, and 38)

[213] Chan, T.F., Wong, C.-K.: Total variation blind deconvolution. *IEEE Transactions on Image Processing* **7**(3), 370–375 (1998) (cited on p. 25)

[214] Chan, T.F., Vese, L.A.: Active contours without edges. *IEEE Transactions on Image Processing* **10**(2), 266–277 (2001) (cited on p. 25)

[215] Abhishek, A., Strauss, T.: Solving the Electrical Impedance Tomography Problem with a DeepONet Type Neural Network: Theory and Application. preprint arXiv:2407.17182 (2024) (cited on pp. 26, 34, 35, and 37)

[216] Gouk, H., Frank, E., Pfahringer, B., Cree, M.J.: Regularisation of neural networks by enforcing Lipschitz continuity. *Machine Learning* **110**(2), 393–416 (2021) (cited on pp. 27 and 49)

[217] Chen, K., Wang, C., Yang, H.: Let data talk: data-regularized operator learning

theory for inverse problems. preprint arXiv:2310.09854 (2023) (cited on pp. 27 and 33)

- [218] Marzouk, Y.: Discussion of “Experimental Design and Modeling for Forward-Inverse Maps” by R. Barton & M. Morris, appearing in *Technometrics*. *Technometrics* **67**(3), 391–393 (2025) (cited on p. 28)
- [219] Bhattacharya, K., Cao, L., Stepaniants, G., Stuart, A., Trautner, M.: Learning memory and material dependent constitutive laws. preprint arXiv:2502.05463 (2025) (cited on p. 29)
- [220] Berner, J., Liu-Schiaffini, M., Kossaifi, J., Duruisseaux, V., Bonev, B., Azizzadenesheli, K., Anandkumar, A.: Principled approaches for extending neural architectures to function spaces for operator learning. preprint arXiv:2506.10973 (2025) (cited on p. 30)
- [221] Zaheer, M., Kottur, S., Ravanbakhsh, S., Poczos, B., Salakhutdinov, R.R., Smola, A.J.: Deep sets. In: *Advances in Neural Information Processing Systems*, vol. 30 (2017) (cited on p. 31)
- [222] Qi, C.R., Yi, L., Su, H., Guibas, L.J.: PointNet++: Deep hierarchical feature learning on point sets in a metric space. In: *Advances in Neural Information Processing Systems*, vol. 30, pp. 5105–5114 (2017) (cited on p. 31)
- [223] Chiu, S.-T., Hong, J., Braga-Neto, U.: DeepOSets: Non-autoregressive in-context learning of supervised learning operators. preprint arXiv:2410.09298 (2024) (cited on p. 32)
- [224] Arridge, S., Hauptmann, A., Korolev, Y.: Inverse problems with learned forward operators. In: Bubba, T.A. (ed.) *Data-driven Models in Inverse Problems*, pp. 73–106. Walter de Gruyter GmbH & Co KG (2024). Chap. 3 (cited on pp. 33, 39, and 41)
- [225] Aspri, A., Korolev, Y., Scherzer, O.: Data driven regularization by projection. *Inverse Problems* **36**(12) (2020) (cited on pp. 33, 39, 40, and 41)
- [226] Dittmer, S., Kluth, T., Maass, P., Otero Baguer, D.: Regularization by architecture: A deep prior approach for inverse problems. *Journal of Mathematical Imaging and Vision* **62**(3), 456–470 (2020) (cited on p. 33)
- [227] Castro, J., Muñoz, C., Valenzuela, N.: The Calderón’s problem via DeepONets. *Vietnam Journal of Mathematics*, 1–32 (2024) (cited on pp. 34, 35, and 37)
- [228] Castro, J.: The Kolmogorov infinite dimensional equation in a Hilbert space via deep learning methods. *Journal of Mathematical Analysis and Applications* **527**(2) (2023) (cited on p. 35)

[229] Benyamini, Y., Lindenstrauss, J.: Geometric Nonlinear Functional Analysis vol. 48. American Mathematical Society (1998) (cited on p. 36)

[230] Alberti, G.S., Santacesaria, M.: Calderón’s inverse problem with a finite number of measurements. In: Forum of Mathematics, Sigma, vol. 7 (2019). Cambridge University Press (cited on p. 37)

[231] Alberti, G.S., Santacesaria, M.: Infinite-dimensional inverse problems with finite measurements. Archive for Rational Mechanics and Analysis **243**(1), 1–31 (2022) (cited on pp. 37, 38, and 39)

[232] Dugundji, J.: An extension of Tietze’s theorem. Pacific Journal of Mathematics **1**(3), 353–367 (1951) (cited on p. 37)

[233] Engl, H.W., Ramlau, R.: Regularization of inverse problems. In: Encyclopedia of Applied and Computational Mathematics, pp. 1233–1241. Springer (2015) (cited on pp. 39 and 40)

[234] Clason, C.: Regularization of inverse problems. preprint arXiv:2001.00617 (2020) (cited on pp. 40 and 41)

[235] Aspri, A., Frischauf, L., Korolev, Y., Scherzer, O.: Data driven reconstruction using frames and Riesz bases. In: Deterministic and Stochastic Optimal Control and Inverse Problems, pp. 303–318. CRC Press (2021) (cited on p. 41)

[236] Law, K., Stuart, A.M., Zygalakis, K.: Data Assimilation: A Mathematical Introduction. Texts in Applied Mathematics, vol. 62. Springer (2015) (cited on pp. 42, 51, and 61)

[237] Sisson, S.A., Fan, Y., Beaumont, M.: Handbook of Approximate Bayesian Computation. CRC Press (2018) (cited on p. 42)

[238] Cranmer, K., Brehmer, J., Louppe, G.: The frontier of simulation-based inference. Proceedings of the National Academy of Sciences **117**(48), 30055–30062 (2020) (cited on p. 42)

[239] Baldassari, L., Siahkoohi, A., Garnier, J., Solna, K., de Hoop, M.V.: Conditional score-based diffusion models for Bayesian inference in infinite dimensions. In: Advances in Neural Information Processing Systems, vol. 36, pp. 24262–24290 (2023) (cited on pp. 42 and 49)

[240] Schneider, F., Duong, D.-L., Lassas, M., de Hoop, M.V., Helin, T.: An unconditional representation of the conditional score in infinite-dimensional linear inverse problems. preprint arXiv:2405.15643 (2024) (cited on pp. 42 and 49)

[241] Zhao, Y., Lu, H., Jia, J., Zhou, T.: Functional normalizing flow for statistical inverse problems of partial differential equations. preprint arXiv:2411.13277

(2024) (cited on pp. 42 and 61)

[242] Schreuder, N., Brunel, V.-E., Dalalyan, A.: Statistical guarantees for generative models without domination. In: Algorithmic Learning Theory, pp. 1051–1071 (2021). PMLR (cited on p. 44)

[243] Baptista, R., Hosseini, B., Kovachki, N.B., Marzouk, Y.M., Sagiv, A.: An approximation theory framework for measure-transport sampling algorithms. *Mathematics of Computation* **94**(354), 1863–1909 (2025) (cited on p. 44)

[244] Lunz, S., Öktem, O., Schönlieb, C.-B.: Adversarial regularizers in inverse problems. In: Advances in Neural Information Processing Systems, vol. 31 (2018) (cited on p. 44)

[245] Afkham, B.M., Chung, J., Chung, M.: Learning regularization parameters of inverse problems via deep neural networks. *Inverse Problems* **37**(10) (2021) (not cited)

[246] Haltmeier, M., Nguyen, L.: Regularization of inverse problems by neural networks. In: Handbook of Mathematical Models and Algorithms in Computer Vision and Imaging: Mathematical Imaging and Vision, pp. 1065–1093. Springer (2023) (not cited)

[247] Mukherjee, S., Dittmer, S., Shumaylov, Z., Lunz, S., Öktem, O., Schönlieb, C.-B.: Data-driven convex regularizers for inverse problems. In: ICASSP 2024-2024 IEEE International Conference on Acoustics, Speech and Signal Processing (ICASSP), pp. 13386–13390 (2024). IEEE (not cited)

[248] Tan, H.Y., Cai, Z., Pereyra, M., Mukherjee, S., Tang, J., Schönlieb, C.-B.: Unsupervised training of convex regularizers using maximum likelihood estimation. preprint arXiv:2404.05445 (2024) (not cited)

[249] Zhang, Y., Leong, O.: Learning difference-of-convex regularizers for inverse problems: A flexible framework with theoretical guarantees. preprint arXiv:2502.00240 (2025) (not cited)

[250] Soh, Y.S., Chandrasekaran, V.: Learning semidefinite regularizers. *Foundations of Computational Mathematics* **19**(2), 375–434 (2019) (cited on p. 49)

[251] Leong, O., O'Reilly, E., Soh, Y.S., Chandrasekaran, V.: Optimal regularization for a data source. *Foundations of Computational Mathematics*, 1–50 (2025) (cited on pp. 44 and 49)

[252] Trillo, N.G., Sanz-Alonso, D.: The Bayesian update: Variational formulations and gradient flows. *Bayesian Analysis* **15**(1), 29–56 (2020) (cited on p. 45)

[253] Ruthotto, L., Haber, E.: An introduction to deep generative modeling. *GAMM-Mitteilungen* **44**(2) (2021) (cited on p. 45)

[254] Song, Y., Shen, L., Xing, L., Ermon, S.: Solving inverse problems in medical imaging with score-based generative models. In: International Conference on Learning Representations (2022) (cited on pp. 45 and 49)

[255] Dimakis, A.G., Bora, A., Van Veen, D., Jalal, A., Vishwanath, S., Price, E.: Deep generative models and inverse problems. *Mathematical Aspects of Deep Learning* **400** (2022) (not cited)

[256] Bohra, P., Pham, T.-a., Dong, J., Unser, M.: Bayesian inversion for non-linear imaging models using deep generative priors. *IEEE Transactions on Computational Imaging* **8**, 1237–1249 (2023) (not cited)

[257] Scarlett, J., Heckel, R., Rodrigues, M.R., Hand, P., Eldar, Y.C.: Theoretical perspectives on deep learning methods in inverse problems. *IEEE Journal on Selected Areas in Information Theory* **3**(3), 433–453 (2023) (not cited)

[258] Zhao, Z., Ye, J.C., Bresler, Y.: Generative models for inverse imaging problems: From mathematical foundations to physics-driven applications. *IEEE Signal Processing Magazine* **40**(1), 148–163 (2023) (cited on p. 45)

[259] Al-Ghattas, O., Chen, J., Sanz-Alonso, D., Waniorek, N.: Covariance operator estimation: Sparsity, lengthscale, and ensemble Kalman filters. *Bernoulli* **31**(3), 2377–2402 (2025) (cited on p. 46)

[260] Alberti, G.S., Hertrich, J., Santacesaria, M., Sciuotto, S.: Manifold learning by mixture models of VAEs for inverse problems. *Journal of Machine Learning Research* **25**(202), 1–35 (2024) (cited on p. 47)

[261] Gonzalez, M., Almansa, A., Delbracio, M., Musé, P., Tan, P.: Solving Inverse Problems by Joint Posterior Maximization with a VAE Prior. In: (KHIPU) Latin American Meeting in Artificial Intelligence (2019) (cited on p. 47)

[262] Arjovsky, M., Chintala, S., Bottou, L.: Wasserstein generative adversarial networks. In: International Conference on Machine Learning, pp. 214–223 (2017). PMLR (cited on p. 48)

[263] Carreira-Perpinan, M.A., Hinton, G.: On contrastive divergence learning. In: International Workshop on Artificial Intelligence and Statistics, pp. 33–40 (2005). PMLR (cited on p. 49)

[264] Hyvärinen, A., Dayan, P.: Estimation of non-normalized statistical models by score matching. *Journal of Machine Learning Research* **6**(4) (2005) (cited on p. 49)

[265] Hauptmann, A., Mukherjee, S., Schönlieb, C.-B., Sherry, F.: Convergent regularization in inverse problems and linear plug-and-play denoisers. *Foundations of Computational Mathematics*, 1–34 (2024) (cited on pp. 49 and 60)

[266] Basu, S., Jammalamadaka, S.R., Liu, W.: Stability and infinitesimal robustness of posterior distributions and posterior quantities. *Journal of Statistical Planning and Inference* **71**(1-2), 151–162 (1998) (cited on pp. 50 and 52)

[267] Basu, S.: Uniform stability of posteriors. *Statistics & Probability Letters* **46**(1), 53–58 (2000) (cited on p. 52)

[268] Diaconis, P., Freedman, D.: On the consistency of Bayes estimates. *The Annals of Statistics*, 1–26 (1986) (not cited)

[269] Owhadi, H., Scovel, C.: Qualitative robustness in Bayesian inference. *ESAIM: Probability and Statistics* **21**, 251–274 (2017) (cited on p. 50)

[270] Sprungk, B.: On the local Lipschitz stability of Bayesian inverse problems. *Inverse Problems* **36**(5) (2020) (cited on pp. 50 and 52)

[271] Garbuno-Inigo, A., Helin, T., Hoffmann, F., Hosseini, B.: Bayesian posterior perturbation analysis with integral probability metrics. preprint arXiv:2303.01512 (2023) (cited on pp. 50 and 51)

[272] Trevisan, D.: Wide deep neural networks with Gaussian weights are very close to Gaussian processes. preprint arXiv:2312.11737 (2023) (cited on pp. 51 and 52)

[273] Cvetković, N., Lie, H.C.: Upper and lower bounds for local Lipschitz stability of Bayesian posteriors. preprint arXiv:2505.23541 (2025) (cited on p. 50)

[274] Dunbar, O.R., Nelsen, N.H., Mutic, M.: Hyperparameter optimization for randomized algorithms: A case study on random features. *Statistics and Computing* **35**(3), 1–28 (2025) (cited on pp. 50 and 62)

[275] Girolami, M., Febrianto, E., Yin, G., Cirak, F.: The statistical finite element method (statFEM) for coherent synthesis of observation data and model predictions. *Computer Methods in Applied Mechanics and Engineering* **375** (2021) (cited on p. 50)

[276] Dolera, E., Mainini, E.: Lipschitz continuity of probability kernels in the optimal transport framework. *Annales de l’Institut Henri Poincaré (B) Probabilités et Statistiques* **59**(4), 1778–1812 (2023). Institut Henri Poincaré (cited on p. 51)

[277] Alberti, G.S., De Vito, E., Lassas, M., Ratti, L., Santacesaria, M.: Learning the optimal Tikhonov regularizer for inverse problems. In: *Advances in Neural Information Processing Systems*, vol. 34, pp. 25205–25216 (2021) (cited on pp. 53, 54, 55, and 56)

[278] Alberti, G.S., De Vito, E., Helin, T., Lassas, M., Ratti, L., Santacesaria, M.: Learning sparsity-promoting regularizers for linear inverse problems. preprint arXiv:2412.16031 (2024) (cited on p. 55)

[279] Kabri, S., Auras, A., Riccio, D., Bauermeister, H., Benning, M., Moeller, M., Burger, M.: Convergent data-driven regularizations for CT reconstruction. *Communications on Applied Mathematics and Computation* **6**(2), 1342–1368 (2024) (cited on pp. 56 and 57)

[280] Ratti, L.: Learned reconstruction methods for inverse problems: Sample error estimates. In: Bubba, T.A. (ed.) *Data-driven Models in Inverse Problems*, pp. 163–200. Walter de Gruyter GmbH & Co KG (2024). Chap. 5 (cited on pp. 53 and 55)

[281] Webb, A.R.: Functional approximation by feed-forward networks: a least-squares approach to generalization. *IEEE Transactions on Neural Networks* **5**(3), 363–371 (1994) (cited on p. 56)

[282] Venkatakrishnan, S.V., Bouman, C.A., Wohlberg, B.: Plug-and-play priors for model based reconstruction. In: 2013 IEEE Global Conference on Signal and Information Processing, pp. 945–948 (2013). IEEE (cited on p. 59)

[283] Meinhardt, T., Moller, M., Hazirbas, C., Cremers, D.: Learning proximal operators: Using denoising networks for regularizing inverse imaging problems. In: *Proceedings of the IEEE International Conference on Computer Vision*, pp. 1781–1790 (2017) (cited on p. 59)

[284] Gilton, D., Ongie, G., Willett, R.: Deep equilibrium architectures for inverse problems in imaging. *IEEE Transactions on Computational Imaging* **7**, 1123–1133 (2021) (cited on p. 59)

[285] Ryu, E., Liu, J., Wang, S., Chen, X., Wang, Z., Yin, W.: Plug-and-play methods provably converge with properly trained denoisers. In: *International Conference on Machine Learning*, pp. 5546–5557 (2019). PMLR (cited on p. 59)

[286] Belkouchi, Y., Pesquet, J.-C., Repetti, A., Talbot, H.: Learning truly monotone operators with applications to nonlinear inverse problems. *SIAM Journal on Imaging Sciences* **18**(1), 735–764 (2025) (cited on p. 59)

[287] Fang, Z., Buchanan, S., Sulam, J.: What’s in a Prior? Learned Proximal Networks for Inverse Problems. In: *The Twelfth International Conference on Learning Representations* (2024) (cited on p. 59)

[288] Pesquet, J.-C., Repetti, A., Terris, M., Wiaux, Y.: Learning maximally monotone operators for image recovery. *SIAM Journal on Imaging Sciences* **14**(3), 1206–1237 (2021) (cited on p. 60)

[289] Bouman, C.A., Buzzard, G.T.: Generative plug and play: Posterior sampling for inverse problems. In: 2023 59th Annual Allerton Conference on Communication, Control, and Computing (Allerton), pp. 1–7 (2023). IEEE (cited on p. 60)

[290] Ebner, A., Haltmeier, M.: Plug-and-play image reconstruction is a convergent regularization method. *IEEE Transactions on Image Processing* **33**, 1476–1486 (2024) (cited on p. 60)

[291] Khelifa, N., Schönlieb, C.-B., Sherry, F.: Enhanced denoising and convergent regularisation using Tweedie scaling. In: International Conference on Scale Space and Variational Methods in Computer Vision, pp. 185–197 (2025). Springer (cited on p. 60)

[292] Al-Jarrah, M., Hosseini, B., Taghvaei, A.: Fast filtering of non-Gaussian models using amortized optimal transport maps. *IEEE Control Systems Letters*, 1670–1675 (2025) (cited on p. 61)

[293] Bach, E., Baptista, R., Luk, E., Stuart, A.M.: Learning optimal filters using variational inference. preprint arXiv:2406.18066 (2024) (not cited)

[294] Zhou, X.-H., Liu, Z.-R., Xiao, H.: BI-EqNO: Generalized approximate Bayesian inference with an equivariant neural operator framework. preprint arXiv:2410.16420 (2024) (cited on p. 61)

[295] Colbrook, M.J., Antun, V., Hansen, A.C.: The difficulty of computing stable and accurate neural networks: On the barriers of deep learning and Smale’s 18th problem. *Proceedings of the National Academy of Sciences* **119**(12) (2022) (cited on p. 61)

[296] Antun, V., Renna, F., Poon, C., Adcock, B., Hansen, A.C.: On instabilities of deep learning in image reconstruction and the potential costs of AI. *Proceedings of the National Academy of Sciences* **117**(48), 30088–30095 (2020) (not cited)

[297] Boche, H., Fono, A., Kutyniok, G.: Limitations of deep learning for inverse problems on digital hardware. *IEEE Transactions on Information Theory* **69**(12), 7887–7908 (2023) (not cited)

[298] Gottschling, N.M., Antun, V., Hansen, A.C., Adcock, B.: The troublesome kernel: On hallucinations, no free lunches, and the accuracy-stability tradeoff in inverse problems. *SIAM Review* **67**(1), 73–104 (2025) (not cited)

[299] Evangelista, D., Loli Piccolomini, E., Morotti, E., Nagy, J.G.: To be or not to be stable, that is the question: understanding neural networks for inverse problems. *SIAM Journal on Scientific Computing* **47**(1), 77–99 (2025) (cited on p. 61)

[300] Burger, M., Roith, T.: Learning in image reconstruction: A cautionary tale. *SIAM News* **57**(08) (2024) (cited on p. 61)

[301] Cleary, E., Garbuno-Inigo, A., Lan, S., Schneider, T., Stuart, A.M.: Calibrate, emulate, sample. *Journal of Computational Physics* **424** (2021) (cited on p. 62)